

BRIGHAM YOUNG UNIVERSITY

GEOLOGY

S T U D I E S

GEOLOGICAL SOCIETY OF AMERICA



FIELD TRIP GUIDE BOOK



1997 ANNUAL MEETING • SALT LAKE CITY, UTAH



PART *1* ONE

EDITED BY PAUL KARL LINK AND BART J. KOWALLIS

V O L U M E 4 2 • 1 9 9 7

PROTEROZOIC TO RECENT STRATIGRAPHY, TECTONICS, AND VOLCANOLOGY, UTAH, NEVADA, SOUTHERN IDAHO AND CENTRAL MEXICO

Edited by
Paul Karl Link and Bart J. Kowallis

BRIGHAM YOUNG UNIVERSITY GEOLOGY STUDIES

Volume 42, Part I, 1997

CONTENTS

Neoproterozoic Sedimentation and Tectonics in West-Central Utah	Nicholas Christie-Blick	1
Proterozoic Tidal, Glacial, and Fluvial Sedimentation in Big Cottonwood Canyon, Utah	Todd A. Ehlers, Marjorie A. Chan, and Paul Karl Link	31
Sequence Stratigraphy and Paleoecology of the Middle Cambrian Spence Shale in Northern Utah and Southern Idaho	W. David Liddell, Scott H. Wright, and Carlton E. Brett	59
Late Ordovician Mass Extinction: Sedimentologic, Cyclostratigraphic, and Biostratigraphic Records from Platform and Basin Successions, Central Nevada	Stan C. Finney, John D. Cooper, and William B. N. Berry	79
Carbonate Sequences and Fossil Communities from the Upper Ordovician-Lower Silurian of the Eastern Great Basin	Mark T. Harris and Peter M. Sheehan	105
Late Devonian Alamo Impact Event, Global Kellwasser Events, and Major Eustatic Events, Eastern Great Basin, Nevada and Utah	Charles A. Sandberg, Jared R. Morrow and John E. Warme	129
Overview of Mississippian Depositional and Paleotectonic History of the Antler Foreland, Eastern Nevada and Western Utah	N. J. Silberling, K. M. Nichols, J. H. Trexler, Jr., P. W. Jewell and R. A. Crosbie	161
Triassic-Jurassic Tectonism and Magmatism in the Mesozoic Continental Arc of Nevada: Classic Relations and New Developments	S. J. Wyld, and J. E. Wright	197
Grand Tour of the Ruby-East Humboldt Metamorphic Core Complex, Northeastern Nevada: Part 1 — Introduction & Road Log	Arthur W. Snoke, Keith A. Howard, Allen J. McGrew, Bradford R. Burton, Calvin G. Barnes, Mark T. Peters, and James E. Wright	225
Part 2: Petrogenesis and thermal evolution of deep continental crust: the record from the East Humboldt Range, Nevada	Allen J. McGrew and Mark T. Peters	270

Part 3: Geology and petrology of Cretaceous and Tertiary granitic rocks, Lamoille Canyon, Ruby Mountains, Nevada	Sang-yun Lee and Calvin G. Barnes	276
Part 4: Geology and geochemistry of the Harrison Pass pluton, central Ruby Mountains, Nevada	Bradford R. Burton, Calvin G. Barnes, Trina Burling and James E. Wright	283
Hinterland to Foreland Transect through the Sevier Orogen, Northeast Nevada to North Central Utah: Structural Style, Metamorphism, and Kinematic History of a Large Contractional Orogenic Wedge	Phyllis Camilleri, W. Adolph Yonkee, Jim Coogan, Peter DeCelles, Allen McGrew, Michael Wells	297
Part 2: The Architecture of the Sevier Hinterland: A Crustal Transect through the Pequop Mountains, Wood Hills, and East Humboldt Range, Nevada	Phyllis Camilleri and Allen McGrew	310
Part 3: Large-Magnitude Crustal Thickening and Repeated Extensional Exhumation in the Raft River, Grouse Creek and Albion Mountains	Michael L. Wells, Thomas D. Hoisch, Lori M. Hanson, Evan D. Wolff, and James R. Struthers	325
Part 4: Kinematics and Mechanics of the Willard Thrust Sheet, Central Part of the Sevier Orogenic Wedge, North-central Utah	W. A. Yonkee	341
Part 5: Kinematics and Synorogenic Sedimentation of the Eastern Frontal Part of the Sevier Orogenic Wedge, Northern Utah	W. A. Yonkee, P. G. DeCelles and J. Coogan	355
Bimodal Basalt-Rhyolite Magmatism in the Central and Western Snake River Plain, Idaho and Oregon	Mike McCurry, Bill Bonnichsen, Craig White, Martha M. Godchaux, and Scott S. Hughes	381
Bimodal, Magmatism, Basaltic Volcanic Styles, Tectonics, and Geomorphic Processes of the Eastern Snake River Plain, Idaho	Scott S. Hughes, Richard P. Smith, William R. Hackett, Michael McCurry, Steve R. Anderson, and Gregory C. Ferdock	423
High, Old, Pluvial Lakes of Western Nevada	Marith Reheis, and Roger Morrison	459
Late Pleistocene-Holocene Cataclysmic Eruptions at Nevado de Toluca and Jocotitlan Volcanoes, Central Mexico	J. L. Macias, P. A. Garcia, J. L. Arce, C. Siebe, J. M. Espíndola, J. C. Komorowski, and K. Scott	493

A Publication of the
Department of Geology
Brigham Young University
Provo, Utah 84602

Editor

Bart J. Kowallis

Brigham Young University Geology Studies is published by the Department of Geology. This publication consists of graduate student and faculty research within the department as well as papers submitted by outside contributors. Each article submitted is externally reviewed by at least two qualified persons.

Cover photos taken by Paul Karl Link.

Top: Upheaval Dome, southeastern Utah.

Middle: Lake Bonneville shorelines west of Brigham City, Utah.

Bottom: Bryce Canyon National Park, Utah.

ISSN 0068-1016
9-97 700 23348/24218

Preface

Guidebooks have been part of the exploration of the American West since Oregon Trail days. Geologic guidebooks with maps and photographs are an especially graphic tool for school teachers, University classes, and visiting geologists to become familiar with the territory, the geologic issues and the available references.

It was in this spirit that we set out to compile this two-volume set of field trip descriptions for the Annual Meeting of the Geological Society of America in Salt Lake City in October 1997. We were seeking to produce a quality product, with fully peer-reviewed papers, and user-friendly field trip logs. We found we were bucking a tide in our profession which de-emphasizes guidebooks and paper products. If this tide continues we wish to be on record as producing "The Last Best Geologic Guidebook."

We thank all the authors who met our strict deadlines and contributed this outstanding set of papers. We hope this work will stand for years to come as a lasting introduction to the complex geology of the Colorado Plateau, Basin and Range, Wasatch Front, and Snake River Plain in the vicinity of Salt Lake City. Index maps to the field trips contained in each volume are on the back covers.

Part 1 "Proterozoic to Recent Stratigraphy, Tectonics and Volcanology: Utah, Nevada, Southern Idaho and Central Mexico" contains a number of papers of exceptional interest for their geologic synthesis. Part 2 "Mesozoic to Recent Geology of Utah" concentrates on the Colorado Plateau and the Wasatch Front.

Paul Link read all the papers and coordinated the review process. Bart Kowallis copy edited the manuscripts and coordinated the publication via Brigham Young University Geology Studies. We would like to thank all the reviewers, who were generally prompt and helpful in meeting our tight schedule. These included: Lee Allison, Genevieve Atwood, Gary Axen, Jim Beget, Myron Best, David Bice, Phyllis Camilleri, Marjorie Chan, Nick Christie-Blick, Gary Christenson, Dan Chure, Mary Droser, Ernie Duebendorfer, Tony Ekdale, Todd Ehlers, Ben Everitt, Geoff Freethy, Hugh Hurlow, Jim Garrison, Denny Geist, Jeff Geslin, Ron Greeley, Gus Gustason, Bill Hackett, Kimm Harty, Grant Heiken, Lehi Hintze, Peter Huntoon, Peter Isaacson, Jeff Keaton, Keith Ketner, Guy King, Mel Kuntz, Tim Lawton, Spencer Lucas, Lon McCarley, Meghan Miller, Gautam Mitra, Kathy Nichols, Robert Q. Oaks, Susan Olig, Jack Oviatt, Bill Perry, Andy Pulham, Dick Robison, Rube Ross, Rich Schweickert, Peter Sheehan, Norm Silberling, Dick Smith, Barry Solomon, K.O. Stanley, Kevin Stewart, Wanda Taylor, Glenn Thackray and Adolph Yonkee. In addition, we wish to thank all the dedicated workers at Brigham Young University Print Services and in the Department of Geology who contributed many long hours of work to these volumes.

Paul Karl Link and Bart J. Kowallis, Editors

The Grand Tour of the Ruby–East Humboldt Metamorphic Core Complex, Northeastern Nevada: Part 1—Introduction & Road Log

ARTHUR W. SNOKE

Department of Geology and Geophysics, University of Wyoming, Laramie, Wyoming 82071-3006

KEITH A. HOWARD

U.S. Geological Survey, MS 975, 345 Middlefield Road, Menlo Park, California 94025

ALLEN J. MCGREW

Department of Geology, The University of Dayton, Dayton, Ohio 45469-2364

BRADFORD R. BURTON

Department of Geology and Geophysics, University of Wyoming, Laramie, Wyoming 82071-3006

CALVIN G. BARNES

Department of Geosciences, Texas Tech University, Lubbock, Texas 79409-1053

MARK T. PETERS

Woodward-Clyde Federal Services, 1180 Town Center Drive, Las Vegas, Nevada 89134

JAMES E. WRIGHT

Department of Geology and Geophysics, Rice University, Houston, Texas 77251

ABSTRACT

The purpose of this geological excursion is to provide an overview of the multiphase developmental history of the Ruby Mountains and East Humboldt Range, northeastern Nevada. Although these mountain ranges are commonly cited as a classic example of a Cordilleran metamorphic core complex developed through large-magnitude, mid-Tertiary crustal extension, a preceding polyphase Mesozoic contractional history is also well preserved in the ranges. An early phase of this history involved Late Jurassic two-mica granitic magmatism, high-temperature but relatively low-pressure metamorphism, and polyphase deformation in the central Ruby Mountains. In the northern Ruby Mountains and East Humboldt Range, a Late Cretaceous history of crustal shortening, metamorphism, and magmatism is manifested by fold-nappes (involving Archean basement rocks in the northern East Humboldt Range), widespread migmatization, injection of monzogranitic and leucogranitic magmas, all coupled with sillimanite-grade metamorphism. Following Late Cretaceous contraction, a protracted extensional deformation partially overprinted these areas during the Cenozoic. This extensional history may have begun as early as the Late Cretaceous or as late as the mid-Eocene. Late Eocene and Oligocene magmatism occurred at various levels in the crust yielding mafic to felsic orthogneisses in the deep crust, a composite granitic pluton in the upper crust, and volcanic rocks at the surface. Movement along a west-rooted, extensional shear zone in the Oligocene and early Miocene led to core-complex exhumation. The shear zone produced mylonitic rocks about 1 km thick at deep crustal levels, and an overprint of brittle detachment faulting at shallower levels as unroofing proceeded. Megabreccias and other synextensional sedimentary deposits are locally preserved in a tilted, upper Eocene through Miocene stratigraphic sequence. Neogene magmatism included the emplacement of basalt dikes and eruption of rhyolitic rocks. Subsequent Basin and Range normal faulting, as young as Holocene, records continued tectonic extension.

INTRODUCTION AND ORGANIZATION OF THE FIELD GUIDE

The Ruby Mountains and East Humboldt Range form two adjoining ranges in northeastern Nevada, each reaching approximately a mile above surrounding lowlands, and together over 80 mi (~130 km) long (Fig. 1). They lie within the late Cenozoic Basin and Range province, in a region that was also the site of part of the Cordilleran miogeocline during the Neoproterozoic to early Mesozoic. This area was subjected to multiple episodes of plutonism, metamorphism, and deformation in the Mesozoic, and was in the hinterland of the Sevier orogenic belt during the late Mesozoic and early Tertiary. Finally, it was subjected to a complex history of volcanism, sedimentation, and crustal extension during the Cenozoic. For many years the Ruby Mountains and East Humboldt Range has been recognized as a classic example of a Cordilleran metamorphic core complex (e.g., Crittenden et al., 1980). The large magnitude Cenozoic crustal extension associated with core complex development has exposed an important window into middle crustal rocks of the Sevier hinterland and provides an opportunity to study the Mesozoic root zone of the Cordilleran fold-and-thrust belt. Because of the complex overprinting of multiple episodes of deformation, magmatism, and metamorphism in this area—some during contraction and some during extension—a major problem in interpreting the geology of the Ruby Mountains and East Humboldt Range has always been deciphering to which event a particular fabric, structural feature, or plutonic body was associated. Although significant progress has been made in recent years toward sorting out the deformational, magmatic, and metamorphic chronology of the Ruby Mountains and East Humboldt Range, the complexity and overprinting of events must always be considered whenever any rock body in the Ruby Mountains and East Humboldt Range is examined.

In part, this guidebook article has been modified from Snoke and Howard (1984). However, during the past thirteen years and continuing to the present, there have been substantial new geologic studies in the Ruby-East Humboldt area and thus a prime purpose of this trip is to highlight results from these new studies. In that light, this article is divided into the following sections: (1) an introductory section written by Snoke and Howard that summarizes previous work and provides a brief geologic framework for the trip; (2) a detailed roadlog prepared by Snoke with contributions from McGrew and Peters, Howard, and Burton; and (3) a set of three short reports on new results of ongoing studies on metamorphic petrology in the East Humboldt Range (McGrew and Peters), geochemistry of granites in the upper Lamoille Canyon area (Lee and Barnes), and geology and geochemistry of the Harrison Pass pluton

(Burton, Barnes, Burling, and Wright). For convenience, guidebook article figures are numbered sequentially, and the "References cited" section is cumulative.

ACKNOWLEDGMENTS

Recent field studies in the Ruby Mountains by Snoke and Howard were supported by NSF grant EAR-9627958, and the geochemical studies on the Harrison Pass pluton and granitic rocks of upper Lamoille Canyon were supported by NSF grant EAR-9627814. Additional support for geochemical studies on the Harrison Pass pluton were provided by the Department of Geosciences, Texas Tech University, and INAA data were obtained at the Lunar and Planetary Institute through the courtesy of Graham Ryder. Ken Johnson is thanked for his assistance in the field. Some geochemical data on granitic rocks of the upper Lamoille Canyon area were obtained through a DOE reactor sharing grant from Oregon State University. McGrew and Peters thank Steve Wickham and many co-workers for their collaborative efforts in this region over the past several years. In addition, Peters acknowledges the support of Woodward-Clyde Federal Services and grants from the NSF and Geological Society of America. McGrew acknowledges early support from NSF EAR-87-07435 awarded to A.W. Snoke and most recently a University of Dayton Research Council Seed Grant. The field studies of Burton were partially supported by a Geological Society of America research grant. Burton thanks Barbara E. John of the University of Wyoming for many instructive discussions about the mechanics of pluton emplacement and petrogenesis of granitic rocks. The authors thank Phyllis A. Camilleri, W. Adolph Yonkee, and Paul K. Link for their critical review comments on an earlier version of the manuscript. Their many useful suggestions greatly improved the clarity and overall presentation of this field trip guide.

PREVIOUS GEOLOGIC STUDIES

Geologists of the Fortieth Parallel Survey first recognized the anomalously high metamorphic grade of rocks within the Ruby Mountains and East Humboldt Range (at that time both ranges were referred to as the Humboldt Range) and consequently inferred a Precambrian age for these rocks (King, 1878). Robert P. Sharp was the first geologist to study the ranges comprehensively and reported on the geomorphology (1940), glacial deposits (1938), flanking Tertiary deposits (1939a), Paleozoic stratigraphy and structure (1942), and basin-and-range faulting (1939b). Among his many perceptive observations, Sharp established that the ranges are horsts bounded by normal fault systems and reported that granitic material is intermingled with metasedimentary rocks in the metamorphic core of the ranges with an overall increase in the amount of granite

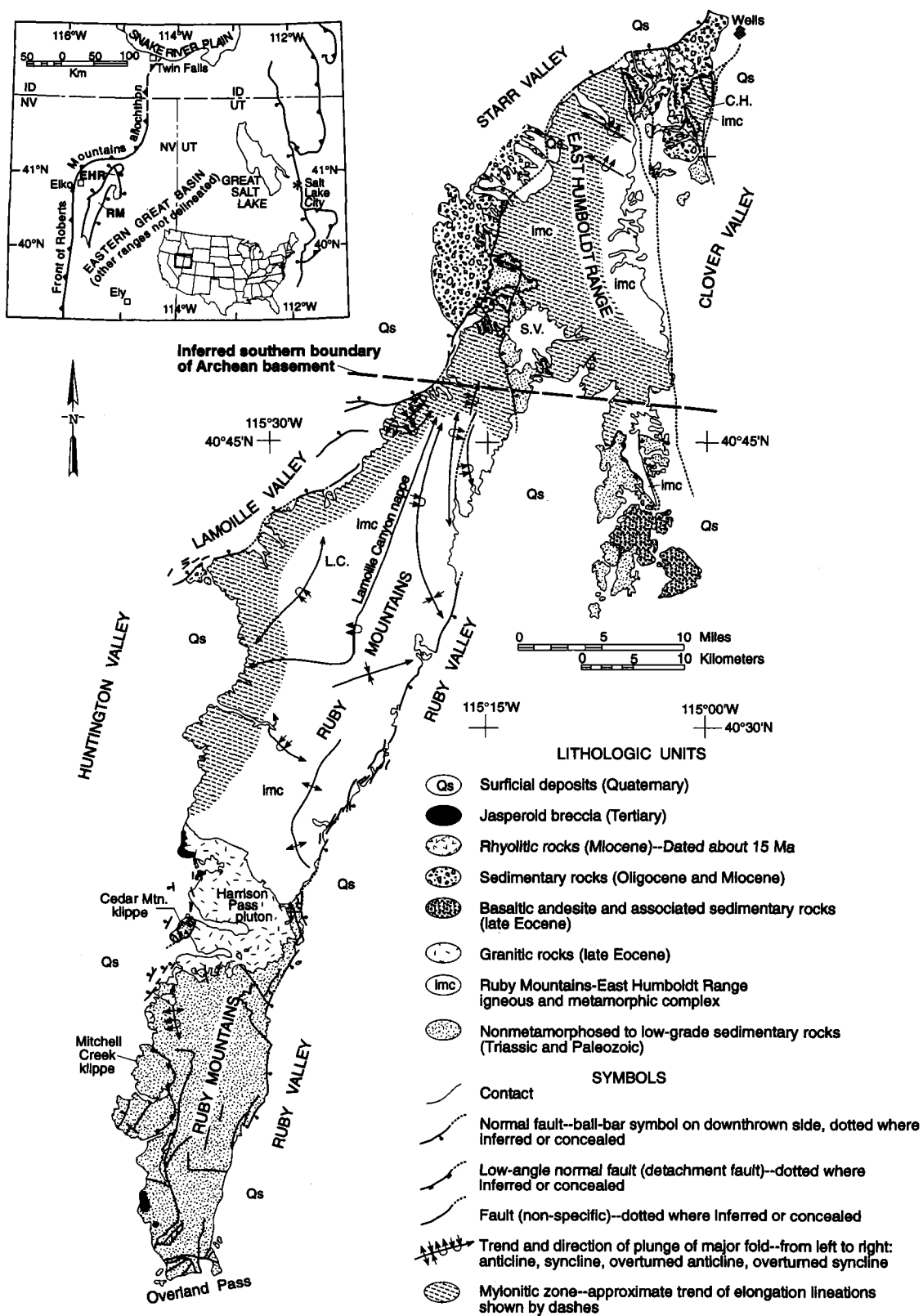


Figure 1. Generalized geologic map of the Ruby Mountains-East Humboldt Range, Nevada. C.H. = Clover Hill, S.V. = Secret Valley, L.C. = Lamoille Canyon.

southward toward the Harrison Pass area (Fig. 1). There, a composite pluton, now known to be late Eocene (~36 Ma; see Swisher and Prothero [1990] for determination of Eocene-Oligocene boundary), separates a migmatitic terrane from a homocline of Cambrian to Mississippian carbonate, shale, and quartzite strata (Sharp, 1942). He also proposed that similar Paleozoic strata were the protoliths for marble and metaquartzite in the northern part of the range (Sharp, 1939b, 1942). Many of the major geologic elements of the ranges were recognized as a result of the studies of Sharp and other early workers: (1) unmetamorphosed lower and middle Paleozoic strata in the southern Ruby Mountains, (2) a migmatitic core of granitic and upper amphibolite facies metamorphic rocks exposed throughout most of the remainder of the ranges, (3) outliers of upper Paleozoic strata on the range flanks and in the Secret Creek gorge area between the ranges, and (4) Tertiary continental strata.

Snelson's (1957) mapping in the East Humboldt Range and northernmost Ruby Mountains added another important element, a thick mylonitic zone developed in the metamorphic and igneous rocks, structurally separated from overlying upper Paleozoic strata by low-angle faults. Snelson (1957) inferred that this mylonite zone, as well as associated low-angle faults that typically place unmetamorphosed sedimentary rocks onto a highly metamorphosed footwall, were manifestations of a Mesozoic décollement zone related to regional contraction. Armstrong and Hansen (1966) inferred that a regional, mobile metamorphic infrastructure developed in the Phanerozoic, based in part on Tertiary K-Ar ages obtained from the Ruby Mountains and other metamorphic rocks in the eastern Great Basin.

Willden and Kistler (1969, 1979) further documented the Paleozoic strata in the southern Ruby Mountains. Detailed geologic mapping and structural studies in the migmatitic rocks of the northern Ruby Mountains by Howard (1966, 1971, 1980) established the presence of a coherent metasedimentary stratigraphy metamorphosed to amphibolite facies (Fig. 2). This stratigraphy outlines large-scale recumbent folds and persists even where commingled granite constitutes half or even 90 per cent of the exposures. Howard (1966, 1980) also divided the igneous and metamorphic complex of the northern Ruby Mountains into a migmatitic metamorphic infrastructure and a structurally higher mylonitic zone. This subdivision has proven to be useful throughout the Ruby Mountains and East Humboldt Range (Snoke et al. 1990b), and we use this nomenclature in this article.

In 1971 Snoke began a study of the transition from the migmatitic infrastructure into the mylonitic zone and included klippen of unmetamorphosed rocks within his initial map area in the northernmost Ruby Mountains. As this study progressed, he realized that Tertiary rocks were

involved in the low-angle faulting that characterized the upper levels of the structural pile (Snoke, 1975). During the summer of 1981, mylonitic rocks were discovered in the mid-Tertiary Harrison Pass pluton (Snoke et al., 1982) and the concept evolved that much of the mylonitization was Tertiary in age rather than Mesozoic as had been assumed since Snelson's (1957) descriptions of the mylonitic rocks of the East Humboldt Range and northernmost Ruby Mountains. U-Pb geochronology coordinated with geologic mapping established that many of the mylonitic plutonic bodies in the Ruby Mountains and East Humboldt Range were Tertiary intrusive bodies subsequently deformed in a ductile shear zone (Wright and Snoke, 1986, 1993) and consequently the recognition of a Tertiary shear zone became a fundamental element in the structural chronology. The cooling history of the mylonitic shear zone and migmatitic infrastructure has been explored by various thermochronometric studies (Armstrong and Hansen, 1966; Kistler et al., 1981; Dallmeyer et al., 1986; Dokka et al., 1986; McGrew and Snee, 1994). While geochronological studies indicated the importance of plastic Tertiary deformation in the Ruby Mountains and East Humboldt Range, kinematic studies of the mylonitic rocks provided important clues to the overall geometry of the mylonitic shear zone including the recognition of a west-rooted, plastic-to-brittle fault system with top to the west-northwest motion along the west flank of both the Ruby Mountains and East Humboldt Range (Snoke and Lush, 1984; Mueller and Snoke, 1993a). The mylonitic zone has been studied with thermobarometric techniques which indicated that the deeper parts of the mylonitic shear zone were deformed under amphibolite-facies conditions (Hurlow et al., 1991). Recrystallization grain-size studies also provided information on paleostress during mylonitization (Hacker et al., 1990). These studies coupled with geologic mapping indicate that the mylonitic shear zone is about 1 kilometer thick, extensional in character and rooted to the west, exhibits a plastic-to-brittle history during exhumation, involved plutonic rocks as young as 29 Ma, and is cut by younger normal faults related to late Cenozoic Basin and Range extension.

The fold-nappes originally recognized by Howard (1966, 1980) in the northern Ruby Mountains have always been a major geologic curiosity in this part of the Sevier hinterland. Studies in the East Humboldt Range have now demonstrated that a basement-cored (Archean) fold-nappe is exposed in the northern part of that range (Lush et al., 1988; McGrew, 1992). The age of this fold-nappe is still controversial, but Allen McGrew has made a strong case for Late Cretaceous development based on detailed geologic mapping and some sparse U-Pb dating of associated granitic rocks. McGrew (1992) concluded that the fold-nappe formed during crustal contraction associated with

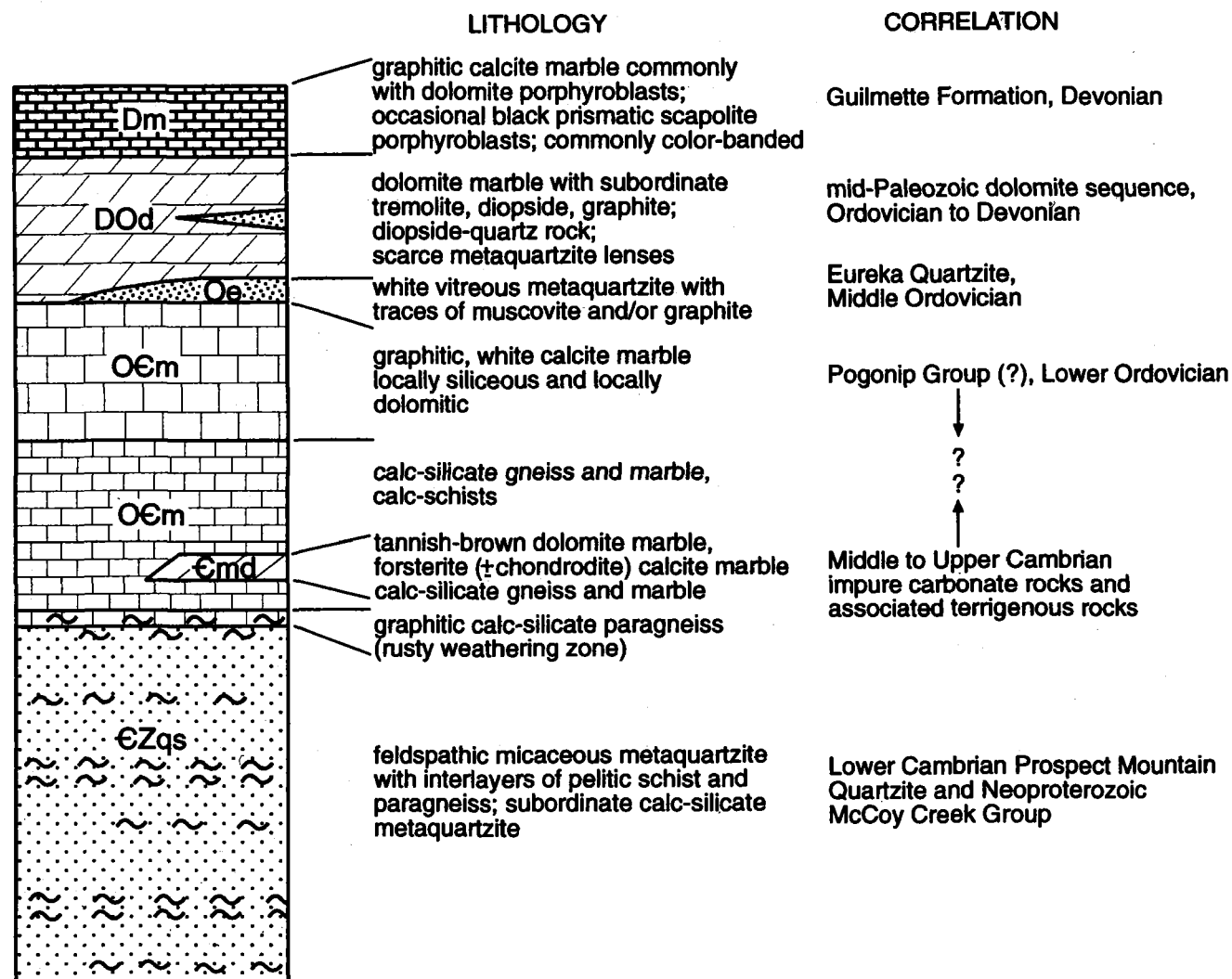


Figure 2. Schematic stratigraphic column of metasedimentary rock units (after Howard, 1971; Snoke, 1980).

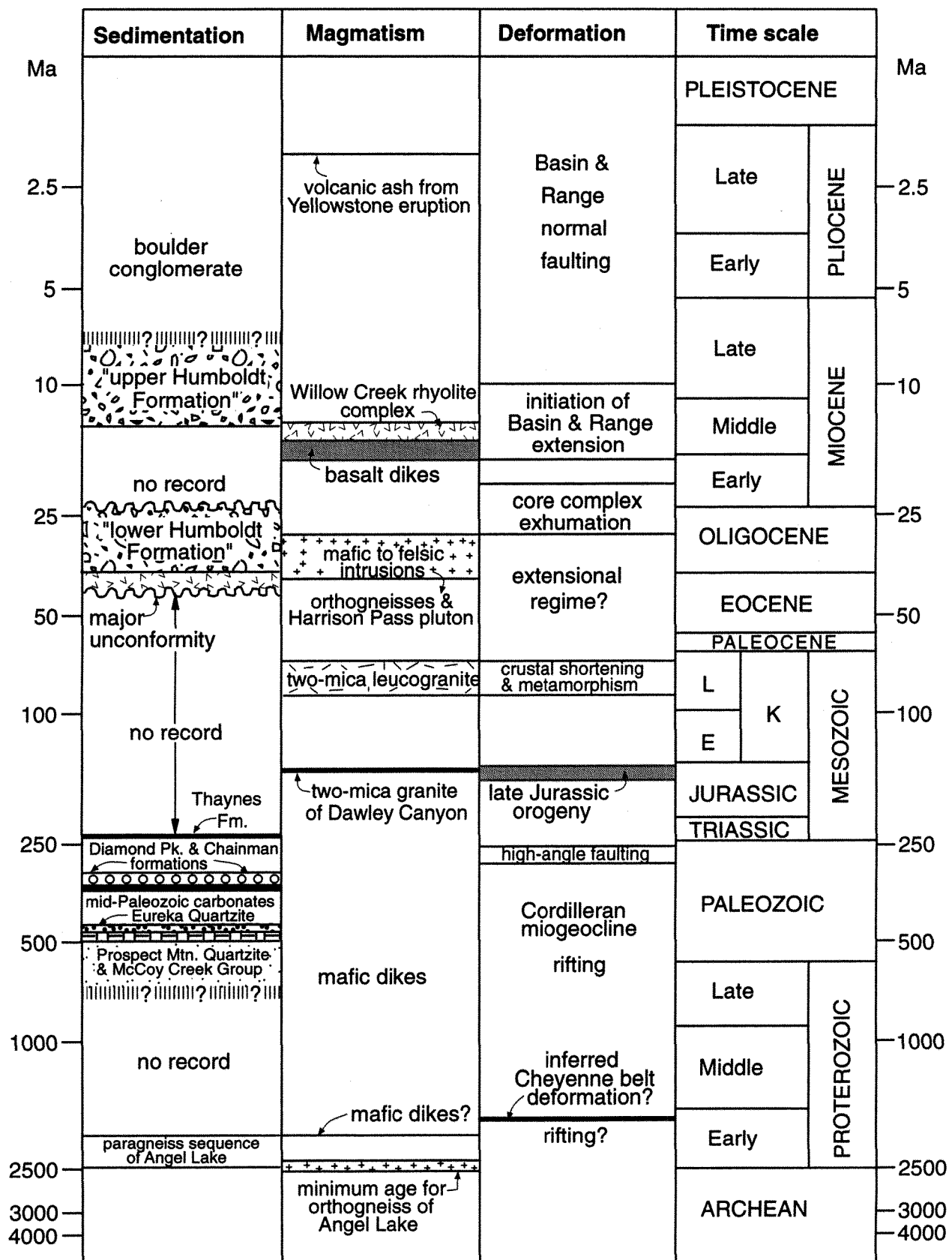
the Sevier orogeny and was subsequently strongly overprinted by a large-scale Tertiary shear zone during core complex development. The magnitude of Late Cretaceous deformation, magmatism, and metamorphism in the Ruby Mountains and East Humboldt Range is still just being explored via geologic mapping and coordinated radiometric dating, but ongoing studies on the relationship between granite emplacement and deformation in the Lamoille Canyon area may provide an important key to this history. We will study some of these important relationships in upper Lamoille Canyon on DAY THREE of the field trip.

An important recent discovery is that a pervasive elongation lineation (sometimes defined by sillimanite), widespread in parts of the migmatitic infrastructure of the northern Ruby Mountains, developed during the Tertiary

(MacCready et al., 1993, in press). The development of this infrastructure lineation may in part overlap the development of the west-northwest lineation of the mylonitic shear zone. The key evidence for this conclusion is that selected Tertiary plutonic orthogneisses of the infrastructure, dated by U-Pb radiometric techniques, contain this fabric.

GEOLOGIC FRAMEWORK

The Ruby Mountains–East Humboldt Range records a polyphase Mesozoic–Cenozoic history of deformation (Fig. 3). Although a complex Mesozoic history is inferred to have affected the entire Ruby Mountains–East Humboldt Range prior to core complex development, this early history is best understood in the Ruby Mountains. In the central Ruby Mountains, Hudc (1990, 1992) identified three phases of penetrative deformation and two amphibolite-



facies metamorphic events, all of which he interpreted as broadly synchronous with the emplacement of Late Jurassic two-mica granite (Hudec and Wright, 1990). Metamorphic monazite from a pelitic schist in the northern Ruby Mountains yielded a Late Cretaceous U-Pb date suggesting a younger high-temperature metamorphic event in that area (Snok et al., 1979). Sillimanite-bearing, pegmatitic leucogranite intimately interlayered with upper amphibolite-facies metamorphic rocks in the northern Ruby Mountains (Lamoille Canyon area) has also yielded a Late Cretaceous monazite date (Wright, Snok, Howard, and Barnes, unpublished data; Snok et al., 1992). These data suggest the importance of Late Cretaceous granitic magmatism and metamorphism during the evolution of the high-grade, migmatitic core of the Ruby Mountains (Kistler et al., 1981; Snok et al., 1992). In summary, the Mesozoic history of the Ruby Mountains (and perhaps also the East Humboldt Range) involved at least two thermal pulses—one in the Late Jurassic clearly associated with granitic pluton emplacement, and one in the Late Cretaceous associated with tectonic thickening and the production of leucogranites (Snok, 1994).

Tertiary intrusion in the Ruby Mountains-East Humboldt Range was areally widespread, occurred over an extensive time period (40–29 Ma), and is well-documented by U-Pb geochronology (Wright and Snok, 1993; Fig. 3). Tertiary intrusions exhibit a broad range in composition from mafic quartz diorite to leucogranite; the intrusions occur as dikes, sills, and large sheet-like bodies. Wall-rock contacts range from sharp to diffuse. Some bodies clearly cross-cut wall-rock structures (e.g., foliation), whereas other bodies are subparallel to wall-rock structures or appear to share the same fabric elements.

Superposed on this polyphase magmatic, metamorphic, and deformational history is the top-to-the-west-north-west, normal-sense mylonitic shear zone of Tertiary age

(Snok and Lush, 1984). The physical conditions of mylonitization include a broad range of P–T conditions, as different levels of the shear zone are exposed along >100 km of strike (Snok et al., 1990a; Hacker et al., 1990; Hurlow et al., 1991). As the shear zone evolved and uplift and tectonic denudation progressed, the character of extensional deformation changed from plastic to brittle, with low-angle normal faults localized in the mylonitic shear zone. These low-angle faults dismembered macroscopic folds related to the earlier periods of deformation, and they juxtaposed upper crustal, unmetamorphosed to low-grade metamorphic rocks against rocks originally resident in the middle crust. The mylonitic deformation was thus part of a long-lived, extensional fault system (e.g., Mueller and Snok, 1993a). Activity on this fault system began in the Eocene and has continued into the Holocene, thereby indicating a protracted history of exhumation for the Ruby Mountains–East Humboldt core complex.

ROAD LOG

DAY ONE

Salt Lake City International Airport to Wells, Nevada via Interstate 80 West (Fig. 4).

There will be no formal geologic stops along our route from the Salt Lake City International Airport to Wells, Nevada (Fig. 4). However, a brief summary of the physiography and geology that we traverse along this segment of the field trip is included in this road log as well as some references.

After leaving the Salt Lake City International Airport, we drive west toward the Great Salt Lake Desert. Our route takes us around the north end of the Oquirrh Mountains near Magna, where complex folding of the Pennsylvanian–Permian Oquirrh Group is well exposed in the North Oquirrh thrust plate (Tooker and Roberts, 1970). Shore-

Figure 3. Geologic history of the Ruby Mountains and East Humboldt Range, Nevada, including sedimentation, magmatism, and deformation. Only selected stratigraphic units are delineated in the sedimentation column. Logarithmic time scale in Ma; geologic time scale after Palmer (1983). This diagram was designed after Dickinson (1991, figure 5). The age of the Archean orthogneiss of Angel Lake is from Lush et al. (1988), the age range for the mid-Tertiary orthogneisses is from Wright and Snok (1993), and the age range of the Willow Creek rhyolite complex is from E. H. McKee (unpublished data). The age range of the Miocene basalt dikes is based on data reported in Snok (1980) and Hudec (1990). The age range of the leucogranites (90 to 70 Ma) is based on data summarized in Snok et al. (1992) as well as the unpublished U-Pb radiometric ages of J. E. Wright. The age of the two-mica granite of Dawley Canyon is from Hudec and Wright (1990). The age range for the exhumation of the core complex is based on data reported in Dallmeyer et al. (1986), Dokka et al. (1986), and Wright and Snok (1993). The stratigraphic age range for the "lower Humboldt Formation" (late Eocene to Oligocene) is based on paleontological data reported in Good et al. (1995). The age range of the late Eocene volcanic and associated rocks in the East Humboldt Range is based on data summarized in Brooks et al. (1995). The presence of ash deposits erupted from the Yellowstone volcanic plateau is based on a preliminary identification made by A. M. Sarna-Wojcicki (personal. comm., 1992) of a sample of vitric ash collected by Snok from near the center of section 7, T. 34 N, R. 59 E (John Day Creek, Soldier Peak 7 1/2 minute quadrangle).

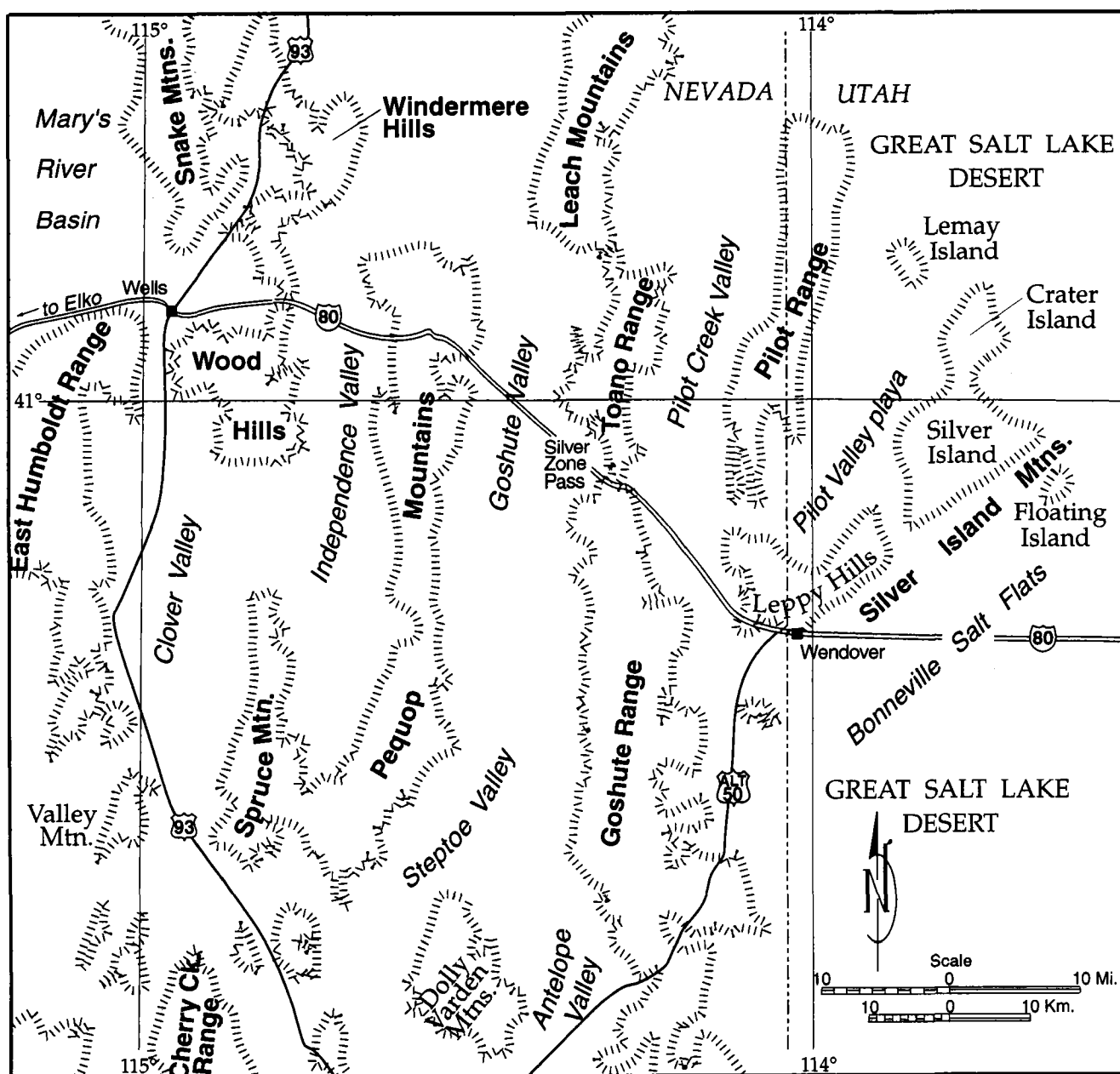
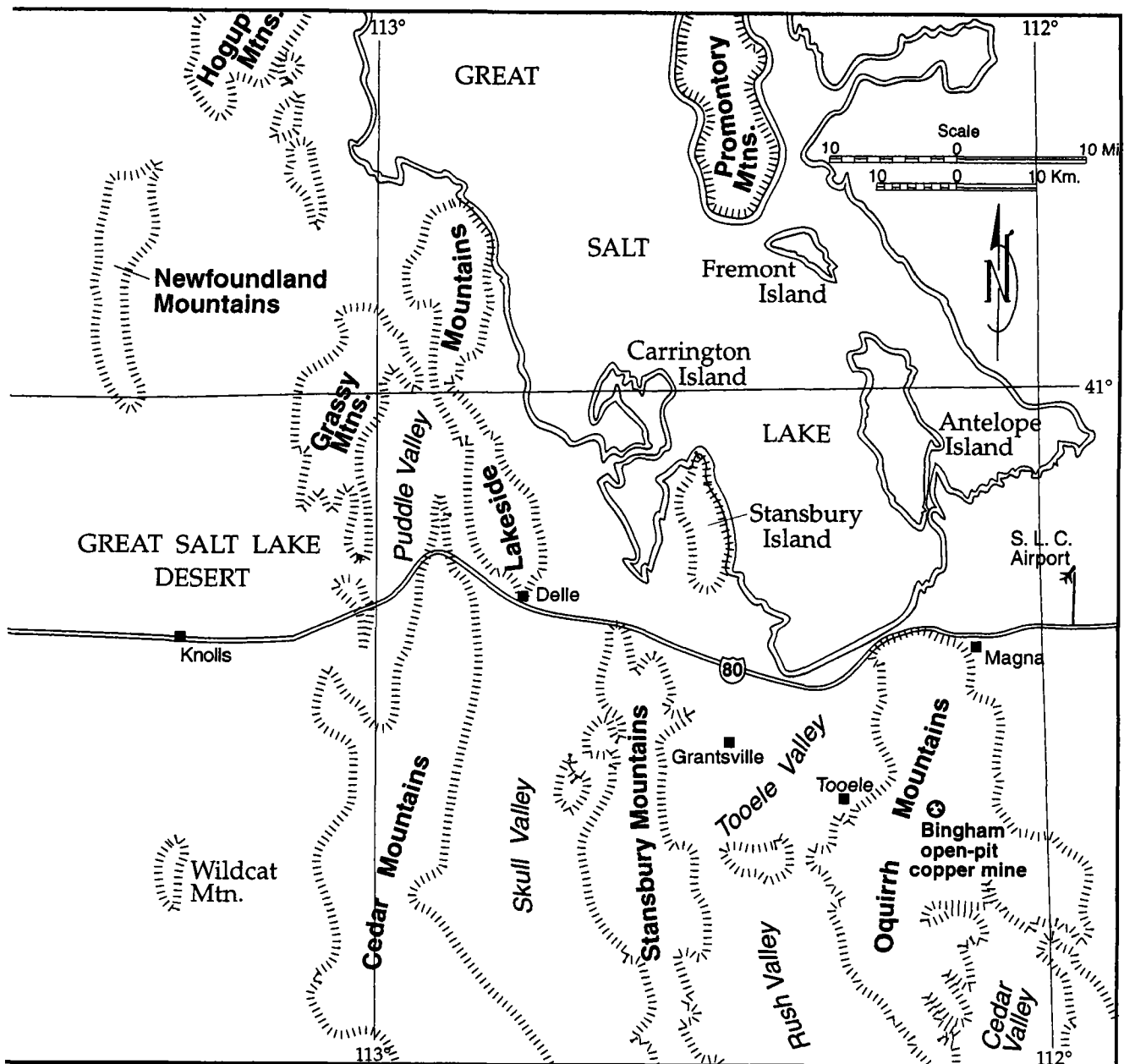


Figure 4. Map showing route (along I-80 West) from Salt Lake City International Airport to Wells, Nevada (see geologic description of the route on DAY ONE).

line features related to Pleistocene Lake Bonneville, studied by G. K. Gilbert (1890), are also well preserved along the margin of the Oquirrh Mountains. Further south on the east side of the range, in the Bingham Canyon area, units of the Oquirrh Group are complexly intruded by late Eocene granitic stocks, dikes, and sills (Lanier et al., 1978; Warnars, et al., 1978). Possible cogenetic volcanic rocks occur on the east side of the range and have yielded late Eocene and Oligocene radiometric ages (Moore, 1973;

Warnars et al., 1978; Moore and McKee, 1983). Extensive copper mineralization is associated with the epizonal granitic intrusions and adjacent sedimentary country rocks. The Bingham copper deposit is one of the largest in the world with pre-mining reserves estimated at almost 3 billion tons of 0.67 per cent copper ore (Babcock et al., 1995).

The large, barren island within the Great Salt Lake to the north is Antelope Island, which has been preserved as a state park and is known for the largest buffalo herd in



the State of Utah (Doelling, 1989). The island is 15 miles long and about 5 1/2 miles wide and exposes a wide range of rocks including extensive exposures of Paleoproterozoic and Archean(?) rocks of the Farmington Canyon complex (Doelling et al., 1990). These Precambrian rocks are in the footwall of the Willard thrust, a regional thrust fault well exposed in the Wasatch Mountains to the east (Camilleri et al., this volume). Lake Bonneville deposits are also well-preserved on the island, and shoreline levels are clearly notched into the ridges of the island (Doelling, 1989; Doelling et al., 1990).

After passing across Tooele Valley, we will skirt the north end of the Stansbury Mountains where excellent shore features of Lake Bonneville are also well-preserved. The structural geology of this range is controversial. Rigby (1958) mapped several large-scale folds in the range and argued that they were cut by high-angle faults. Tooker and Roberts (1971) and Tooker (1983) postulated that imbricate, east-directed thrusting was the dominant structural pattern of the range and related this deformation to the Sevier orogeny (Armstrong, 1968). Cashman (1992) found that some of the folding in the range is related to blind

faulting in the subsurface, and interpreted the whole range as in the hanging wall of the Tintic Valley thrust, an unexposed regional thrust postulated to exist east of the range. Deseret Peak (11,031 ft [3,364 m]), the highest peak in the range, is underlain by massive, light-colored Cambrian Tintic Quartzite (Rigby, 1958).

West of the Stansbury Mountains, we cross the northern end of Skull Valley and pass immediately south of the Lakeside Mountains (Young, 1955). Near the northern end of the Cedar Mountains, we cross low hills composed of Pennsylvanian-Permian rocks prior to entering the Great Salt Lake Desert. Near Knolls, the Newfoundland Mountains are visible north of I-80, there Allmendinger and Jordan (1984) documented an older-over-younger thrust (Desert Peak thrust) that is intruded by a Late Jurassic (~160 Ma) granitic stock. They also mapped low-angle normal faults, some of which are intruded by Jurassic granitic dikes thus indicating a mid-Mesozoic history of contraction, extension, and magmatism.

As we approach the Nevada State Line, the Silver Island Mountains, a northeast-trending range that begins near Wendover, Utah–Nevada forms the skyline. The northeastern end of the Silver Island Mountains is called Crater Island and this area was recently studied in detail by Miller and Allmendinger (1991) who mapped a set of north- and northeast-striking normal faults and an associated north-northwest dextral strike-slip fault system which predate a ~160-Ma pluton. These authors argued that these relationships, coupled with other examples of coeval Jurassic extension and magmatism, suggest a Jurassic regional extensional event in northwest Utah, whereas Jurassic contraction is characteristic of several localities in northeast Nevada.

Near Wendover, Utah–Nevada, several large roadcuts expose Upper Devonian Guilmette Formation (Schaeffer, 1960). West of Wendover, tilted 12-Ma rhyolite unconformably overlies Permian rocks (Miller and Camilleri, 1992). Beyond Wendover, Pilot Peak (named by J. C. Fremont; elevation = 10,704 ft [3,265 m]) in the Pilot Range to the north forms a prominent landmark that has guided many pioneers, including the ill-fated Donner-Reed party of 1846. The geology of the Pilot Range and environs has been studied by Miller et al. (1987), Miller and Hoisch (1992), and Miller and Lush (1981). The basic structural feature of the range is the Pilot Peak décollement, a low-angle normal fault that separates a footwall of metamorphosed Cambrian and Neoproterozoic clastic rocks from a hanging-wall plate consisting of unmetamorphosed miogeoclinal rocks ranging in age from Permian to Cambrian. A small, ~39-Ma pluton (Bettridge Creek Granodiorite) and associated dikes cut all rocks and structures below the décollement, as well as intrude the décollement, thereby

indicating that ductile deformation had ceased by the late Eocene (Miller et al., 1987).

At Silver Zone Pass in the Toano Range, we pass through a granitic pluton (chiefly hornblende-biotite granodiorite) dated as Jurassic (~160 Ma, J. E. Wright, personal comm., 1997). Glick (1987) most recently mapped this area and proposed that the metasedimentary wall rocks experienced Jurassic regional metamorphism and deformation prior to emplacement of the pluton. Miller and Camilleri (1992) confirmed that the pluton intruded and contact metamorphosed previously regionally metamorphosed Cambrian strata.

West of the Toano Range, we cross the broad Goshute Valley. Interpretations of east-west-striking, migrated seismic reflection profiles across the basin (Effimoff and Pinezich, 1981; Anderson et al., 1983) indicated an asymmetric basin bounded on the east flank by a major low-angle fault. Strecker et al. (1996) recognized two syntectonic Tertiary seismic sequences—one recording an early sag stage and a younger sequence recording an expansion of the stratigraphic section across an intrabasin graben. Strecker et al. (1996) argued that the early sequence formed in response to a planar normal fault, whereas the younger sequence formed in response to listric growth faulting.

After we pass Oasis, we begin a long climb to Pequop Summit. During this climb up the east flank of the northern Pequop Mountains, we begin our traverse in upper Eocene volcanic and sedimentary rocks that rest unconformably on folded and faulted Devonian through Permian strata (Brooks et al., 1995, their figure 4). The highway then traverses through various upper and middle Paleozoic sedimentary units. Past Pequop Summit, the Upper Devonian Guilmette Formation forms spectacular gray carbonate cliffs as the highway descends down Maverick Canyon.

After crossing Independence Valley, we pass the northern end of the Wood Hills at Moor Summit where east-dipping Miocene Humboldt Formation(?) is exposed in low roadcuts. The Wood Hills and adjacent Pequop Mountains were studied by C. H. Thorman for his Ph. D. dissertation research project at the University of Washington (1962), supervised by late Professor Peter Misch. Thorman (1970) recognized a mappable, metamorphosed lower Paleozoic stratigraphy as well as several low-angle faults. This area was subsequently studied by P. A. Camilleri for her Ph. D. dissertation (1994) at the University of Wyoming, and a recent published paper by Camilleri and Chamberlain (1997) provides new structural, stratigraphic, metamorphic, and geochronologic data on the area. An important conclusion of Camilleri and Chamberlain (1997) is that the peak of regional, Barrovian metamorphism was during Late Cretaceous time and subsequently the area experienced a complex extensional history.

After crossing Moor Summit, the highway grades gradually down hill into the town of Wells, originally named Humboldt Wells in reference to the creeks and springs that mark the origin of the Humboldt River. This ends the roadlog for DAY ONE; we stay in Wells overnight, and on DAY TWO we examine parts of the East Humboldt Range, the high mountain range southwest of the town.

DAY TWO

Summary of route: Wells to Clover Hill to the northern East Humboldt Range (Angel Lake area) to the southeastern East Humboldt Range to Ruby Valley to Elko (Fig. 5).

<u>Incre.</u> <u>Miles</u>	<u>Cum.</u> <u>Miles</u>	
0.0	0.0	The roadlog starts at the Super 8 Motel, Wells, Nevada. Turn left onto Sixth Street and proceed west.
0.8	0.8	Turn left onto Humboldt Avenue.
0.9	1.7	Intersection of Humboldt Avenue and Angel Lake Highway. Turn right and head toward Angel Lake.
3.5	5.2	Large roadcut (on the right) of conglomerates of the lower part of the Tertiary Humboldt Formation, informally called here the "lower Humboldt Formation" (Thl) (Fig. 6). From this vantage point you can begin to see ahead the northwestern corner of Clover Hill dome, mantled by Tertiary rocks which are in low-angle, normal fault contact onto subjacent metasedimentary rocks. Metamorphic rocks form the dip-slope surface of Clover Hill and are variably mylonitic Ordovician and Cambrian calcite marbles that tectonically overlie mylonitic Cambrian and Neoproterozoic quartzite and schist (Snoke, 1992).
0.3	5.5	To the right are massive exposures of Miocene (about 13.8 Ma) quartz + feldspar-phyric rhyolite porphyry. This lithologic unit forms a laccolithic mass that intruded along the contact between the "Thl2" unit of the lower Humboldt Formation and overlying rhyolite lava flows dated at about 14.8 Ma (Figs. 6 and 7).
0.8	6.3	STOP 2-1 —Overview of the northern East Humboldt Range and a well-exposed, low-angle normal fault contact in roadcut. The following description is modified from STOP 7 of Mueller and Snoke (1993b).

Pull off road to the right into large parking space.

From this locality there is an excellent view of the high country of the northern East Humboldt Range as well as the tree-covered forerange and low-lying foothills. The high country is underlain by amphibolite-facies metamorphic rocks, and is part of the high-grade footwall of the East Humboldt metamorphic core complex (McGrew, 1992). The forerange, however, is underlain by unmetamorphosed upper Paleozoic sedimentary rocks, and the low foothills expose Tertiary sedimentary and volcanic rocks (Fig. 7). These Paleozoic and Tertiary rocks constitute part of the hanging-wall sequence of the East Humboldt Range core complex. The East Humboldt plastic-to-brittle shear zone/detachment fault system originally separated these disparate crustal levels before being offset by late, high-angle normal faults (Mueller and Snoke, 1993a).

A principal feature of the metamorphic terrane is the basement-cored, south-closing, Winchell Lake fold-nappe (Lush et al., 1988; McGrew, 1992). Chimney Rock, a prominent isolated peak (at about azimuth 235°), is composed of orthogneiss and paragneiss that forms the core of this large-scale recumbent fold. The tree-covered forerange consists chiefly of Pennsylvanian and Permian carbonate rocks (Ely Limestone, Pequop Formation, Murdock Mountain Formation), but also includes Pennsylvanian and Mississippian Diamond Peak Formation. A prominent high-angle normal fault separates the Paleozoic rocks from the Tertiary strata. Reddish-brown-weathering siliceous breccia (so-called jasperoid) crops out locally along the contact (e.g., at about 240°). Prominent outcroppings in the low-lying Tertiary terrane are lens-like masses of megabreccia derived from middle Paleozoic carbonate rocks; we examine some of these deposits in detail at STOP 2-2. Finally, rhyolite porphyry forms an isolated body along the range front at about azimuth 205°, and a prominent mass of rhyolite is at about 300°.

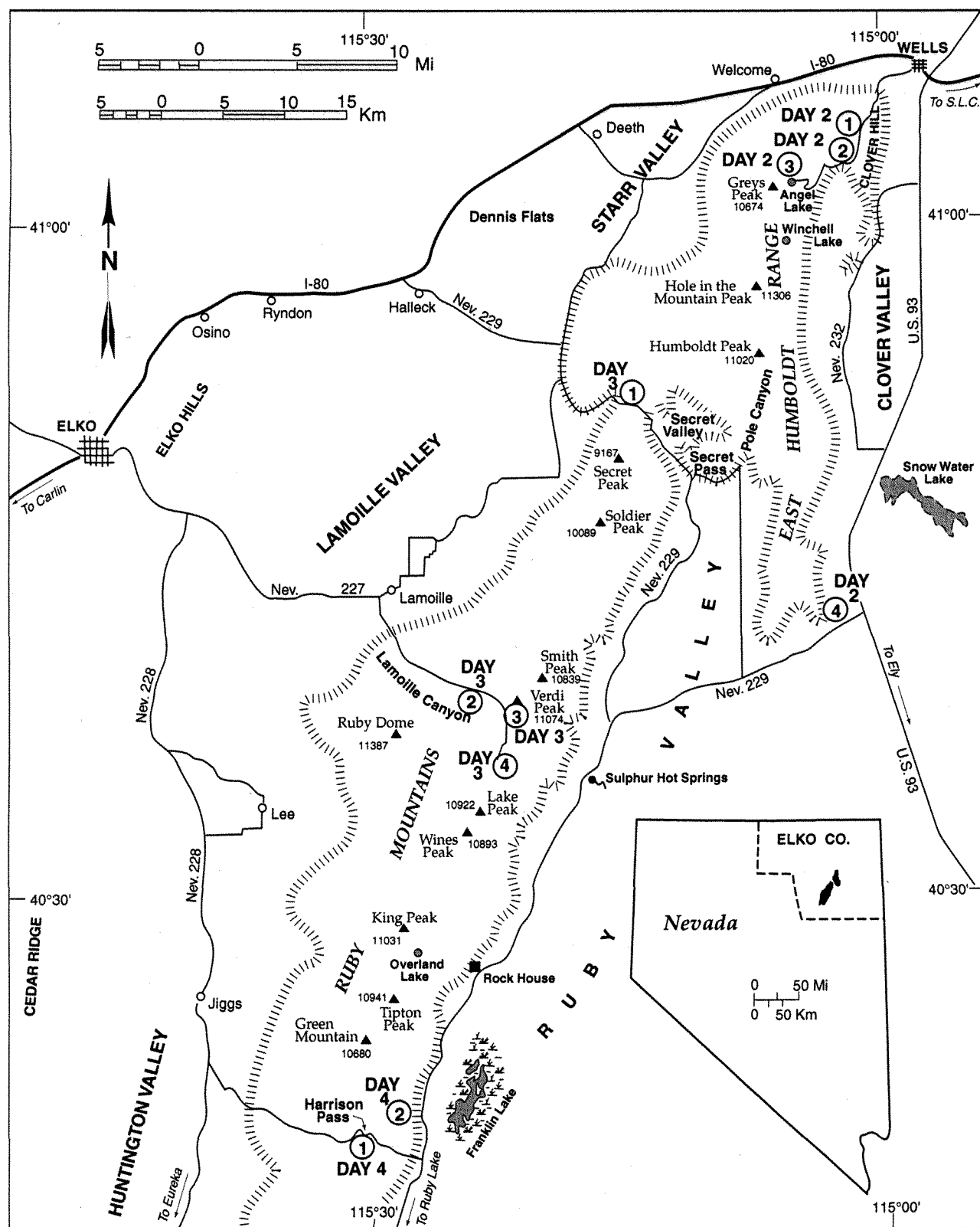


Figure 5. Map of the Ruby Mountains and East Humboldt Range, Nevada, and surrounding areas summarizing the locations of the field trip STOPS for DAY TWO–DAY FOUR. Modified from Snoke and Howard (1984). S.L.C. = Salt Lake City.

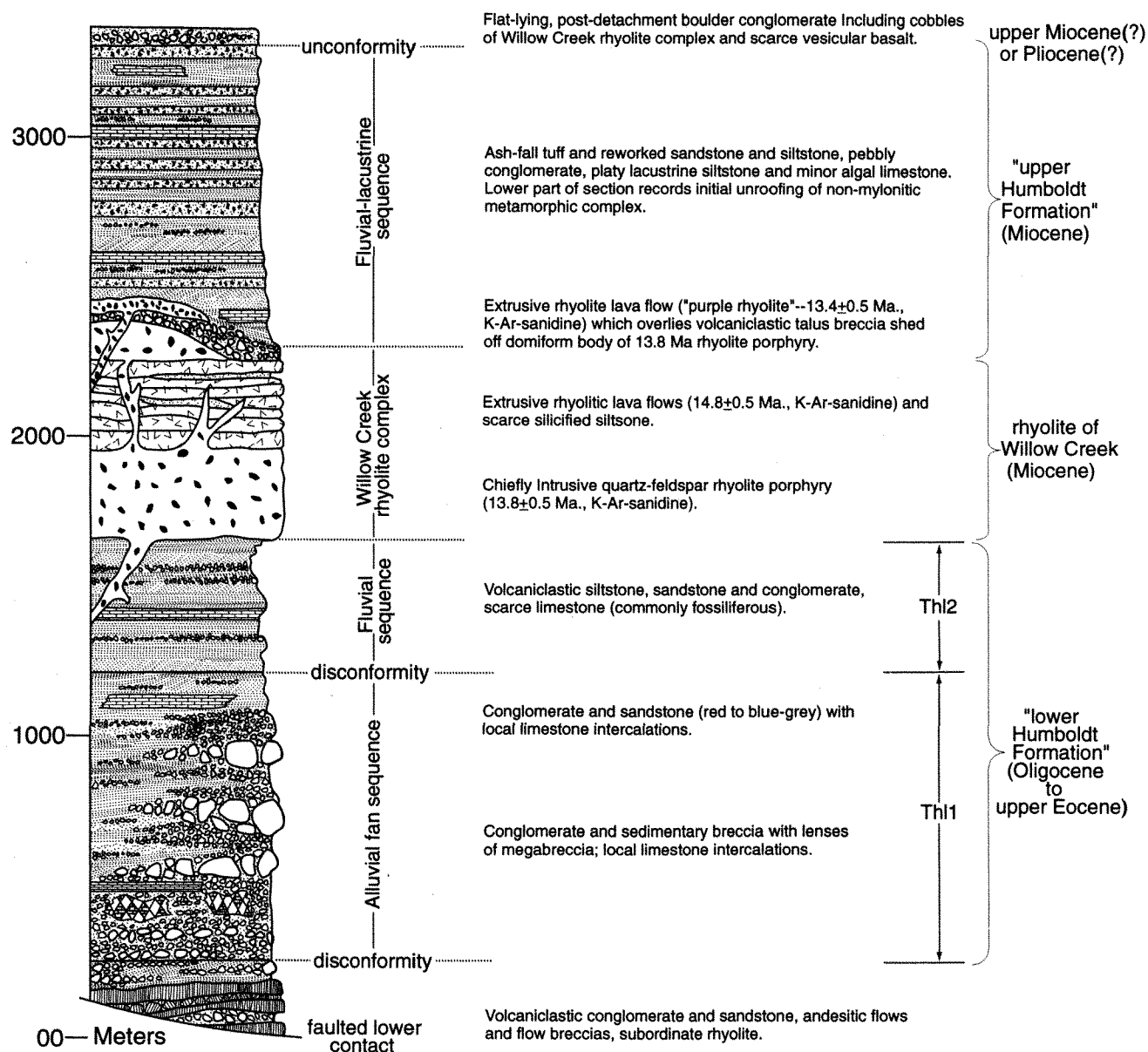


Figure 6. Generalized stratigraphic column of Tertiary rocks in the northeastern East Humboldt Range (modified from Mueller and Snoke, 1993b).

A low-angle normal fault exposed in the west roadcut immediately north of the pull-out separates steeply dipping Miocene conglomerate of the hanging wall from a footwall of platy marble representing Ordovician and Cambrian strata intruded by pegmatitic leucogranite. Red gouge separates these two units, and the top of the marble is brecciated. As the fault is traced northward along strike, a

fault-bounded slice of metadolomite (Silurian and/or Devonian protolith) is present along this tectonic boundary (Fig. 7).

Return to vehicles and continue westward along the Angel Lake Highway.

Roadcut exposure of lacustrine limestone with interbedded conglomerate on right (unit Th11 of Fig. 6). Turn left into flat area across from the west end of the exposure.

1.8 8.1

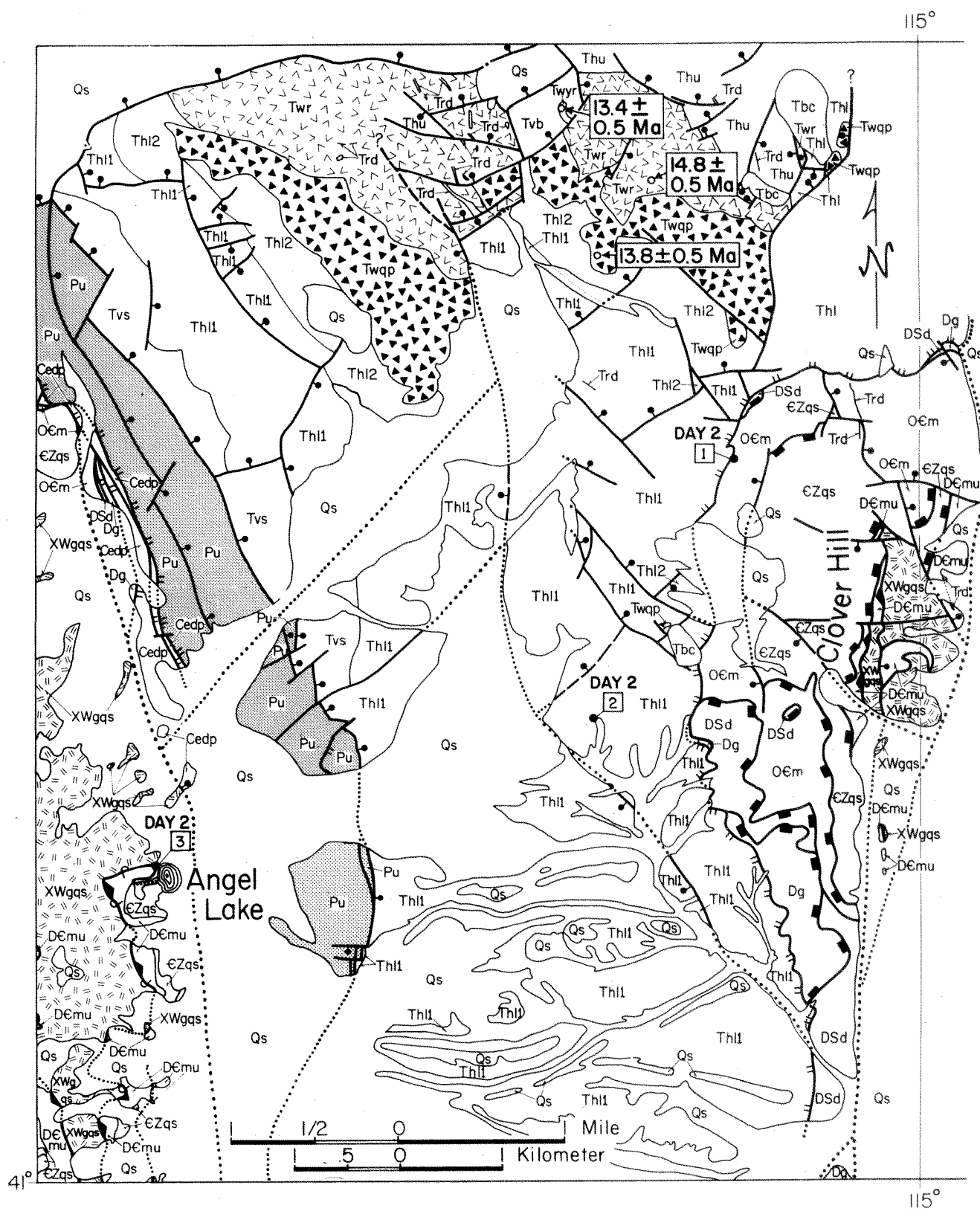






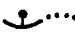

Figure 7. Geologic map of the northeastern East Humboldt Range, Nevada, showing the locations of STOPS 1–3 for DAY TWO.

GEOLOGIC MAP OF THE NORTHEASTERN EAST HUMBOLDT RANGE, NEVADA

Lithologic units

- Qs Surficial deposits (Quaternary)
- Tbc Boulder conglomerate (Pliocene or late Miocene)
- Thu Upper Humboldt Formation (Miocene)
- Twyr Rhyolite (~13.4 Ma)
- Tvb Volcaniclastic breccia (Miocene)
- Twqp Rhyolite quartz porphyry (~13.8 Ma), ^{Trd}// = dikes
- Twr2 Rhyolite (~14.8 Ma)
- Thl Lower Humboldt Fm.--Thl2 & Thl1 (late Eocene ?
& Oligocene)
- Tvs Volcaniclastic conglomerate, sandstone,
andesite - rhyolite (late Eocene)
- Pu Permian undivided (Murdock Mtn. & Pequop formations)
- Cedp Ely Limestone & Diamond Peak Formation
(Carboniferous)
- Dg Guilmette Formation (Devonian)
- DSd Metadolomite (Devonian
& Silurian)
- OEm Impure calcite marble &
calc-silicate rock (Ordo-
vician & Cambrian)
- DCmu Metasedimentary
rocks undivided
(Devonian to
Cambrian)
- EZqs Impure quartzite & schist (Cambrian & Proterozoic Z)
- XWgs Orthogneiss & paragneiss (Archean) & quartzite,
schist, & amphibolite (Proterozoic ?)

Symbols

- | | |
|--|---|
| <p> Contact</p> <p> Pre-folding low-angle fault; over-turned on right</p> <p> Low-angle fault, plastic-to-brittle</p> | <p> Low-angle fault, brittle</p> <p> Normal fault, high-angle; dotted where covered</p> <p> ^{DAY 2}
1 Field trip stop</p> |
|--|---|

STOP 2-2—Megabreccia deposits and surrounding Tertiary strata. *Please watch out for rattlesnakes, especially around the megabreccia outcrop.* The following description is modified from STOP 8 of Mueller and Snoke (1993b).

The roadcut immediately across from the parking place and those to the west provide a useful starting place to examine the megabreccia deposits and encasing beds that are all within the lower Humboldt Formation, (Thl) (Fig. 6). After briefly examining the roadcut exposing lacustrine limestone and conglomerate, walk west up the road (stratigraphically downward) toward the dark gray roadcuts of megabreccia derived from Upper Devonian Guilmette Formation. This megabreccia is one of a group of lens-like masses within the Tertiary lower Humboldt Formation and it both overlies and underlies lacustrine limestone and conglomerate. Therefore, this megabreccia lens, as well as the others, are encased in Tertiary deposits. After examining these roadcut exposures, walk north along the megabreccia lens examining the brecciated internal structure of the deposit. Despite pervasive brecciation, the megabreccia deposits locally display vestiges of relict bedding. If time is available, walk northeastward to another megabreccia lens composed of metadolomite and quartzite derived from Devonian and/or Silurian protoliths. Similar metadolomite and quartzite are exposed in place on Clover Hill to the east.

Return to vehicles and continue westward up the Angel Lake Highway.

- | | | |
|-----|------|--|
| 0.9 | 9.0 | Continue straight on the Angel Lake Highway, past road to Angel Creek campground (on left). |
| 1.3 | 10.3 | Exposure of Pleistocene glacial deposits on right. |
| 0.1 | 10.4 | On right, the beginning of numerous exposures of Permian sedimentary rocks (chiefly Pequop Formation and Park City Group). These unmetamorphosed upper Paleozoic rocks form a high-angle, fault-bounded belt between the high-grade metamorphic rocks of the high country and Tertiary rocks of the foothills. |

- | | | |
|-----|------|---|
| 0.4 | 10.8 | View of Chimney Rock straight ahead. |
| 0.6 | 11.4 | View (to the south-southwest) of rugged exposures of hornblende-biotite quartz dioritic orthogneiss, dated at ~40 Ma by the U-Pb zircon technique (Wright and Snoke, 1993, sample RM-19). |
| 0.1 | 11.5 | Trailhead to Winchell Lake on left. |
| 1.1 | 12.6 | Sharp curve with excellent view of the southwestern flank of Clover Hill and adjacent expanse of Tertiary rocks. |

STOP 2-3—Angel Lake.

This stop affords an opportunity to observe the style of metamorphism and intrusive relationships as well as deformational character of the high-grade, migmatitic infrastructure of the East Humboldt metamorphic core complex. Angel Lake cirque exposes both limbs of the Winchell Lake fold-nappe; although the fold structure is not well displayed in this area because the axial trace of this large-scale fold trends through the middle of a massive Archean orthogneiss sequence. However, the Greys Peak fold, a map-scale parasitic fold on the upper limb of the Winchell Lake fold-nappe, is visible on the east cliff face directly beneath Greys Peak (Fig. 8). Rocks in the upper part of the cirque are overprinted by mylonitic fabrics related to Tertiary extensional deformation. These mylonites gradually give way to coarse-grained gneisses with increasing structural depth. Our traverse will cross the lower limb of the Winchell Lake fold-nappe to the base of the Archean orthogneiss sequence, and will be located entirely within the infrastructure beneath the mylonitic shear zone. This will entail a steep climb with an elevation gain >600 ft over a distance of less than 0.5 mi (0.8 km).

In order from bottom to top, the characteristic rock sequence on the lower limb of the fold-nappe is: (1) a quartzite and schist sequence of probable Early Cambrian to Neoproterozoic age, (2) a thin sequence of calcite marble and calc-silicate paragneiss that is probably Cambrian and Ordovician in age, (3) a discontinuous, thin orthoquartzite layer (<2 m thick) here correlated with the Ordovician Eureka Quartzite, (4) dolo-

mitic marble presumed to correlate with Ordovician to Devonian dolomite, (5) calcite marbles which locally include isolated enclaves of intensely migmatized, rusty-weathering graphitic schist (upper Paleozoic?), (6) severely migmatized quartzitic and quartzo-feldspathic paragneiss inferred to be Paleoproterozoic, and (7) a thick sequence of Archean monzogranite orthogneiss (Lush et al., 1988). The contact between the Neoproterozoic-Paleozoic miogeoclinal sequence (1-5) and Paleoproterozoic(?) paragneiss (unit 6) is inferred to be a pre-folding, premetamorphic fault. The nature of the contact between units (6) and (7) is probably an inverted unconformity.

Small-scale folds occur throughout the transect. Fold hinge lines and stretching lineations show an average orientation of approximately 295°, 5°; and the axial surfaces of small-scale folds are subparallel to foliation, with an average strike and dip of 270°, 15°. Three-dimensional constraints from mapping indicate that the Greys Peak fold and Winchell Lake fold-nappe show the same west-northwest trend as the smaller scale structures. However, there is considerable dispersion in fabric orientations at deep structural levels, and an approximately north-trending lineation of uncertain age occurs locally.

An outcrop of schist near the base of the cirque on the south side yielded an internally consistent P-T estimate of 4.5 kb, 657°C, but this probably reflects relatively late-stage equilibration because localities in the upper part of the cirque yield P-T estimates as high as 8.7 kb, 790°C that probably record an earlier stage in the metamorphic history (see section by McGrew and Peters, this field guide). The most characteristic pelitic mineral assemblage at all structural levels in the northern East Humboldt Range is biotite + sillimanite + garnet + quartz + plagioclase ± K-feldspar ± chlorite ± muscovite ± rutile ± ilmenite. However, scarce relict subassemblages of kyanite + staurolite survive on the upper limb of the Winchell Lake fold-nappe. Late-stage muscovite and chlorite become in-

creasingly prominent in the well-developed mylonitic rocks at higher structural levels. Thermochronologic constraints imply that these assemblages equilibrated between Late Cretaceous and Oligocene time (McGrew and Snee, 1994). ⁴⁰Ar/³⁹Ar muscovite and biotite cooling ages indicate that the range was mostly exhumed by approximately 21.5 Ma.

Stable isotope studies in the northern East Humboldt Range (e.g., Peters and Wickham, 1995) concentrated on Angel Lake cirque and Lizzies Basin to the south. Detailed outcrop and cirque-scale mapping and sampling constrain the isotopic evolution of this core complex over a wide range of structural levels. The degree of ¹⁸O depletion and ¹⁸O/¹⁶O homogenization in the metamorphic rocks correlate strongly with the proportion of intrusive rocks. The stable-isotope systematics at deep structural levels are probably the ultimate product of fluid-rock interaction associated with extension-related magmatism, dominated by leucogranites and monzogranites (Peters and Wickham, 1995).

Locality A. Follow the well-developed path around the south side of the lake to the low bedrock hill labeled "A" on the geologic map (Fig. 8). This locality provides an opportunity to inspect the inferred Cambrian-Neoproterozoic quartzite and schist sequence exposed at the deepest structural levels on the lower limb of the fold-nappe.

The East Humboldt Range is permeated with intrusive rocks of various ages and compositions. In particular, note the abundance of leucogranite at this deep structural level. Here and throughout the traverse, how many distinct generations of leucogranitic rocks can you distinguish? We believe we can distinguish at least four generations of leucogranitic intrusion based on cross-cutting relationships. In addition to the leucogranites, a sheet of biotite monzogranitic orthogneiss occurs near this locality. These small monzogranitic bodies are abundant throughout the Ruby Mountains and East Humboldt Range and have yielded U-Pb zircon

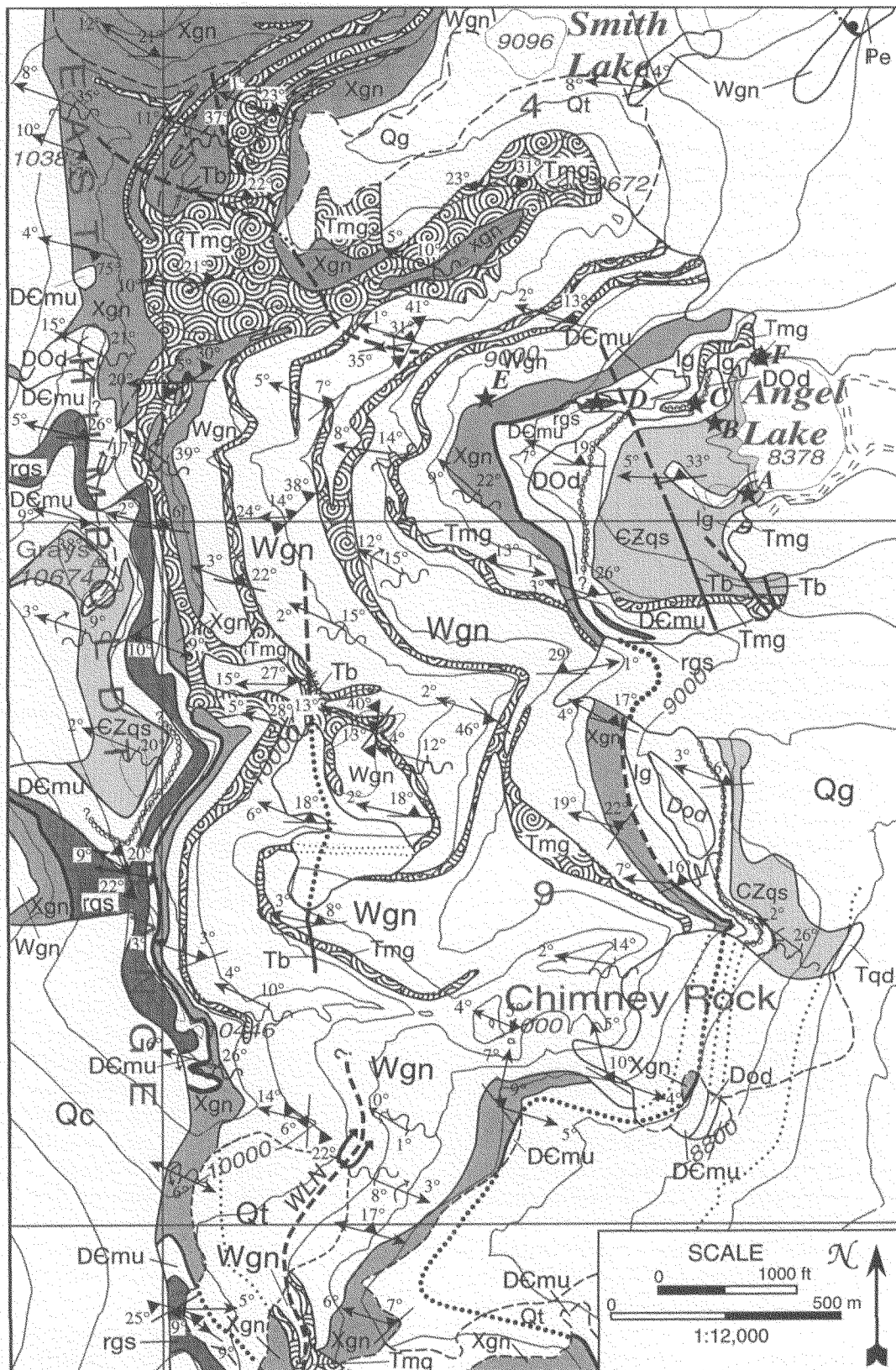
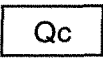
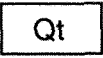
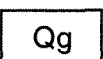
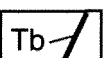

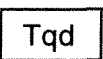
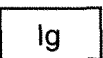


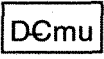

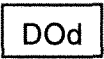
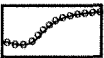
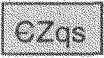

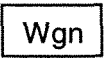
Figure 8. Geologic map of Angel Lake cirque and surrounding areas, with field trip transect (STOP 2-3) labeled (Sites A-F).

Legend

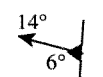
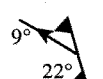
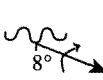


Cenozoic and Mesozoic units

	Colluvium (Quaternary)
	Talus (Quaternary)
	Glacial deposits (Quaternary)
	Basalt dikes (14-17 Ma)
	Biotite monzogranite (~29-Ma)
	Hornblende biotite quartz diorite (~43-Ma)
	Leucogranite (Cretaceous and Tertiary)

Paleozoic and Precambrian units

	Marble, undifferentiated (Devonian to Cambrian)
	Rusty-weathering graphitic schist (Mississippian?)
	Dolomitic marble, undifferentiated (Devonian to Ordovician)
	Eureka quartzite (Ordovician)
	quartzite and schist, undifferentiated (Cambrian and Neoproterozoic)
	Paragneiss sequence of Angel Lake (Paleoproterozoic)
	Orthogneiss sequence of Angel Lake (~2.5 Ga, Archean)

Map Symbols

	Strike and dip of grains-shape and/or compositional foliation with trend and plunge of grain-shape lineation.
	Strike and dip of C'-planes with trend and plunge of slickenlineation.
	strike and dip of axial surface of small-scale fold with trend and plunge of hinge line and vergence indicated where known.
	Surface trace of hinge surface of map-scale recumbent fold (Winchell Lake fold-nappe and Grey's Peak fold)
	Outcrop trace of premetamorphic tectonic contact, dotted where covered, broken where inferred.

ages of ~29 Ma in a variety of locations, including one at the northwest corner of Angel Lake (see Locality F) (Wright and Snoke, 1993, sample RM-5). Consequently, these monzogranitic sheets offer a useful gauge for deciphering the structural chronology of the range. The biotite monzogranitic rocks both cut and are cut by various generations of leucogranites, and some leucogranitic rocks appear to intermingle with the monzogranites. At higher structural levels the monzogranites are clearly overprinted by mylonitic fabrics, providing a crucial constraint on the age of mylonitic deformation. The final phase in the intrusive history of the East Humboldt Range is represented by a series of steeply dipping, amygdaloidal basalt dikes which form three, deeply eroded fissures slicing steeply through the south wall of the cirque. The end of one of these amygdaloidal basalt dikes can be observed near this locality. Similar dikes yield ages of 14 to 17 Ma elsewhere in the Ruby Mountains and East Humboldt Range, providing a younger limit on the age of plastic deformation (Snoke, 1980; Hudec, 1990).

Locality A exposes one of three outcrops near the lake which were the subject of detailed mapping, sampling, and stable isotope analyses (Peters and Wickham, 1995). We will contrast this locality with one of the other two outcrops exposed at Locality B. At Locality A the sample transect crossed a monzogranite–orthogneiss–leucogranite–metaquartzite sequence. Figure 9 presents a schematic summary of the isotopic results for these outcrops. The rocks at Locality A were characterized by significant $^{18}\text{O}/^{16}\text{O}$ homogenization on the scale of meters and substantial ^{18}O depletion of metaquartzite relative to likely protolith values (Peters and Wickham, 1995; and discussion by McGrew and Peters, this field guide).

Locality B. Continue over and around the small hill on the southwest side of the lake and cross the stream to point “B” on the map. The rocks near the base of the slope form a particularly diverse and structurally complex paragneiss se-

quence. Can you find any amphibolite boudins near here? Normally, amphibolite bodies are restricted to the inferred Paleoproterozoic and Archean gneiss sequences, providing a useful guide for correlation. In most cases, they probably represent metamorphosed mafic intrusions that were emplaced during Paleoproterozoic rifting along the southern margin of the Archean Wyoming province. However, here one or two amphibolite bodies occur in the inferred Cambrian and Neoproterozoic quartzite and schist sequence, raising the problem of how these rocks should be correlated. The key to correlation is provided by anomalously high $\delta^{13}\text{C}$ values in the marble units. As discussed in Peters et al. (1992) and Wickham and Peters (1993), the high $\delta^{13}\text{C}$ values probably represent protolith values and allow the assignment of a Neoproterozoic age to these rocks. Thus, carbon isotope analyses in this region provide a strong tool for stratigraphic correlation.

This locality also exposes the second of the three outcrops near the lake that were the subject of detailed mapping, sampling, and stable isotopic analyses. This particular outcrop involves a marble–calc-silicate gneiss–paragneiss–orthogneiss sequence discussed in detail by Peters and Wickham (1995). Figure 9 presents a schematic summary of the isotopic profile for this outcrop, revealing a higher degree of heterogeneity of $^{18}\text{O}/^{16}\text{O}$ on the scale of meters and a smaller degree of isotope depletion as compared with the outcrop visited at Locality A (see discussion in McGrew and Peters, this field guide). We attribute these differences to the lower abundance of intrusive rocks and the higher proportion of marble in this sequence. The marble acted as a flow barrier and a relatively high ^{18}O reservoir.

Locality C. Contour along the base of the slope for a short distance, and then proceed northward up the hill to point “C.” As you walk, notice the interesting small-scale fold and fault relationships in the quartzite and schist sequence, including a rare minor thrust fault. Most

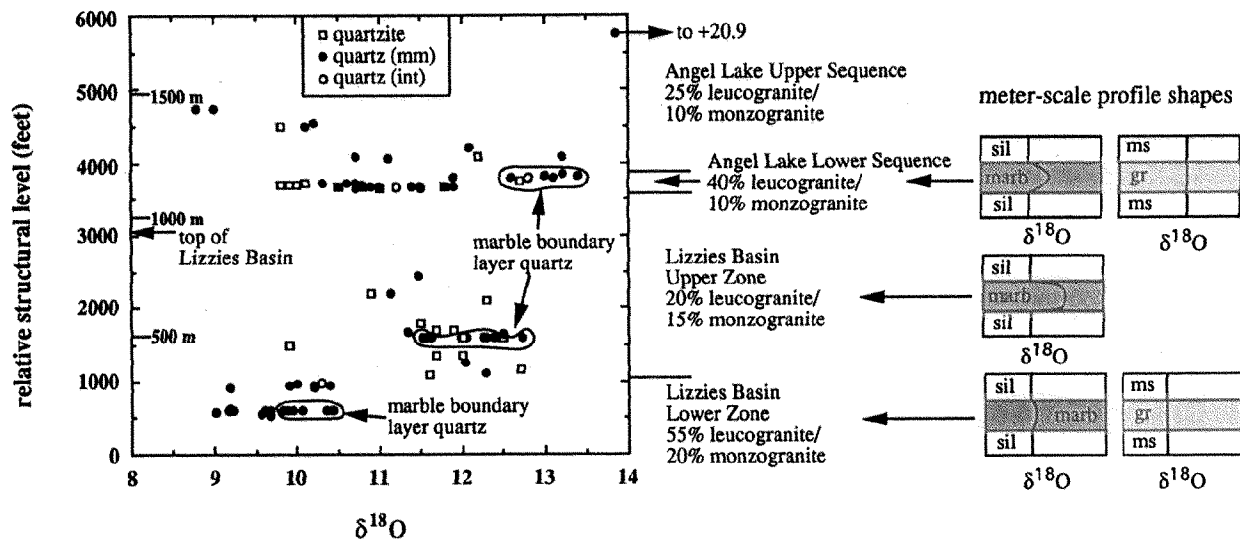


Figure 9. Summary diagram of oxygen isotope data from the northern East Humboldt Range plotted according to relative structural level (data from Wickham and Peters, 1990, 1992; Wickham et al., 1991; and Peters and Wickham, 1995). $\delta^{18}\text{O}$ values are quartz separates in metamorphic (filled circles) and intrusive (open circles) rocks, and quartzite (open squares) whole-rock samples (which closely approximate the quartz $\delta^{18}\text{O}$ values). Also shown is the proportion of leucogranite and biotite monzogranite in four different zones in Angel Lake cirque (which is visited on the field trip, STOP 2-3) and Lizzies Basin, the structurally deepest part of the East Humboldt Range, located approximately 9 km to the south of Angel Lake. Angel Lake cirque is divided into a lower sequence where detailed traverses were completed, and an upper sequence (>8400 feet elevation) where large-scale sampling was done. $\delta^{18}\text{O}$ values for quartz samples collected less than 1 m away from marble layers are indicated by the fields labeled "marble boundary layer quartz." Also shown are the typical shapes of marble-silicate and silicate-silicate profiles at various structural levels (sil-silicate, marb-marble, ms-metasedimentary rock, and gr-granitoid).

shear surfaces exposed in the East Humboldt Range in contrast show normal-sense displacement related to Tertiary extensional tectonism. Where present, approximately 70% of the kinematic indicators observed at deep structural levels are directed top toward the east-southeast, antithetic to the bulk shear sense in the overlying mylonitic zone (McGrew, 1992). This suggests a deep-crustal setting in which extensional deformation was diffusely partitioned into weakly developed, anastomosing antithetic shear systems.

After climbing across the lower marble sequence, pause at an approximately 1-m thick layer of white quartzite that probably correlates with the Ordovician Eureka Quartzite. In nearby mountain ranges, the Upper Cambrian to Middle Ordovician limestone sequence is at least 1 km thick. Assuming that this correla-

tion is correct, here it is possible to walk through the entire section in a vertical distance of just 25 m! Overlying the orthoquartzite is a few meters of dolomitic marble probably equivalent to Upper Ordovician to Devonian dolomites exposed in nearby ranges. Marble and calc-silicate assemblages typically consist of calcite + diopside + quartz \pm dolomite \pm phlogopite \pm plagioclase \pm grossular \pm scapolite \pm K-feldspar \pm sphene \pm amphibole \pm epidote. Peters and Wickham (1994) report that amphibole + grossular + epidote form a secondary subassemblage that records infiltration of water-rich fluids under a metamorphic regime that proceeded from high temperature (600°C – 750°C) to lower temperature ($<525^{\circ}\text{C}$) conditions. This event was probably related to Tertiary extension and associated magmatism. The earlier, primary assemblages proba-

bly equilibrated at ≥ 6 kb, 550°C – 750°C and likely record conditions during Late Cretaceous or mid-Tertiary time.

Locality D. Proceed westward, gaining elevation gradually to point D. At this point, we can see a thin raft of distinctive, rusty-weathering graphitic paragneiss seemingly suspended in a mass of pegmatitic leucogranite. On the upper limb of the fold-nappe, this same rock type forms a continuous layer approximately 25 m thick that in general is only slightly migmatitic. Remarkably, the transition between these two contrasting outcrop styles occurs over a distance of <2 km as this unit is traced from the upper limb of the fold-nappe (where it typically contains $<25\%$ leucogranite) into the hinge zone of the fold-nappe above Winchell Lake (where it contains $>60\%$ leucogranite). These meter-scale leucogranitic bodies are clearly folded around the nose of the fold-nappe, but the fact that isopleths of leucogranite concentration cut the fold-nappe implies that nappe emplacement and leucogranite segregation must have occurred at the same time (McGrew, 1992). The variations in leucogranite abundance are also borne out in cirque-scale estimates summarized in Peters and Wickham (1995). In addition, relict kyanite also disappears over this same interval, being completely replaced by sillimanite on the lower limb of the fold-nappe. Consequently, a preliminary 70–90 Ma U-Pb zircon age (J. E. Wright, unpublished data) on these leucogranitic rocks probably dates both fold-nappe emplacement and a major phase of migmatization and sillimanite zone metamorphism.

Locality E. Climb upward and then proceed westward toward point E. This part of the transect will take us across additional marbles overlying the graphitic schist unit and into and through the overlying Paleoproterozoic(?) paragneiss sequence. Pause momentarily at the contact between the marble and the overlying paragneiss. By inference, this contact is a premetamorphic, prefolding thrust(?) fault of unconstrained, but probably large displacement. You may

wish to inspect the shapes of deformed feldspars in the paragneiss immediately above the contact. Could the rocks near this contact be annealed mylonites? Looking toward the south, notice the thin, white ribs of aplitic leucogranite cutting at high angle through the gneisses. Though clearly quite late, these rocks contain a weak grain-shape foliation suggesting that they intruded during the last gasps of plastic deformation.

Continue across the Paleoproterozoic(?) paragneiss sequence to the exposures of Archean orthogneiss at Locality E. These rocks have a biotite monzogranitic composition and are generally gray in color with a distinctive banded appearance due to segregation of biotite. In addition, they commonly contain large augen of alkali feldspar. U-Pb zircon dating of a sample collected on the north side of the cirque yielded a minimum age of 2520 ± 110 Ma (Lush et al., 1988, sample RM-9).

Locality F. Retrace your steps to the ledge above Locality B, and then contour around to the point labeled “F” at the northwest corner of Angel Lake. As you walk, try to decipher the relative age relationships between leucogranitic intrusions. Some leucogranites are fully involved in folding, whereas others cut folds. Outcrops at Locality F consist predominantly of biotite monzogranitic and leucogranitic orthogneiss. The biotite monzogranite at this locality has yielded an U-Pb zircon age of 29 ± 0.5 Ma (Wright and Snoke, 1993, sample RM-5). Is this sheet of monzogranite folded? Walk around the corner of the outcrop before you decide. Some monzogranitic sheets are clearly involved in folding, but others cut folds, and at map scale a number of monzogranitic bodies cut the Winchell Lake fold-nappe itself, lending credence to the interpretation that the Winchell Lake fold-nappe is Late Cretaceous in age. However, the monzogranitic orthogneisses bear the same west-northwest-trending stretching lineations as the country rock, and at higher structural levels they are overprinted by mylonitic microstructures, thus docu-

menting a Tertiary age for extensional deformation. It seems highly likely that older structures were profoundly transposed during Tertiary deformation, including the Winchell Lake fold-nappe itself.

Return to vehicles and retrace the route to the intersection of the Angel Lake Highway and Humboldt Avenue in Wells (i.e., ~11.7 miles). Turn left onto Humboldt Avenue and drive north toward Wells.

- | | | |
|-----|------|---|
| 0.9 | 26.0 | Turn right onto Sixth Street. |
| 0.8 | 26.8 | Super 8 Motel on right. |
| 0.3 | 27.1 | Intersection with U. S. Highway 93 (Great Basin Highway), turn right (south) onto U. S. 93. |

- | | | |
|-----|------|--|
| 0.5 | 27.6 | Wood Hills on the left and Clover Hill at about 2 o'clock on the right. See comments about the Wood Hills in the road-log for DAY ONE. |
|-----|------|--|

Clover Hill exposes a structurally complex, metamorphosed stratigraphy of Paleozoic and Proterozoic strata intruded by various granitic rocks (Snoke, 1992). A low-angle fault system separates the metamorphic and igneous rocks from weakly to unmetamorphosed middle and upper Paleozoic rocks. The mine on the east face of Clover Hill is chiefly a tungsten prospect (Lipten, 1984).

- | | | |
|-----|------|--|
| 2.0 | 29.6 | Signal Hill, a small conical hill composed of Upper Devonian Guilmette Formation, on the right at about 2 o'clock. |
|-----|------|--|

- | | | |
|-----|------|---|
| 0.4 | 30.0 | The range at 11 o'clock is Spruce Mountain, studied by Hope (1972). In this range, the low-angle Spruce Spring fault separates a footwall of metamorphosed Ordovician through Upper Devonian strata (chiefly low-grade metacarbonate rocks) from a much faulted hanging wall consisting of Mississippian through Permian sedimentary rocks. The metamorphosed stratigraphy of the footwall at Spruce Mountain includes stratigraphic units equivalent to the higher grade metasedimentary rocks exposed in the southeastern East Humboldt Range (e.g., STOP 2-4). |
|-----|------|---|

- | | | |
|-----|------|--|
| 0.9 | 30.9 | Road to Clover Valley on right. |
| 2.1 | 33.0 | Railroad crossing. |
| 1.7 | 34.7 | Road to Tobar on left. From this locality, an excellent view of the east face of the East Humboldt Range is afforded in morning light. The Winchell Lake fold- |

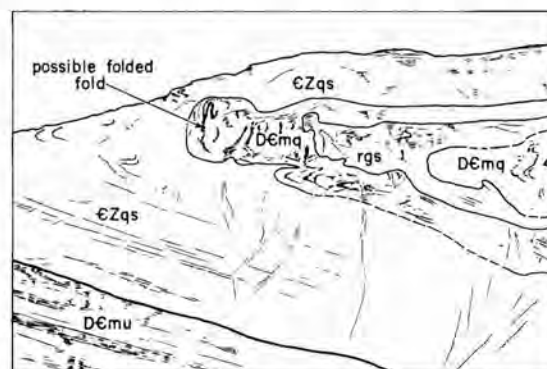


Figure 10. Hinge zone of the Winchell Lake fold-nappe as exposed along the back wall of Winchell Lake cirque on the eastern face of the northern East Humboldt Range. The core of the fold at this locality consists of dark outcrops of rusty-weathering, graphitic paragneiss surrounded by white-weathering Cambrian and Ordovician marble and Ordovician metaquartzite. Enveloping the fold is a thick sequence of Neoproterozoic and Lower Cambrian flaggy quartzite and schist. These metasedimentary rocks, particularly the metaclastic units, all contain abundant sheet-like bodies of leucogranite orthogneiss. The hinge line of this major structure trends west-northwest, approximately parallel to mineral elongation lineations in the deformed rocks. Closure is to the south. To the north, the fold is cored by Archean and Paleoproterozoic gneisses, and a pre-folding low-angle fault is inferred to separate the metasedimentary rocks shown in this photograph from the basement complex enclosed in the core of the fold. CZqs = Cambrian and Neoproterozoic quartzite and schist, rgs = rusty-weathering graphitic schist, DCmq = Cambrian to Devonian metacarbonate rocks and quartzite. DCmu = Cambrian to Devonian metacarbonate rocks.

Photograph by A. W. Snoke, sketch by Phyllis A. Ranz.

nappe is visible at about 280°. See Figure 10 and the accompanying caption for more explanation.

- | | | |
|-----|------|---|
| 2.7 | 37.4 | The northern end of the Cherry Creek Range on the horizon to the left of the road. Pequop Mountains to the east (left). |
|-----|------|---|

Generalized longitudinal cross-section of the East Humboldt Range, Nevada

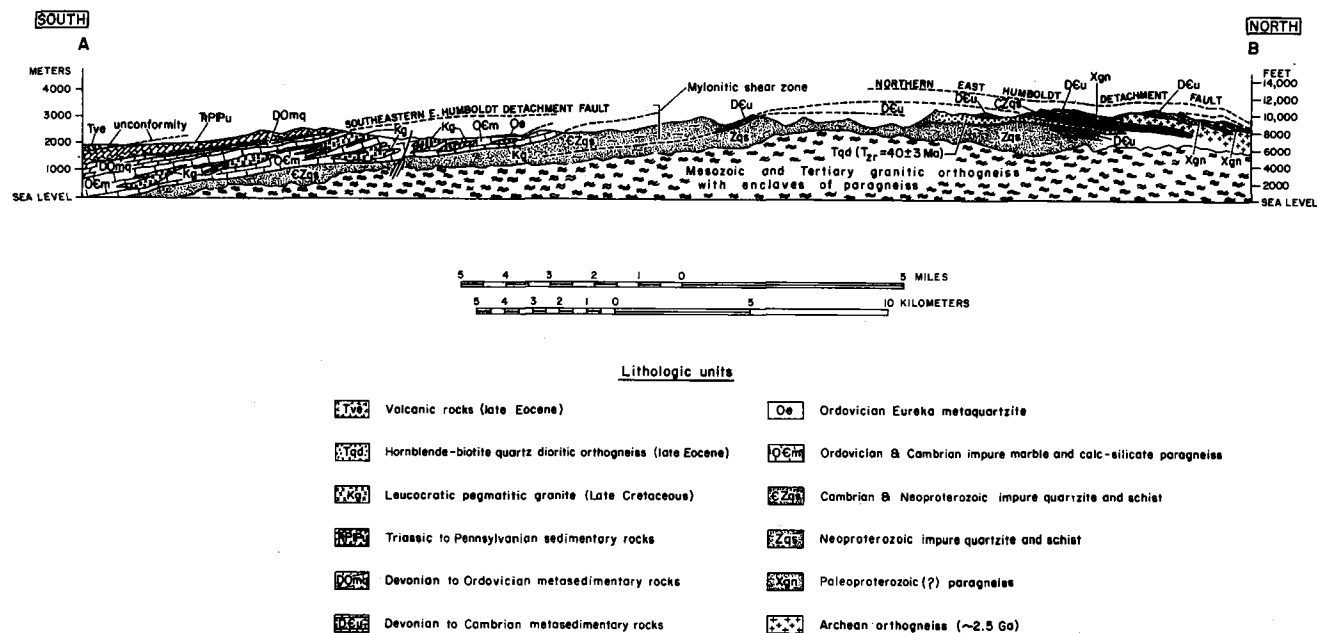


Figure 11. Generalized north-south cross-section of the East Humboldt Range, Nevada. Derived from geologic studies by A. J. McGrew (in the north) and A. W. Snoke (in the south).

- | | | |
|------|-------|---|
| 7.6 | 45.0 | Road to Clover Valley on right. |
| 4.0 | 49.0 | Note the overall southward dipping foliation in the southern East Humboldt Range. This prominent foliation is principally defined by the Tertiary mylonitic shear zone which forms a structural carapace above a migmatitic infrastructure (Fig. 11). Road to ranch on right. |
| 0.3 | 49.3 | Road to ranch on right. |
| 0.9 | 50.2 | Entrance to the Warm Creek Ranch on left. |
| 0.4 | 50.6 | Spruce Mountain ridge at 10 o'clock. |
| 3.1 | 53.7 | Turn right onto Nevada Highway 229 toward Ruby Valley. |
| 1.6 | 55.3 | At 1 o'clock on the skyline is pyramidal Snow Lake Peak in the northern Ruby Mountains. |
| 0.5 | 55.8 | Turn right onto dirt road semicircle and take the far right turn out of the semicircle to proceed northeast to STOP 2-4. |
| 0.75 | 56.55 | Turn left onto the road that passes under the electric lines. |
| 0.35 | 56.9 | Park at outcrop of gray metalimestone adjacent to hills. |

STOP 2-4. Fossiliferous, metamorphosed Guilmette Formation (Fig. 12). The fol-

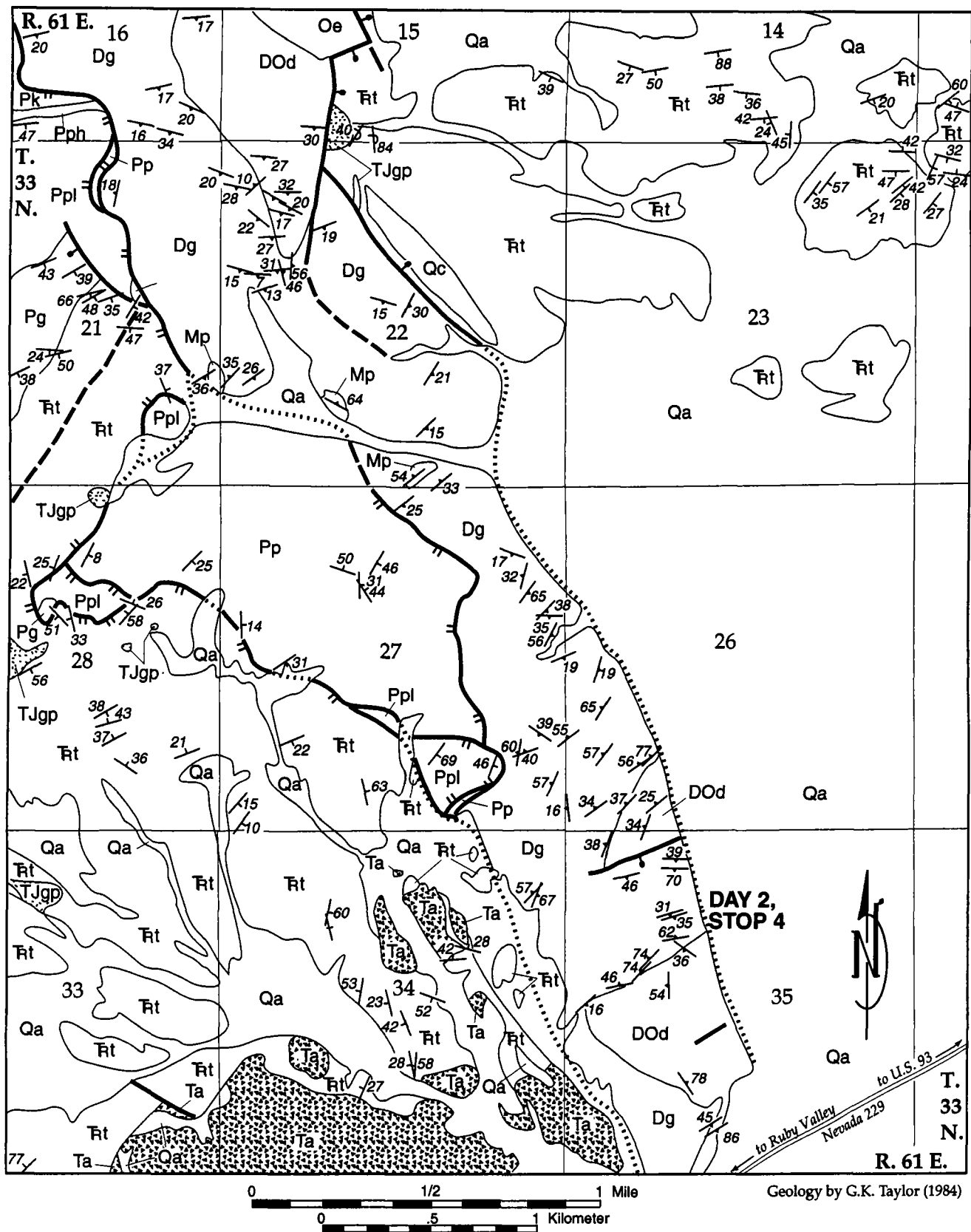
lowing description is modified from STOP 19 of Snoke and Howard (1984).

Metamorphosed Guilmette Formation here is part of a non-migmatitic meta-sedimentary sequence that ranges from Ordovician (Pogonip Group) to Mississippian (upper part of Pilot Shale) and is structurally **above** the main mylonitic shear zone but in turn is structurally overlain by allochthonous upper Paleozoic, lower Mesozoic, and Tertiary rocks (Fig. 12). The rock is a dark to light-gray to white, calcite \pm dolomite marble; color variation is apparently chiefly related to the amount of graphite in the marble. Abundant evidence of ductile flowage is evident in many exposures of the marble including a penetrative foliation, small-scale isoclinal folds, and deformed fossils such as brachiopods, gastropods, and stromatoporoids. As you walk up the hill to the south, you will note that the foliation becomes very steep and eventually you cross a contact with topographically overlying metadolomite. You have actually walked down section into Devonian metadolomite (Simonson Dolo-

		mite, part of DOD on map), and we are, therefore, on the steep limb of an asymmetric fold. Finally, float fragments of hypabyssal intermediate igneous rocks are fairly common and are perhaps intrusive equivalents to a widespread upper Eocene "basaltic andesite unit." We will drive pass poor exposures of this volcanic unit along Nevada 229 as we head west toward Ruby Valley (see note on this locality at cumulative mileage of 59.4).	0.6	83.8	More exposures of Miocene Humboldt Formation on left.
		Turn around retrace route back to Nevada 229.	0.7	84.5	Cross the trace of the approximately north-south-striking Poison Canyon normal fault.
1.1	58.0	Intersection with Nevada 229, turn right onto blacktop road proceed westward toward Ruby Valley.	0.1	84.6	Large roadcut of chiefly mylonitic migmatitic impure quartzite and pelitic schist.
1.4	59.4	Poor exposures of upper Eocene basaltic andesite, flow-brecciated lava (see Brooks et al., 1995).	1.2	85.8	This locality is the beginning of STOP 3-1. See log of DAY THREE for details.
2.6	62.0	Road to North Ruby Valley on right. Stay straight.	0.5	86.3	Roadcut on the right exposes a low-angle normal fault (part of an extensional duplex—see STOP 3-1) that separates dipping Miocene Humboldt Formation from a footwall slice of "broken formation" derived from the Chainman-Diamond Peak formations.
0.7	62.7	At 10 o'clock, the low area in the Ruby Mountains is Harrison Pass underlain by granitic rocks of the Harrison Pass pluton. We will visit this area on the morning of DAY FOUR.			Roadcut exposure of westward-dipping normal fault that has Chainman and Diamond Peak formations in the footwall, and Miocene Humboldt Formation in the hanging wall.
7.5	70.2	Turn right onto Ruby Valley road and proceed northward. Elko is approximately 57 miles from our present location.	0.9	87.7	Secret Peak (9,167 ft [2,796 m]) on the left. Roadcuts expose reddish to lavender fluvial deposits of the Miocene Humboldt Formation. Note that these sedimentary rocks are tilted toward the range.
2.0	72.2	Humboldt Peak (11,020 ft [3,361 m]) is on the skyline to the north. Humboldt Peak consists chiefly of mylonitic impure quartzite and pelitic schist correlative with the Neoproterozoic McCoy Group (of Misch and Hazzard [1962]) and perhaps the Cambrian Prospect Mountain Quartzite. Intercalated with these upper amphibolite-facies metasedimentary rocks are variably deformed granitic rocks including both probable Mesozoic as well as Tertiary intrusive rocks.	0.3	88.0	Holocene fault exposed in creek bank (Secret Creek) on the left. This fault which cuts Quaternary alluvium was originally recognized and described by Sharp (1939b, figure 7) in his classic paper on Basin-Range structure of the Ruby Mountains-East Humboldt Range.
8.5	80.7	North Ruby Valley road on right.	0.2	88.2	Quaternary stream gravels on right.
0.7	81.4	Secret Pass (6,457 ft [1,969 m]).	0.7	88.9	More Quaternary stream gravels on right.
0.4	81.8	Secret Valley on the right. Secret Valley is a structurally controlled feature, bounded on the west by an east-dipping normal fault (Poison Canyon fault, also see below at cumulative mileage point 84.5). Mylonitic impure quartzite and pelitic schist with intercalated granitic rocks form the foothills of the southwestern flank of the East Humboldt Range.	2.1	91.0	Road to the village of Lamoille on left.
		This ends the road log for DAY TWO. For a continuation of the log to Elko, we refer you to the road log for DAY THREE (specifically starting at mileage point 29.2 and following the route in reverse order to Elko). At the turn-off to Lamoille, we thus are 29.2 miles from Elko. We will spend the next two nights in Elko.			
		DAY THREE			
		Summary of route: Elko to Secret Creek gorge (northernmost Ruby Mountains) to Lamoille Canyon to Elko (Fig. 5).			
		<u>Incre.</u> <u>Cum.</u> <u>Miles</u> <u>Miles</u>			
1.4	83.2	Exposure of Miocene Humboldt Formation on the left.	0.0	0.0	Start at Red Lion Inn & Casino, Elko, Nevada.

0.1	0.1	Turn left onto northwest trending road that leads to I-80 entrances.				dated the thrust emplacement of the western assemblage rocks.
0.1	0.2	Turn right into the entrance to I-80 E (i.e., toward Wells and Salt Lake City).	5.2	9.8		An excellent view of the East Humboldt Range straight ahead.
2.0	2.2	View of the Elko Hills on the right. This small range consists of thrust upper Paleozoic sedimentary rocks overlain and intruded by late Eocene(?) silicic igneous rocks. The range was mapped and studied by K.B. Jaeger (1987) for his M.S. thesis research project at the University of Wyoming, and K.B. Ketner (1990) also mapped this range. Although both Jaeger and Ketner agree on many aspects of the geology of the range, they disagree about the amount of intrusive versus extrusive silicic rock exposed in the range. Jaeger (1987) concluded that much of the rhyolitic rocks were part of a shallow intrusive body, whereas Ketner (1990) mapped these rocks as part of a sequence of rhyolite lava flows and pyroclastic tuffs.	0.4	10.2		View to right into northern end of Osino Canyon (cut by the Humboldt River). One of the most controversial contacts regarding the developmental history of the Elko Hills is exposed in a set of railroad cuts along the northwest wall of this canyon. Here Jaeger (1987) interpreted the contact between Tertiary rhyolite and overlying Pennsylvanian–Mississippian Diamond Peak Formation as a deformed contact (locally faulted) along the top of a shallow intrusive body. In contrast Ketner (1990) mapped this contact as a thrust fault related to late Eocene(?) contraction. For further discussion of this controversy see Thorman et al. (1991, STOP 1-3, p. 874–876).
			1.0	11.2		Exit #314 to Ryndon.
1.9	4.1	The East Humboldt Range is on the skyline.	2.3	13.5		Exit #317 to Elburz.
			0.4	13.9		View of the northern Ruby Mountains; the prominent peaks include Secret Peak (9,167 ft [2,796 m]) and Soldier Peak (10,089 ft [3,077 m]).
0.5	4.6	The mountain range on the left is the Adobe Range consisting chiefly of Paleozoic through Triassic sedimentary rocks including allochthonous, western assemblage (eugeoclinal) rocks. The stratigraphy and structure of this area was described by Ketner and Ross (1990). A particularly important structural feature of this range is a large-scale Mesozoic(?) syncline (Ketner and Smith, 1974). According to these authors, the Adobe syncline can be traced to the northern Cortez Mountains where rocks as young as Late Jurassic (Pony Trail Group) are folded. Furthermore, Ketner and Ross (1990) concluded that this folding pre-	2.1	16.0		The topographic low at 2 o'clock is Secret Creek gorge. Note the range-bounding normal fault system prominent along the western flank of the northern Ruby Mountains.
			2.0	18.0		Take exit #321 to Halleck and Ruby Valley.
			1.1	19.1		Cross railroad tracks; Halleck on the right. The Halleck Station was established in 1869 by the Central Pacific Railroad, it once served as a major shipping point for livestock from the local ranches (Patterson, 1977).

Figure 12. Geologic map of part of the southeastern East Humboldt Range, Nevada. **Qa** = Alluvium (Quaternary); **Ta** = basaltic andesite (lavas and breccias) (upper Eocene); **TJgp** = granite porphyry (age uncertain, Tertiary to Jurassic[?]); **TRt** = Thaynes Formation (Lower Triassic); **Pg** = Gerster Limestone (Permian); **Ppl** = Plympton Formation (Permian); **Pph** = phosphorite-bearing strata (Permian); **Pk** = Kaibab Limestone (Permian); **Pp** = Pequop Formation (Permian); **Mp** = Pilot Shale (phyllite and metalimestone) (Mississippian and Devonian[?]); **Dg** = Guilmette Formation (metalimestone and metadolomite) (Devonian); **Dod** = Metadolomite (Devonian to Ordovician); **Oe** = Eureka metaquartzite (Ordovician). Standard symbols for attitudes of bedding and foliation, geologic contacts, and normal faults (except double tick marks on upper plate of brittle, low-angle normal fault [detachment fault]). Faults are dashed where approximate and dotted where concealed. Geology by G. K. Taylor (1984).



- 0.8 19.9 Cross railroad tracks; Secret Peak at 1 o'clock. Note triangular facets related to Holocene normal faulting developed along the west flank of the northern Ruby Mountains.
- 3.0 22.9 Soldier Creek canyon at 2 o'clock with Old Man in the Mountain peak in the background.
- 3.8 26.7 Main entrance to the 71 Ranch on the right.
- 0.4 27.1 Road to Starr Valley on the left. Exposures of Miocene Humboldt Formation form the hills to the left.
- 2.1 29.2 Road to the village of Lamoille on the right. After STOP 3-1, we will take this road to get to Lamoille Canyon (STOP 3-2). For the present, continue straight on Nevada 229.
- 2.2 31.4 Old stream gravels of Secret Creek on left.
- 0.5 31.9 More exposures of stream gravels.
- 0.3 32.2 Beginning of exposures of Miocene Humboldt Formation; south of the road, Secret Creek cuts through an excellent exposure of a Holocene fault (see comment on DAY TWO, mileage point 88.0).
- 0.3 32.5 More exposures of Miocene Humboldt Formation.
- 0.9 33.4 High-angle normal fault contact between the Miocene Humboldt Formation and Mississippian part of the Diamond Peak Formation (here, interlayered sandstone, siltstone, and black mudstone).
- 0.5 33.9 Pull right into large parking space. From here we will walk up the road to **STOP 3-1**. *The following description is modified from STOP 12 of Snoke and Howard (1984). Please watch out for rattlesnakes in this area.*

This stop will consist of a guided traverse through an anastomosing system of distinctive lithologic slices bounded by low-angle normal faults (perhaps best referred to as an extensional duplex structure). The purpose of this traverse is to demonstrate the complex structural style characteristic of the low-angle fault complex, but also to develop the structural chronology between mylonitic deformation, low-angle normal faulting, and high-angle normal faulting. To facilitate the use of this guide, specific localities have been designated (A–H), and the

location of each locality is shown on the accompanying simplified geologic map in Figure 13.

Locality A (roadcut exposure along Nevada 229)—Mylonitic, interlayered migmatitic schist and impure quartzite with subordinate orthogneiss, cut by numerous westward-dipping normal faults. Many of the normal faults are planar, but a few are clearly curvilinear (Fig. 14). Associated with the westward-dipping normal faults are spectacular drag features as well as crushed zones and thin ultramylonitic to cataclastic layers along the fault planes. In addition, flaggy micaceous quartzites with conspicuous mica porphyroclasts ("mica fish") are useful indicators of the sense-of-shear in the mylonite zone. Other mesoscopic criteria useful in the determination of sense-of-shear include asymmetric feldspar porphyroclasts, composite planar surfaces in pelitic schists (S-C-C' fabric), and mesoscopic folds that deform the mylonitic foliation. Well-developed microstructural criteria are also common in these mylonitic rocks (e.g., the mylonitic impure quartzites are classic examples of Type II S-C mylonites of Lister and Snoke, 1984). All these criteria taken together indicate a west-northwest sense-of-shear (top to the west-northwest) throughout the quartzite and schist unit in the northern Ruby Mountains and southwestern East Humboldt Range.

The mylonitic quartzites at this locality as well as other rock types in the Secret Creek gorge area were the subject of a stable isotope study by Fricke et al. (1992) which demonstrated the importance of meteoric water infiltration during mylonitization.

Locality B (roadcut exposure along Nevada 229—west of Locality A)—We have crossed a low-angle normal fault that separates the overlying Horse Creek assemblage from the underlying quartzite and schist unit. The Horse Creek assemblage is diverse and includes impure calcite marble and calc-silicate gneiss and schist (inferred Ordovician and Cambrian protoliths), and mafic to felsic orthogneisses including a distinctive de-

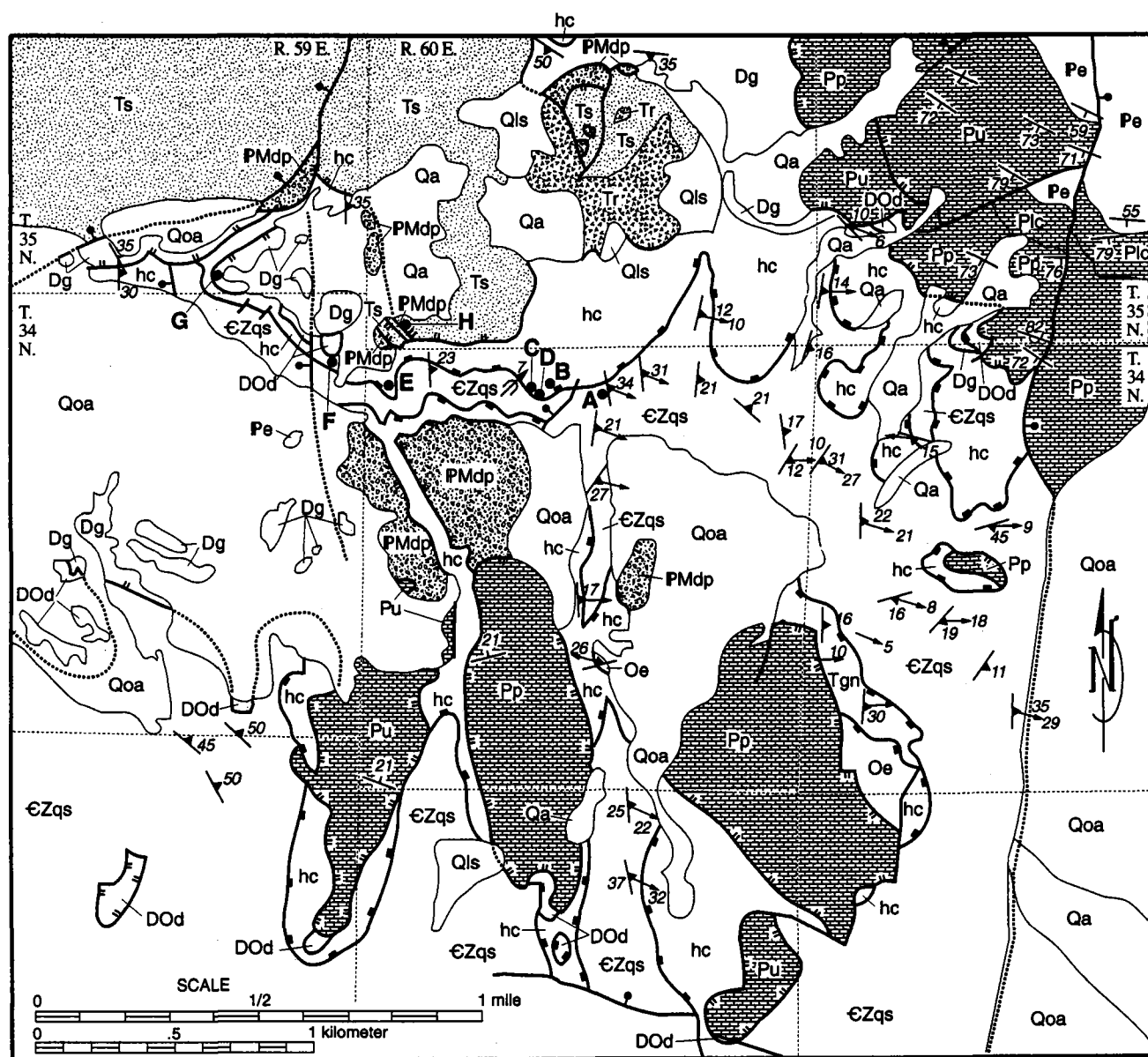


Figure 13. Geologic map of the Secret Creek gorge area, northern Ruby Mountains, Nevada. Modified after Snoke (1980, figure 5). Qa = Alluvium (Quaternary); Qoa = Older alluvium (Quaternary); Qls = Landslide deposits (Quaternary); Ts = Sedimentary rocks (Miocene); Tr = Rhyolite (Miocene); Tgn = Granitic orthogneiss (Tertiary); Pp = Pequop Formation (Permian); Plc = Limestone and conglomerate (Permian); Pu = Permian rocks undivided; Pe = Ely Limestone (Pennsylvanian); PMdp = Diamond Peak Formation (Pennsylvanian and Mississippian); Dg = Guilmette Formation (Devonian); DOd = Metadolomite (Devonian to Ordovician); Oe = Eureka metaquartzite (Ordovician); hc = Horse Creek assemblage (metasedimentary and granitic rocks); CZqs = Impure metaquartzite and schist (Cambrian and Neoproterozoic). Standard symbols for attitude of bedding or foliation, trend and plunge of lineation, hinge line of mesoscopic fold, geologic contacts, and normal faults (except that double tick marks on upper plate of brittle low-angle normal fault [detachment fault] and filled squares on upper plate of plastic-to-brittle low-angle normal fault [detachment fault]). Faults are dotted where concealed. The approximate location of localities A-H are also plotted on the map. Geology by A. W. Snoke.

formed biotite-hornblende mafic quartz diorite. Mylonitic rocks are ubiquitous and include spectacular calc-mylonite containing competent mineral grains and rock clasts. Many of the obvious folds deform the mylonitic foliation and display westward vergence (Fig. 15A). Folded boudins and dismembered folds are other manifestations of a complex strain history (inferred as progressive, non-coaxial deformation). Scarce sheath folds also occur in the Horse Creek assemblage.

Locality C—Folded, mylonitic white quartzite in the Horse Creek assemblage. This westward vergent fold displays rotation of an earlier mylonitic lineation during late folding in the mylonitic shear zone.

Locality D (along the old road)—Disharmonic westward-vergent folds in the Horse Creek assemblage (Fig. 15B). Lithologies include impure calcite marble with mafic pelitic layers, granodioritic augen gneiss, and white quartzite. Note how layer thickness controlled the amplitude and wavelength of the folds.

As we walk from locality D to E along the old road, we will cross the low-angle fault contact between the overlying Horse Creek assemblage and the underlying quartzite and schist unit several times. Note that when the mylonitic foliation in both the upper and lower plates is roughly subparallel, a secondary black ultramylonite is common along this contact (i.e., a ductile-brittle low-angle fault). In other cases, where foliation in the upper plate is highly discordant to foliation in the lower plate, the contact appears to be a brittle low-angle normal fault that has perhaps soled into (i.e., reworked) the earlier ductile-brittle low-angle fault. Furthermore, there are also steeper normal faults that cut the Horse Creek plate.

Locality E—We are presently situated on the Horse Creek assemblage, however, as you look up the canyon you can see the contact between the overlying Horse Creek assemblage and underlying quartzite and schist unit in fine detail. Again note that the mapped low-angle fault

contact is probably composite in character; parts of the contact are a low-angle, ductile-brittle fault and parts are younger, low-angle brittle normal faults that have soled into the older ductile-brittle fault. These relations suggest a continuum from the mylonitic shear zone deformation to brittle low-angle normal faulting.

Locality F—As we climb the slope above the old road we will cross two low-angle normal faults. The lower fault (the main break in metamorphic grade and here the top of the mylonitic zone) separates the Horse Creek assemblage from a slice of low-grade metadolomite; the upper fault separates the metadolomite from a structurally higher slice of low-grade but fossiliferous Upper Devonian Guilmette Formation (metalsilicite). Remember that low-angle normal faults are structurally below, and as you will soon realize, there are more low-angle normal faults structurally above involving younger rocks.

When you reach the top of the hill (i.e., the resistant gray exposures of Guilmette Formation), if you look approximately east-southeast (i.e., toward the paved road), you will see a portion of a roadcut (locality H). This roadcut is topographically and structurally above your present position. In the roadcut, Mississippian and Pennsylvanian Diamond Peak Formation is structurally overlain by Miocene Humboldt Formation. Therefore, another low-angle normal fault must separate the Guilmette Formation from the Diamond Peak Formation and Humboldt Formation. If you include the ductile-brittle low-angle fault that separates the Horse Creek assemblage from the structurally lower quartzite and schist unit, there are at least five low-angle normal faults in the immediate area that attenuate a stratigraphic section that includes rocks ranging in age from Neoproterozoic to Miocene. In this area, the order of units is such that younger rocks are faulted onto older rocks, so that the section is attenuated. These characteristics closely resemble so-called "chaos structure" originally described by Noble (1941) from the Death Valley region (Wernicke and Burchfiel, 1982).

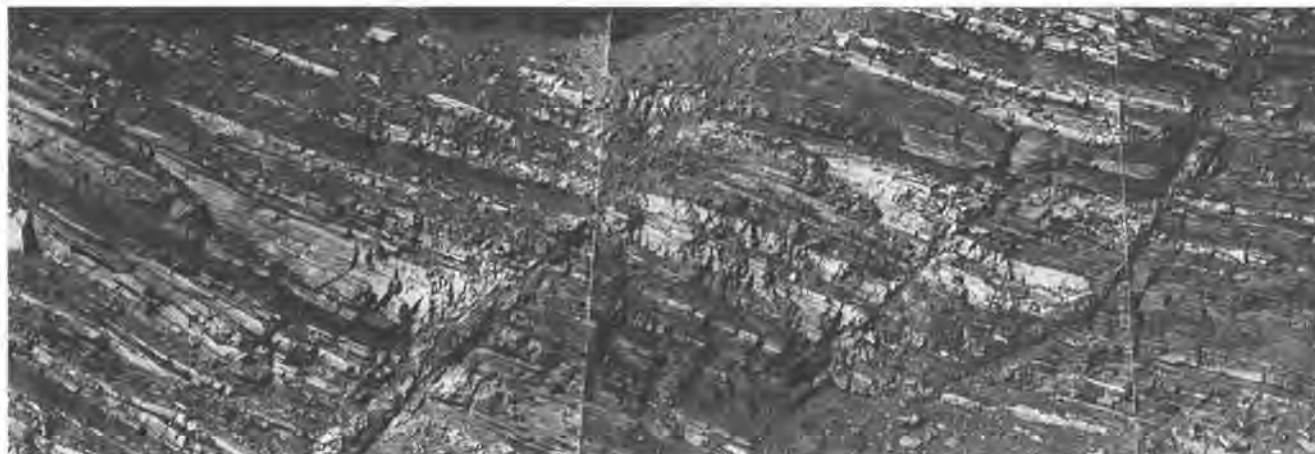


Figure 14. Composite photograph of roadcut (along north side of Nevada 229) in mylonitic, interlayered migmatitic schist and impure quartzite cut by westward-dipping normal faults (both planar and listric), Secret Creek gorge area. Thus roadcut is near locality A on Figure 13 and is 4 to 5 m high. Photograph by A. W. Snoke.

As we walk from locality F to G, we are traversing through poorly exposed slices of chiefly low-grade, middle Paleozoic metacarbonate rocks (Devonian Guilmette Formation and Ordovician to Devonian metadolomite but also sparse metamorphosed Ordovician Eureka Quartzite) structurally above the top of the mylonitic Horse Creek assemblage. In a few places along this portion of the traverse, the exhumed structural top of the Horse Creek assemblage is exposed; note that the orthogneissic rocks are commonly retrograded (chloritic alteration) at these locations. The role of abundant fluids along this important low-angle normal fault is clearly indicated. Furthermore, the retrogression indicates that the brittle low-angle normal faulting, at least in part, evolved under lower grade conditions than the mylonitic rocks (biotite in the mylonitic orthogneisses is retrograded to chlorite at the structural top of the Horse Creek assemblage).

Locality G—Slice of mylonitic Ordovician Eureka Quartzite structurally beneath non-mylonitic but brecciated, low-grade Guilmette Formation and structurally above mylonitic Horse Creek assemblage. The Eureka Quartzite at this locality is a somewhat fractured quartz mylonite. The surface of the exposure appears tectonically polished with a near hori-

zontal west-northwest-trending slickenside lineation. The overlying Guilmette Formation is a medium gray, highly calcite-veined, low-grade metalimestone. A similar tectonic slice of Guilmette Formation exposed south of Secret Creek gorge yielded Late Devonian conodonts with $CAI = 5 \frac{1}{2}$ suggesting that the host rock reached 300°C to 350°C (A. Harris, written communication, 1982).

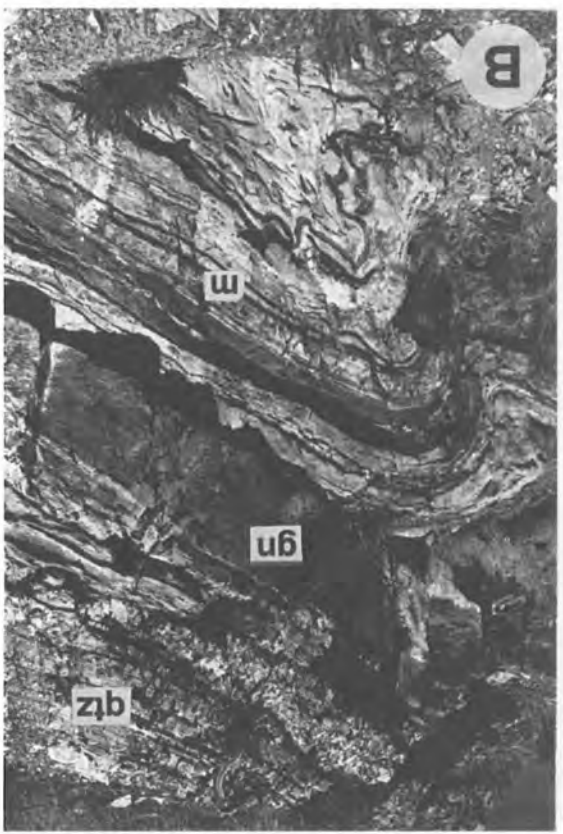
Locality H (along Nevada 229, at parking area)—Tuffaceous siltstone and sandstone of the Humboldt Formation in low-angle normal fault contact with Mississippian and Pennsylvanian Diamond Peak Formation. The Diamond Peak Formation is a thin tectonic slice structurally above the mylonitic Horse Creek assemblage and the low-grade Guilmette Formation metalimestone. Note that bedding in the Diamond Peak Formation has been dismembered; and the formation, which here consists of pebble conglomerate, grit, siltstone, sandstone, and black mudstone, takes on the overall appearance of "broken formation."

Upon completion of the traverse, please congregate near the vehicles in the parking area (adjacent to locality H).

We will now turn the vehicles around and retrace our route to the road to Lamoille (~4.7 miles to the east-southeast).

4.7	38.6	Turn left onto the road that goes to Lamoille.			Quartzite which overlies dolomite marble (Devonian to Ordovician) to the left but is below calcite marble (Ordovician to Cambrian) to the right. The calcite marble, in turn, is overlain to the right by Eureka Quartzite on the right-side-up limb of the anticline. This fold has a curvilinear hinge line that appears to trace an arc through 180°; it is thus a large-scale sheath fold.
2.1	40.7	Secret Peak at 10 o'clock. Just to the right of Secret Peak you can see a landslide scar that developed on May 30, 1983, after intense Spring rains coupled with a rapid snow melt. Note triangular facets along the west flank of the northern Ruby Mountains; a sketch of these facets were included in Sharp (1939b, figure 6).			Hidden Lakes uplift, a north-south trending fold with a core of upper amphibolite facies Neoproterozoic and Lower Cambrian, metamorphosed Prospect Mountain Quartzite, is at 9 o'clock.
1.6	42.3	Road to Starvation Canyon on the left (private property, permission required to drive on this road). Note small offset of Quaternary fan deposits indicating recent Holocene faulting (fault scarp is accentuated by vegetation).	3.9	52.3	Bear left onto Clubline Road.
1.75	44.05	Ninety degree turn in road. To the left is Soldier Peak at 9 o'clock.	3.5	55.8	Turn left.
0.95	45.0	Fort Halleck historical marker. Fort Halleck (1867–1886) was established to protect the California Emigrant trail and construction work on the Central Pacific Railroad. The fort was named for Henry Wagner Halleck who was Commander-in-Chief of the United States Army in 1867.	0.4	56.2	Enter the village of Lamoille (elevation = 5,890 ft [1,796 m]). Turn right onto Nevada 227.
			1.1	57.3	Turn left onto the road that leads into the Lamoille Canyon Recreation Area.
			1.2	58.5	Road climbs onto a piedmont moraine of the Lamoille substage of glaciation. The Lamoille Canyon glacier that deposited this moraine was ~12 miles long (Sharp, 1938).
0.3	45.3	Cross Soldier Creek.			Watch ahead for fault scarp cutting the moraine.
0.85	46.15	Road up Soldier Creek Canyon on left.			
1.25	47.4	Cross John Day Creek.			
1.0	48.4	A recumbent anticline is exposed in the foothills between Cold Creek and Soldier Creek on your left. This fold is best defined by the bouldery white slopes that expose metamorphosed Ordovician Eureka Quartzite. The bouldery white slope on the left as you face the range (i.e., look eastward) is inverted Eureka	0.3	58.8	Entrance to Ruby Dome Ranch on right.
			0.5	59.3	At ditch, the road climbs the late Quaternary fault scarp that cuts the moraine.
			0.4	59.7	Continue past right turnoff to Powerhouse picnic area.
			0.2	59.9	Roadcut in mylonitic orthogneiss of Thorpe Creek, an extensive sill of garnet-two-mica leucogranite gneiss. This

Figure 15. Deformational features in the Tertiary mylonitic shear zone as exposed in the Secret Creek gorge area, northern Ruby Mountains (STOP 3-1). **A**, Fold in mylonitic orthogneiss with thickened hinge zone and attenuated limbs (Locality B on Figure 13). Note that the mylonitic foliation (i.e., gneissic layering) of the shear zone is deformed by this fold. **B**, Late, post-mylonitic folds in the mylonitic shear zone (Locality D on Figure 13). The main rock types are *m*, impure calcite marble with pelitic interlayers; *gn*, biotite granodiorite orthogneiss; and *qtz*, flaggy white quartzite. This exposure is part of a cascade of asymmetric, west-verging folds within the mylonitic shear zone. These folds illustrate the non-coaxial character of deformation in the shear zone, wherein layers were folded in the shortening field despite an overall extensional deformation. Note the disharmonic nature of the folding, controlled by contrasting layer thickness and competency. Hammer used for scale is lying on the outcrop above small bush lower right. **C**, Large clast of massive and competent quartz-bearing hornblende gabbrodiorite encased in mylonitic calcite marble. The area of photograph **D** is outlined. **D**, Rotated clast of competent paragneiss (indicated by arrow and label) in mylonitic calcite marble. Note that a mylonitic fluxion structure is deflected around the clast which itself contains a mylonitic foliation. Both foliations developed during a continuous, non-coaxial extensional deformation. Photographs by A. W. Snoke.



SNOKE, ET AL.: RUBY-EAST HUMBOLDT CORE COMPLEX, NEVADA

		intrusive unit has yielded U-Pb monazite ages of ~36–39 Ma (Wright and Snoke, 1993; MacCready et al., in press).			
0.2	60.1	Lamoille Canyon sign and pullout on right. We are presently in the mylonitic zone that forms a carapace above the migmatitic metamorphic infrastructure, exposed at structural deeper levels in Lamoille Canyon.	0.4	63.5	Lower cliffs above (north of) the road are gneissic pegmatitic leucogranite containing pods of calc-silicate rock and impure calcite marble inverted on the lower limb of the Lamoille Canyon fold-nappe.
0.4	60.5	Roadcut exposes pegmatitic leucogranite with enclaves of calc-silicate rock and sillimanite-bearing pelitic schist of the Ordovician and Cambrian impure marble/calc-silicate unit (Fig. 2). At this location, the unit is in an inverted position on the lower limb of the Lamoille Canyon fold-nappe. We are passing into the infrastructure which is an upper amphibolite facies, granite-rich zone structurally beneath the Tertiary mylonitic shear zone.	0.4	63.9	Wall of quartzite across the canyon contains a deep vertical cleft that probably hides a Miocene basalt dike. Such dikes typically weather recessively in clefts. Some of the basalt dikes are amygdaloidal and were evidently emplaced at relatively shallow depths.
0.2	60.7	Roadcuts along lower Lamoille Canyon are chiefly mixtures of pegmatitic leucogranite gneiss and darker gneisses of uncertain parentage. The pegmatitic leucogranite gneiss predominates in this relatively deep part of the infrastructure.	0.9	64.8	STOP 3-2 —Thomas Canyon campground. <i>The following description is modified from STOP 8 of Snoke and Howard (1984) and Howard (1987). See Figure 16 for a geologic map of the northern Ruby Mountains indicating the location of this STOP and others in Lamoille Canyon. Representative cross sections for the northern Ruby Mountains are shown in Figure 17.</i>
1.2	61.9	The large talus blocks above and below the road include: (1) the granodiorite gneiss of Seitz Canyon (medium-grained biotite granodiorite gneiss) and (2) pegmatitic leucogranite gneiss.			This locality is deep within the migmatitic, metamorphic infrastructure of the Ruby Mountains core complex. The high cliff to the northwest, across Lamoille Canyon, is composed of Cambrian-Neoproterozoic Prospect Mountain Quartzite above intensely folded Ordovician-Cambrian calc-silicate paragneisses. We are therefore looking at the inverted limb of the Lamoille Canyon fold-nappe. Note the contrasting styles of pegmatitic leucogranite in the two stratigraphic units: sills in the calc-silicate paragneiss unit and irregular dikes in the quartzite. Furthermore, especially note the two curved, rainbow-shaped dikes of biotite monzogranite in the left part of the cliff; each are about 6–7 m thick. The dikes truncate compositional layering and foliation in the wall rocks (that is, sillimanite-bearing, micaceous feldspathic quartzite). Four zircon and two monazite fractions were analyzed with U-Pb techniques from the dike on the right (Wright and Snoke, 1993). The two monazite fractions yield a crystallization age of 29 ± 0.5 Ma for
0.5	62.4	Road to Camp Lamoille on the right. Continue on the main road up the canyon.			
0.45	62.85	High cliff to the northwest (uphill to the left) exposes a nose of the granodiorite gneiss of Seitz Canyon in the core of the Lamoille Canyon fold-nappe. The gray gneiss is enveloped by brown Prospect Mountain Quartzite.			
0.25	63.1	This large roadcut includes a mixture of granitic rocks of probable Cretaceous and Tertiary age. A strongly foliated, gray granitic orthogneiss (Cretaceous?) is intruded by pegmatitic leucogranite gneiss (Late Cretaceous?). Both of these units are intruded by a 29-Ma biotite monzogranite dike (RM-15 in Wright and Snoke, 1993). Angular fragments of pegmatitic leucogranite gneiss occur in the biotite monzogranite dike. At the western end of this roadcut is a dark quartz dioritic dike that intrudes pegmatitic leucogranite			

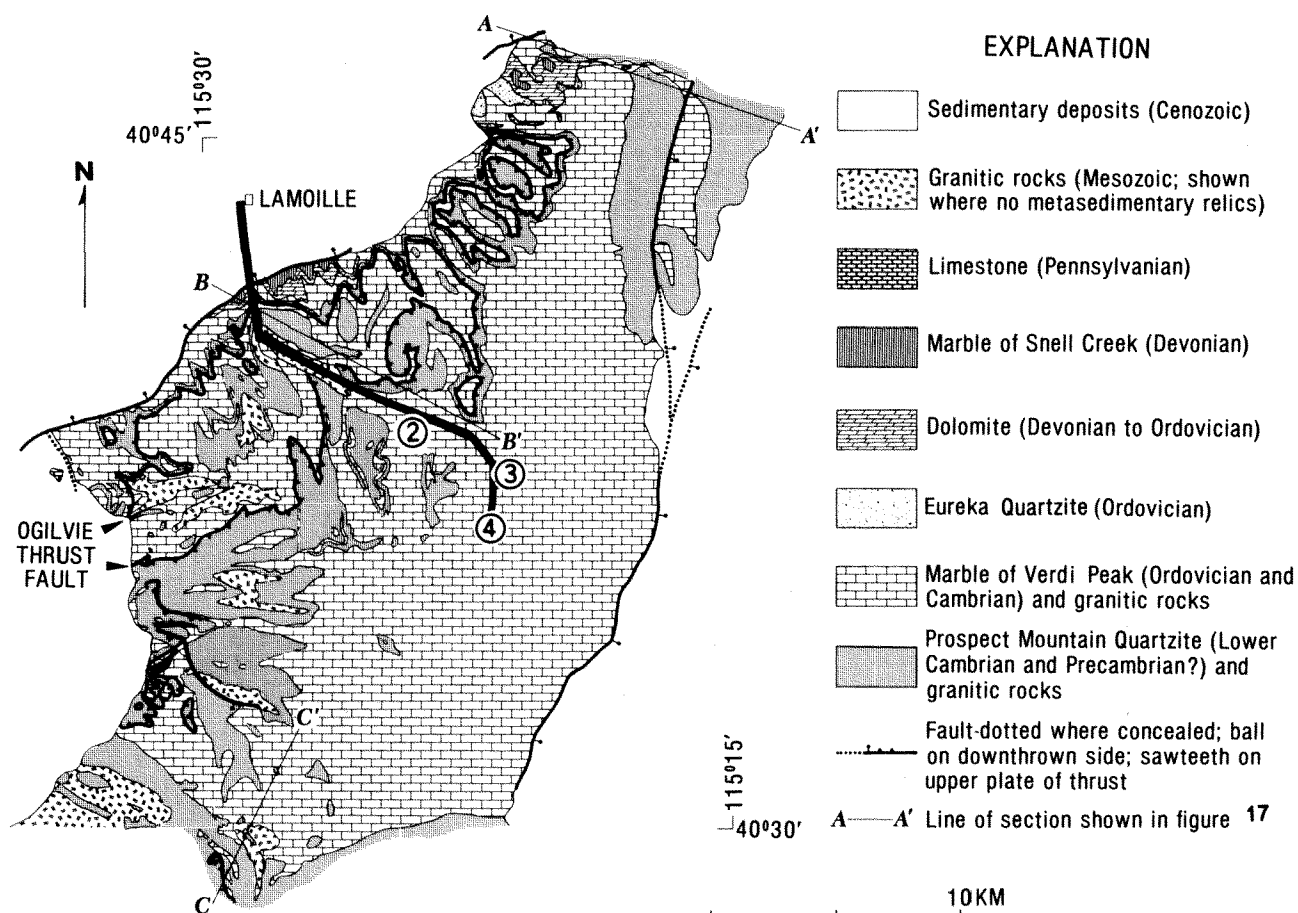


Figure 16. Geologic map of part of the northern Ruby Mountains (modified from Howard [1980], figure 3) showing STOPS 3-2-3-4 along the Lamoille Canyon Road.

this sample. The zircon analyses yield a less precise, lower concordia intercept of 26 ± 8 Ma, which is analytically indistinguishable from the monazite analyses. The analyzed sample is equigranular, medium grained, and apparently undeformed; the other dike is weakly foliated parallel to the dike walls.

The southwest wall of Lamoille Canyon above the Thomas Canyon campground exposes thick sills of pegmatitic leucogranite (Late Cretaceous?, see STOP 3-3 for radiometric age data on possibly similar intrusive rocks) intruded into calcite marble and calc-silicate paragneiss (Ordovician and Cambrian protoliths) (Fig. 18A). Above the marble/calc-silicate rock unit is a thin sliver of quartzite, then more

marble/calc-silicate rocks, capped by brown cliffs of quartzite. The stratigraphic section is inverted; the overlying brown cliffs are the Cambrian and Neoproterozoic Prospect Mountain Quartzite. The sliver of quartzite, interpreted as an inverted thrust slice of the Prospect Mountain Quartzite (Howard, 1987), can be traced for miles. When this inferred thrust sliver is restored to a pre-folding position it and others pinch out to the west, suggesting west-directed thrusting (Snook and Howard, 1984, figure 10).

Continue past roadside pullout for valley overlook and view of hanging valleys. Outcrops of buff marble and white pegmatitic leucogranite are above the road on the left (east).

1.7 66.5
0.6 67.1

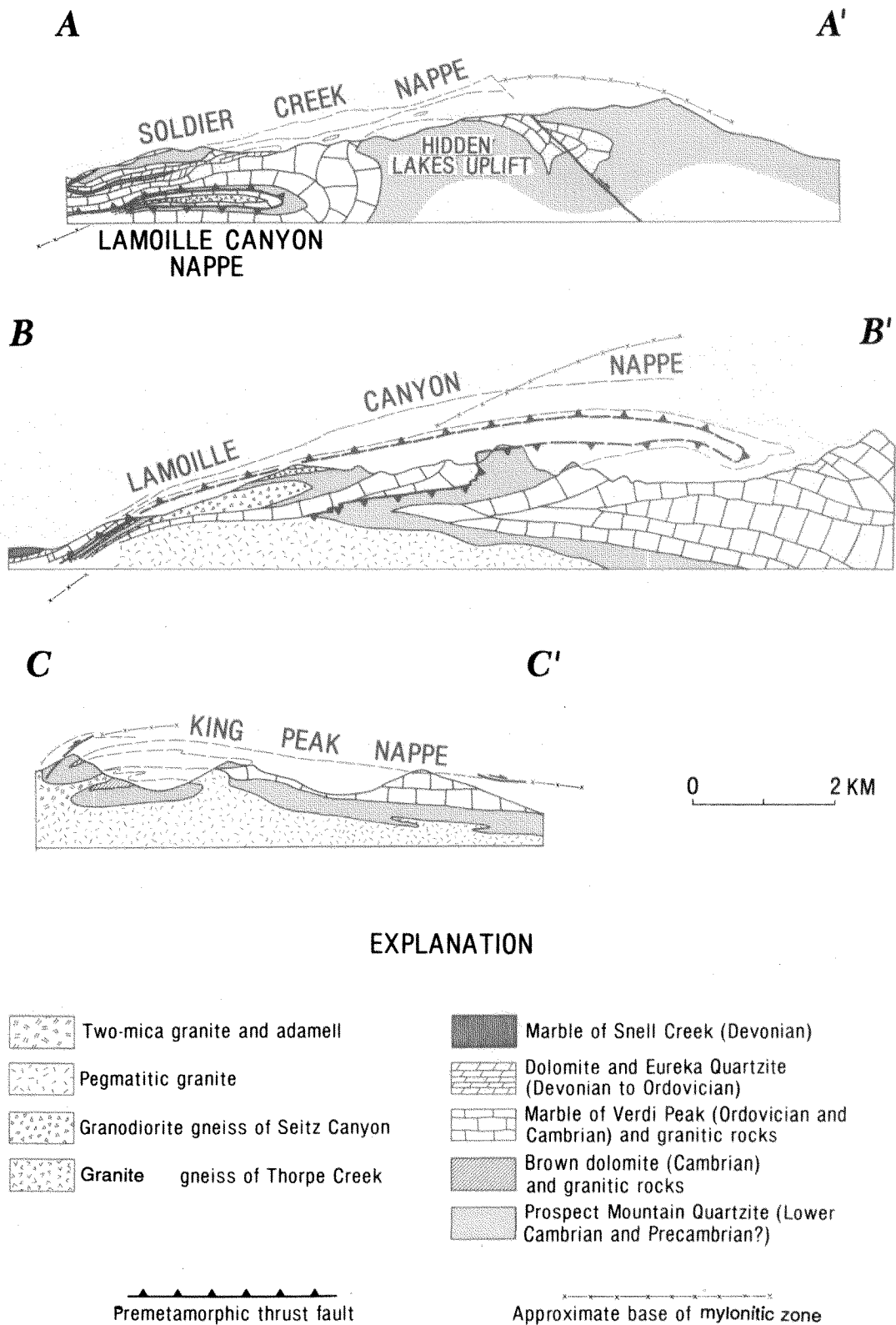


Figure 17. Cross sections along Lamoille Canyon (BB') and other locations in the northern Ruby Mountains (modified from Howard [1980], figure 4). Cross-section lines located on Figure 16.

0.4 67.5 Roadcuts are pegmatitic leucogranite gneiss and enclaves of folded calc-silicate paragneiss, part of STOP 3-3.

0.2 67.7 **STOP 3-3**—Turn left into Terraces day-use area and drive to parking area (0.1 mi). There is a charge (presently \$2) to park here.

View stop of hinge of Lamoille Canyon fold-nappe at Terraces day-use area. *The following description is modified from STOP 6 of Snoke and Howard (1984) and Howard (1987).*

Bring binoculars, if available, and assemble on the large flat outcrop of gneissic pegmatitic leucogranite in the picnic grounds. From this locality we can view the hinge of the recumbent Lamoille Canyon fold-nappe (Fig. 18B). The view northward down the canyon shows brown cliffs of Prospect Mountain Quartzite (Neoproterozoic and Cambrian) forming an eastward closing fold nose with metacarbonate rocks (Ordovician and Cambrian) wrapping around it. Within the quartzite nose is a repetition of the stratigraphically higher unit of marble and calc-silicate rocks, separated from the quartzite unit by an inferred pre-folding thrust fault (Ogilvie thrust).

The outcrops of pegmatitic leucogranite gneiss that we are standing on, and along the Lamoille Canyon road just below, contain sillimanite and monazite; enclaves of calc-silicate paragneiss are common. Monazite from the leucogranite yielded a U-Pb date of ~83 Ma (J. E. Wright, unpublished data, cited in Wright and Snoke, 1993), suggesting a Late Cretaceous emplacement age.

0.2 67.9 Return to main road and turn left (i.e., continue up the canyon).

0.8 68.7 "Avalanche chute" parking area on right. Continue to the end of the canyon.

1.3 70.0 **STOP 3-4**—End of the road, parking lot, and trailhead at elevation ~8,800 ft (2,684 m).

The walls of upper Lamoille Canyon expose a variety of granitic rocks occurring as dikes, sills, and sheet-like intrusive bodies; metasedimentary enclaves of impure calcite marble, calc-silicate paragneiss, and pelitic schist (Ordovician

and Cambrian protoliths) are intermixed with the granitic rocks (Fig. 18C). The prominent rugged, light-colored peak to the north down the valley is Verdi Peak (11,074 ft [3,378 m]). The saddle in the ridge along the skyline to the south is Liberty Pass (~10,500 ft [3,202 m]); the peak (11,032 ft [3,365 m]) to right of the pass is an unnamed feature that rises above Lamoille Lake. On another visit, when you have more time, we recommend a hike up to Lamoille Lake or beyond—this high country is spectacular for hiking, especially from mid-July through early September.

The Ruby Crest Trail begins at the end of the road (~8,800 ft at trailhead sign) and continues south for about 40 mi (64 km) along the crest of the Ruby Mountains to Harrison Pass. We will walk south a short distance along the trail with the chief objective being to examine some of the intrusive granitic rocks and metasedimentary enclaves. A new, collaborative research project (University of Wyoming, Texas Tech University, U.S. Geological Survey, and Rice University and funded by the National Science Foundation) is in progress to study the petrogenesis, age, emplacement mechanisms, and deformational history of the granitic rocks in this area. Evidence indicates that most, if not all, of these granitic rocks are either Late Cretaceous or Tertiary in age; look for evidence for consistent cross-cutting relationships between the various types of granitic rocks (Fig. 19).

The trailhead begins at the sign near the parking lot. After crossing the bridge with railing, the first outcrop along the trail is a banded, foliated, and lineated two-mica granitic orthogneiss with sparse garnet and sillimanite (Cretaceous or Jurassic?). This granitic gneiss contains an enclave of calc-silicate paragneiss and is intruded by pegmatitic, two-mica leucogranite gneiss (Late Cretaceous?). Continue along the trail until you reach an exposure of foliated biotite monzogranite (Oligocene?) cut by several pegmatite dikes (note: this outcrop is located just before you cross a second bridge). From this locality verge off the trail to the





Figure 18. Views of the Lamoille Canyon area showing relationships between intrusive granitic rocks, upper amphibolite-facies metasedimentary wall rocks, and large-scale structural features. **A**, Southwest wall of Lamoille Canyon, above the mouth of Thomas Canyon, showing a complex network of sills and dikes of granitic rocks intruded into calcite marble and calc-silicate paragneiss (Ordovician and Cambrian protoliths) (near STOP 3-2). **B**, The Lamoille Canyon fold-nappe as exposed on the north wall of Lamoille Canyon. The hinge of the nappe is outlined by brown-weathering cliffs of upper amphibolite facies Prospect Mountain Quartzite (Cambrian and Neoproterozoic). The quartzite nose is surrounded by calcite marble and calc-silicate paragneiss (Ordovician and Cambrian protolith) pervasively intruded by numerous sills of white-weathering pegmatitic leucogranite. Calcite marble and calc-silicate paragneiss also occur in the core of the fold and have been interpreted by Howard (1966) as the Cambrian and Ordovician unit in the originally lower plate of the pre-metamorphic and pre-folding Ogilvie thrust fault. **C**, East wall of upper Lamoille Canyon exposing a granitic dike-sill complex intruded into upper amphibolite-facies calc-silicate paragneiss and impure calcite marble (Ordovician and Cambrian protoliths) (near STOP 3-4). Photographs by A. W. Snoke

right following an azimuth of $\sim 280^\circ$. This trend will lead you to an excellent exposure of foliated, and locally banded, biotite > muscovite granitic orthogneiss cut by dikes and irregular bodies of pegmatitic leucogranite. At this exposure there is also a "Z-shaped" medium-grained biotite leucogranite body. Is it part of the Tertiary biotite monzogranite suite? From this locality, we will traverse to a large exposure that has been studied in detail by Sang-yun Lee (summarized in section by Lee and Barnes, this field guide).

We will return to the parking lot via the stock trail. If you haven't already noticed, the steep east wall of upper Lamoille Canyon exposes a superb granitic dike and sill complex intruded into impure calcite marble and calc-silicate paragneiss (Fig. 18C), and the view is excellent from the stock trail in the afternoon.

This is the last stop for DAY THREE. We will drive back down the canyon (approximately 12.6 mi) and turn left at the intersection with Lamoille Highway and thus return to Elko.

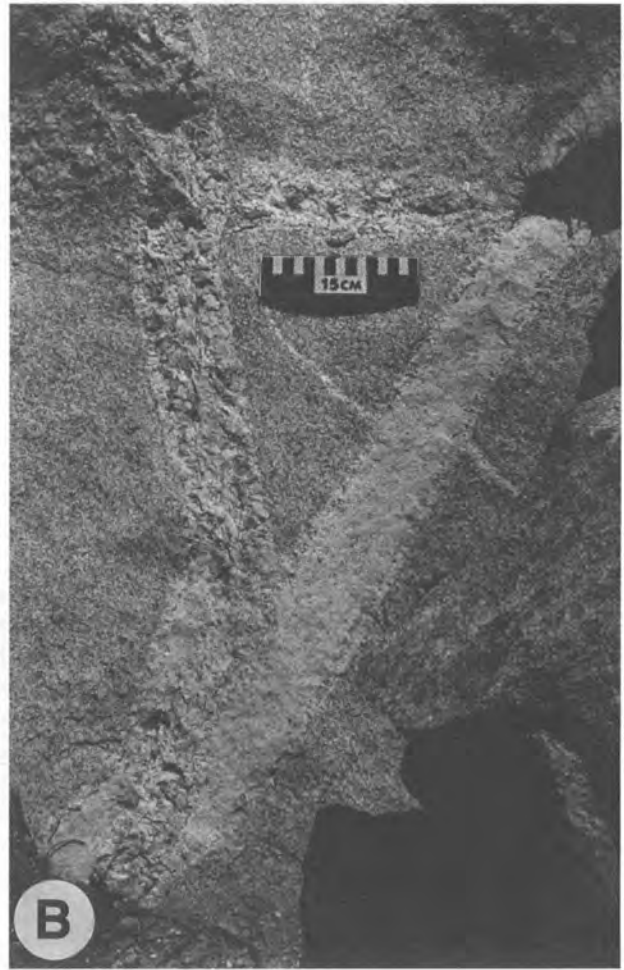
DAY FOUR

Elko to Harrison Pass to Ruby Valley (Road Canyon area)
to Salt Lake City.

Incre. Cum.
Miles Miles

0.0	0.0	Start at Red Lion Inn & Casino, Elko, Nevada.	0.3	4.8	Exposures of the Eocene cherty limestone unit on left.
0.6	0.6	Northeast Nevada Museum.	0.2	5.0	Lamoille summit and exposures of Elko Formation on the left.
0.4	1.0	Turn left (south) onto 12th Street.	0.1	5.1	View of the west flank of the northern Ruby Mountains. The large canyon to the southeast is Lamoille Canyon, the focus of several stops on DAY THREE.
0.4	1.4	Cross the Humboldt River.			The smooth, west-dipping flank of the range is principally controlled by foliation in ~1-km thick mylonitic shear zone.
0.5	1.9	Turn left at "T" onto Lamoille Highway (Nevada 228).	2.2	7.3	Stop light. Intersection of Lamoille Highway and Spring Valley Parkway on left.
0.2	2.1	For information about the Humboldt National Forest turn left and proceed to Headquarters but for our trip stay straight.	0.4	7.7	Turn right onto Nevada Highway 228 and proceed toward Jiggs.
0.4	2.5	Road to City of Elko municipal landfill.			Note dip slope formed on flaggy rocks of the mylonitic shear zone on the west flank of the Ruby Mountains.
2.0	4.5	The roadcut exposures on the left expose some of the oldest Tertiary rocks in Nevada (Solomon et al., 1979; Solomon and Moore, 1982). These rocks referred to as the "conglomerate, sandstone, and shale unit" by Solomon et al. (1979), include a tuff layer dated by the K-Ar method (biotite) at 43.3 ± 0.4 Ma. These rocks underlie fossiliferous Eocene rocks (cherty limestone unit of Smith and Ketner, 1976) as well as the upper Eocene and Oligocene(?) Elko Formation and, therefore, must be Eocene or older. The dated tuff is apparently one of the earliest manifestations of Tertiary volcanism in Nevada (Solomon et al., 1979).	3.3	11.0	Entering tribal lands.
			0.7	11.7	Mountain range at 2 o'clock is the Piñon Range. This area has been studied by Smith and Ketner (1978).
			0.7	12.4	Leaving tribal lands.
			0.4	12.8	South Fork Recreation Area road on the right.
			5.9	18.7	Twin Bridges on the right. The red soils are developed on the "conglomerate, sandstone, siltstone, and limestone" unit (Eocene?) of Smith and Howard (1977). Cherty limestone (Eocene), however, forms the bulk of the hill immediately west of the Twin Bridges area.
		These Paleogene rocks form the core of a normal-faulted, northeast-plunging anticline. The folding and normal faulting must pre-date 35 Ma, because relatively flat-lying and unfaulted Oligocene andesite (exposed about 2 km to the southwest) unconformably overlies the deformed older Tertiary rocks (Solomon and Moore, 1982).	1.6	20.3	Road to Lee on the left. Note light-colored exposures of Miocene Humboldt Formation in roadcut on left. Pebble conglomerate in this section of Humboldt Formation contains abundant lithic clasts presumably derived from the Ruby Mountain igneous-metamorphic complex. Mylonitic clasts are not present, and the dominant clast-types are leucocratic granitic rocks and various impure calcite marbles and calc-schists.

Figure 19. Intrusive relationships among granitoids exposed in upper Lamoille Canyon area. **A**, Irregular dark dike of biotite tonalite (Tertiary?) intruded into two-mica pegmatitic granite gneiss (Late Cretaceous?). Note head of hammer near upper edge of photograph. **B**, Equigranular biotite monzogranite, correlated with the 29-Ma suite, intruded by three generations of pegmatite-aplite dikes. The youngest dike exhibits a distinctive texture characterized by coarse sheaves of muscovite. **C**, Composite enclave of dark-colored calc-silicate paragneiss (lower center) and concordant, equigranular, two-mica granitic gneiss (upper center) within two-mica pegmatitic granite gneiss. The pegmatitic leucogranite gneiss is correlated lithologically with the rock dated near the Terraces day-use area as Late Cretaceous by U-Pb isotopic analysis on monazite. Photographs by A. W. Snoke.



0.45	20.75	Cross the South Fork of the Humboldt River.			Jiggs Fire Station and school. The village is named for the comic strip character of the same name; it was originally called Skelton, then Hylton, and finally Jiggs in 1918 (Patterson, 1977). During the 1970s and early 1980s, the Huntington Valley area, southwest of Jiggs, was the site of an exploratory drilling program for hydrocarbons (Schalla, 1992). Five deep wildcat wells were drilled and substantial oil and gas shows were reported. Pan American #1 Jiggs-USA, drilled in 1971, reached a total depth of 13,600 ft (4,145 m), making it the deepest well drilled in Huntington Valley. All five wells penetrated Cenozoic sedimentary and volcanic rocks as much as 11,040 ft (3,367 m) thick, including the Elko, Indian Well, Humboldt, and Hay Ranch formations which lie unconformably on Pennsylvanian and Mississippian rocks. Sub-surface maps based on drilling and seismic data indicate a pronounced northward dip for the Paleozoic-Cenozoic unconformity as well as a horst block bounded by generally north-south-striking normal faults (Schalla, 1992).
3.15	23.9	View up Rattlesnake Canyon on left.			
0.9	24.8	Pearl Peak at 11 o'clock. North of Pearl Peak is Harrison Pass.			
0.3	25.1	Road to Lee on left.			
4.0	29.1	Tree-covered hill north-northwest of Pearl Peak is Cedar Mountain which is chiefly composed of allochthonous, unmetamorphosed Devonian sedimentary rocks (Devils Gate Limestone and Nevada Formation) that lie structurally above granitic rocks of the Harrison Pass pluton. Willden et al. (1967) recognized cataclastic textures in the underlying granitic rocks as well as the overall allochthonous character of the Devonian rocks at this locality. These authors argued that the klippe was a manifestation of west-to-east Tertiary thrusting (i.e., contractional deformation). Snoke and Howard (1984, their Stop 16) suggested that this klippe as well as several westward-dipping, siliceous breccia sheets north of the klippe along the west flank of the Ruby Mountains are part of an extensional allochthon related to post-emplacement normal or detachment faulting. Blackwell et al. (1984, 1985), Reese (1986), Hudec (1990), and Burton (in preparation) indicate that a low-angle normal fault forms the base of the klippe and breccia sheets and that this fault (an originally steeper, west-dipping normal fault) as well as the Harrison Pass pluton and environs have been tilted eastward, perhaps as much as 30°, in the footwall of a west-rooted normal fault system.	0.9	34.8	Excellent view of Cedar Mountain at 11 o'clock with Pearl Peak in the background.
			0.4	35.2	Dip slopes of siliceous breccia ("jasperoid") sheet at 10 o'clock.
			2.1	37.3	Continue straight toward the Ruby Lake National Wildlife Refuge.
			0.9	38.2	Another excellent view of tree-covered Cedar Mountain. View of dip slope of siliceous breccia sheet at 9 o'clock.
1.7	30.8	Excellent view of Cedar Mountain klippe, west of Harrison Pass.	2.2	40.4	Pavement ends.
			0.8	41.2	View of the sprawling ridge north of Toyn Creek. This area is an especially important locality to study age relationships between intrusive phases of the Harrison Pass pluton. Here, numerous biotite ± muscovite monzogranite sills and dikes as well as pegmatite, alaskite, and aplite dikes intrude the megacrystic biotite ± hornblende granodiorite phase of the Harrison Pass pluton.
1.8	32.6	Robinson Mountain at 2 o'clock is part of a widespread rhyolitic to dacitic ash-flow tuff unit that forms a major part of the Oligocene Indian Well Formation (Smith and Ketner, 1976). A detailed paleomagnetic-structural study of these rocks was reported on by Palmer et al. (1991).			
1.3	33.9	Village of Jiggs (elevation = 5,476 ft [1,670 m]) and Jiggs Bar. Jiggs serves as an important center of communication in this ranching community and is the site of many local activities as well as the	0.3	41.5	Road on the left goes up Green Mountain Creek.
			1.6	43.1	Another view at 10 o'clock of the ridge north of Toyn Creek.

0.2	43.3	Outcrop of composite mafic dike with commingled(?) felsic component on north side of the road.			granitic suite can be seen in the distance to the northwest. These rocks weather a distinctive orange color and are exposed on the flank of two prominent knobs in the distance.
1.3	44.6	The road crosses a prominent outcrop of vein quartz in granitic rocks of the Harrison Pass pluton. This northeast-striking vein is shown on the geologic map of Willden and Kistler (1969).	0.3	48.5	Turn around and retrace our route back to the main road.
1.5	46.1	Beginning of numerous rounded exposures of megacrystic granodiorite on both the right and left sides of the road.	1.4	49.9	Intersection with Harrison Pass road, turn right.
1.8	47.9	Turn right onto dirt track at Harrison Pass (elevation = 7,248 ft [2,211 m]), once known as Fremont Pass.	0.1	50.0	Exposure of closely spaced joints in granodiorite phase of the Harrison Pass pluton.
0.3	48.2	STOP 4-1. Harrison Pass view stop. This locality affords an excellent view of the late Eocene (~36 Ma) Harrison Pass pluton and environs (see Burton et al., this field trip guide including a geologic map and cross section of the pluton). The extensive set of outcrops to the north are chiefly comprised of megacrystic granodiorite. A good view into Ruby Valley as well as parts of various ranges (including Spruce Mountain and Medicine Range) is visible to the east. The roof zone of the pluton is also exposed on the east side of the range. The contact is located at the change in vegetation cover on several ridges that can be seen to the east. The southern contact is along the near-side of a long ridge that extends west from Pearl Peak, directly to the south. Paleozoic sedimentary rocks on this ridge are folded in the contact aureole of the pluton, whereas south of this point the Paleozoic rocks form an eastward dipping homocline (Sharp, 1942; Willden and Kistler, 1979). The northern contact of the pluton cannot be seen from this locality. To the west is the Cedar Mountain klippe (discussed previously at mileage point 29.1). The view west down Toyn Creek affords a look into Huntington Valley with the Piñon Range in the distance on the horizon.	0.8	50.8	Fresh, coarse-grained, megacrystic biotite monzogranite of the older granodiorite unit of the Harrison Pass pluton in roadcut on left.
			0.1	50.9	Buildings on right are remains of the Star Tungsten mine, discovered in 1916 or 1917. The mine chiefly produced scheelite from skarn deposits along the contact between the Harrison Pass pluton and metacarbonate country rocks.
			0.1	51.0	Additional remains of Star Tungsten mine on left. Approximate contact between granitic rocks of the Harrison Pass pluton and metacarbonate rocks of the Paleozoic country-rock sequence.
			0.1	51.1	Exposure of porphyritic dikes from the Harrison Pass pluton (immediately before crossing cattle guard). Metacarbonate rocks of the Ordovician Pogonip Group underlie the adjacent hills, and these rocks are pervasively intruded by dikes and apophyses of the Harrison Pass pluton.
			0.1	51.2	Contact metamorphosed metacarbonate rocks in the aureole of the Harrison Pass pluton. Locally the metacarbonate rocks are characterized by large porphyroblasts of vesuvianite.
			0.9	52.1	More exposures of metacarbonate rocks in the aureole of the Harrison Pass pluton.
			0.9	53.0	Interesection of the Harrison Pass road with the Ruby Valley road, turn left (i.e., proceed northward). The prominent hill directly south is composed of west-dipping Pennsylvanian Ely Limestone, down-faulted from the main part of the range (Hudec, 1990).
					South end of Franklin Lake on the right at about 2 o'clock.

- 1.3 54.3 Turn left onto the dirt road up Road Canyon.
- 0.3 54.6 Cross creek.
- 0.55 55.15 Head frame for mine workings on right.
- 0.05 55.2 Park near remains of buildings. These buildings and several small winzes at the crest of the ridge to the north comprise the Eddie claims of the Valley View mining district (Lapointe et al., 1991). These prospects were developed on tungsten-manganese skarn deposits in the contact aureole of the Harrison Pass pluton; however, the claims were not productive.

STOP 4-2. Contact zone between Harrison Pass pluton and metamorphosed Paleozoic wall rocks.

Proceed northward by ascending a north-south-trending ridge through complexly folded roof rocks. Small amplitude folds plunge to the southeast and define a conical distribution on a stereonet. The stratigraphic sequence here is attenuated by as much as 70% in comparison to the inferred equivalent sequence exposed to the south near Pearl Peak. Continue your ascent to about the 7000-foot elevation where the contact between the Harrison Pass pluton and Cambrian impure metacarbonate rocks is exposed. In this area and along the west-facing slope of this ridge to about the 7300-foot elevation, slabs of contact-metamorphosed Cambrian wall rocks are exposed within a sheeted zone of the pluton margin. Wall-rock slabs are separated by dikes and sills of leucocratic phases considered part of the granodioritic suite of the Harrison Pass. The wall-rock slabs consist of carbonaceous argillite, phyllite, impure quartzite, and calc-silicate rocks. At this locality, the pluton-wall-rock contact is discordant, whereas by looking south across Road Canyon you can see the transition to a concordant roof zone.

The contact between the Harrison Pass pluton and metasedimentary wall rocks is irregular, but is approximately coincident with the edge of the coniferous forest on this ridge as well as on the ridge to the south. The contact consists of both steep- and shallow-dipping segments and

thus exhibits an overall stair-step geometry. Along the contact, blocks of wall rock are separated by dikes and sills of leucocratic granitic rock. Brittle fracture played a key role in the emplacement of the dikes and sills as well as in the development of the stair-step contact. However, folding of the wall rocks also occurred during the emplacement of the Harrison Pass pluton. At approximately the 7300-foot elevation is a prominent outcrop of folded siliceous wall rock with a folded sill of leucogranite in its core.

Turn vehicles around and retrace our route back to the Ruby Valley road (~0.9 mi).

- | | | |
|-----|------|--|
| 0.9 | 56.1 | Intersection with Ruby Valley road, turn left (i.e., proceed northward). |
| 3.7 | 59.8 | Exposures of Jurassic two-mica granite of Dawley Canyon on the left at about 10 o'clock. |
| 1.1 | 60.9 | Stone buildings on right. Exposure of two-mica granite of Dawley Canyon on left is the site where a sample for U-Pb dating was collected in 1980 from which J. E. Wright found an age on monazite of 153 ± 1 Ma (Hudec, 1990; Hudec and Wright, 1990). |
| 1.8 | 62.7 | Rock House on left. |
| 0.7 | 63.4 | Road to Overland Lake trailhead on left. Exposures of two-mica granite of Dawley Canyon to the west. |
| 1.5 | 64.9 | Cross Overland Creek. |
| 1.2 | 66.1 | Humboldt Peak (11,020 ft [3,361 m]) on the skyline at 11 o'clock. Southeast East Humboldt Range at 10 o'clock. |
| 3.8 | 69.9 | Road to the abandoned Battle Creek mines on left. This road also serves as a public access road to the Humboldt National Forest. |
| 2.0 | 71.9 | Ruby Valley Fire Department Station #2 on left. Lake Peak (10,922 ft [3,331 m]) at 10 o'clock. |
| 0.5 | 72.4 | Ruby Valley school on left, built in 1962. Another view of Lake Peak northwest of the school. |
| 5.0 | 77.4 | Pavement begins. |
| 0.7 | 78.1 | Massive exposures of sillimanite-grade metaquartzite at 11 o'clock. Joe Billy Basin at 10 o'clock. |
| 1.4 | 79.5 | End of Nevada 767, turn right onto Nevada 229 and proceed eastward. This is the end of the road log for DAY FOUR. |

Our present location is the same as mileage point 70.2 on DAY TWO of the trip but today we approached this locality from the south rather than from the east as we did on DAY TWO. Thus, you can refer to the road log material that pre-

ceded mileage point 70.2 on DAY TWO as we now drive toward U. S. 93, Wells, and eventually Salt Lake City, the site of the 1997 Annual Meeting of The Geological Society of America.

Grand Tour—Part 2: Petrogenesis and thermal evolution of deep continental crust: the record from the East Humboldt Range, Nevada

ALLEN J. MCGREW

Department of Geology, The University of Dayton, Dayton, Ohio 45469-2364

MARK T. PETERS

Woodward-Clyde Federal Services, 1180 Town Center Drive, Las Vegas, Nevada 89134

INTRODUCTION

The northern part of the East Humboldt Range, Nevada, provides a rare opportunity to explore the petrogenetic environment of deep levels in the middle crust during both large-scale Mesozoic contraction and Cenozoic regional extension. On this segment of the field trip, we will explore evidence bearing on the character of the metamorphic and magmatic history of this terrane, and attempt to link these constraints to the rheology and tectonic evolution of the middle crust during the Mesozoic and Cenozoic.

TECTONIC SETTING

The northern East Humboldt Range forms the northernmost and perhaps the deepest seated part of the footwall of the Ruby Mountains–East Humboldt Range metamorphic core complex (Fig. 1). The western flank of the range forms a dip-slope on a gently inclined, normal-sense mylonitic shear zone at least 1 km thick, whereas the eastern flank of the range is bounded by a younger, steep east-dipping range-front normal fault that cuts through the metamorphic core complex to expose a spectacular natural cross-section (Figs. 10 and 11). Like other parts of the Ruby Mountains–East Humboldt Range, the northern East Humboldt Range records a complicated, polyphase history beginning with tectonic deep burial before the Late Cretaceous followed by deep-crustal tectonism during the Late Cretaceous to Oligocene and tectonic exhumation during Oligocene to early Miocene time. An important contrast between the northern East Humboldt Range and other parts of the Ruby Mountains–East Humboldt Range is that it exposes the only known outcrops of Archean rocks in the State of Nevada. Based on U-Pb geochronology and Sr, Nd, and Pb isotopic geochemistry, Wright and Snoke (1993) argue that the East Humboldt Range and Ruby Mountains are underlain by contrasting

crustal basement provinces of Archean and Proterozoic age, respectively (Fig. 1).

The structural architecture of the northern East Humboldt Range is dominated by two kilometer-scale features: a large, southward-closing, basement-cored recumbent fold known as the Winchell Lake fold-nappe, and the >1-kilometer thick mylonitic shear zone referred to above (Figs. 10 and 11) (Snoke and Lush, 1984; McGrew, 1992). We present evidence that the Winchell Lake fold-nappe was emplaced originally during the Late Cretaceous but was later transposed during Tertiary mylonitic shearing. An Archean orthogneiss occupies the core of the Winchell Lake fold-nappe and is surrounded by probable Paleoproterozoic paragneiss (Lush et al., 1988). Folded around this Precambrian gneiss complex, and separated from it by an inferred prefolding, premetamorphic fault, is a metasedimentary sequence of quartzite, schist, and marble that probably correlates with the Neoproterozoic to Mississippian (?) miogeoclinal sequence of the eastern Great Basin. The inferred Paleozoic marble sequence repeats twice more at depth beneath the Winchell Lake fold-nappe, with a thick sequence of probable Neoproterozoic paragneiss intervening (see fig. 7B in Camilleri et al., this volume) (McGrew, 1992; Peters et al., 1992; Wickham and Peters, 1993). Inferred premetamorphic tectonic contacts bound each major package of rocks, and a thick sheet of hornblende-biotite quartz dioritic orthogneiss dated at 40 ± 3 Ma (U-Pb zircon, Wright and Snoke, 1993, RM-19) cuts gently across the various allochthons, including the tectonic slide at the base of the Winchell Lake fold-nappe. Numerous intrusions of biotite monzogranitic orthogneiss which are part of a widespread 29-Ma suite of dikes and sheets also cut the various allochthons, but are partially involved in folding and extensively overprinted by the mylonitic deformation (McGrew, 1992; Wright and Snoke, 1993). Taken together, the East Humboldt Range forms a stacked sequence of allochthons assembled during a complex,

polyphase tectonic history. A portion of the same stacked structural sequence is exposed east of the northern East Humboldt Range in the "Clover Hill" area (Snoke, 1992).

PRESSURE-TEMPERATURE HISTORY

Developing a pressure-temperature-time history (PTt path) for the East Humboldt Range depends critically on integrating quantitative thermobarometry with available cooling age constraints from radiometric dating and with relative age constraints developed from interpretive petrography and careful field observation. Below we first discuss constraints on the pressure-temperature path based on traditional petrography, field relationships, and quantitative thermobarometry, and then we integrate time-temperature constraints developed from radiometric dating in order to synthesize a PTt-path for the northern East Humboldt Range from the Late Cretaceous to early Miocene.

Petrographic and thermobarometric constraints

The northern East Humboldt Range exposes a diverse suite of metamorphic rocks, including leucogranitic to dioritic orthogneiss, amphibolite, calcite and dolomite marble, calc-silicate paragneiss, pelitic schist, and quartzite. The strongest constraints on the PTt history of the northern East Humboldt Range come from pelitic schists and to a lesser extent from amphibolites and calc-silicate paragneisses. For convenience, in the discussion below we will adopt emplacement of the Winchell Lake fold-nappe as a benchmark for notation of relative age relationships, designated by the subscript "n." Thus, M_n refer to metamorphism inferred to be synchronous with fold-nappe emplacement whereas M_{n-1} refers to metamorphic mineral growth predating fold-nappe emplacement, and M_{n+1} refers to metamorphic mineral growth postdating fold-nappe emplacement.

In general, metamorphic mineral assemblages show little geographic variation throughout the northern East Humboldt Range. However, the oldest phase in the metamorphic history of the northern East Humboldt Range is preserved only on the upper limb of the Winchell Lake fold-nappe where scarce subassemblages of kyanite \pm staurolite + biotite persist locally as inclusion suites in garnet. Kyanite also survives locally in the matrix of some pelitic schists where it is mantled or pseudomorphosed by later sillimanite. At present, the only constraint on the age of this kyanite-bearing subassemblage is that it must pre-date formation of the Winchell Lake fold-nappe because the sillimanite that replaces it is itself pre- to early synkinematic with fold-nappe emplacement. However, by analogy with similar assemblages in the Wood Hills and Clover Hill to the east, we suggest that the kyanite-bearing assemblages (M_{n-1}) in the northern East Humboldt Range prob-

ably record tectonic burial in the Late Jurassic and/or Early Cretaceous (Hodges et al., 1992; Snoke, 1992; Camilleri and Chamberlain, 1997).

The characteristic peak metamorphic assemblage in pelitic schists consists of biotite + sillimanite + garnet + quartz + plagioclase \pm K-feldspar \pm muscovite \pm chlorite \pm rutile \pm ilmenite. In a few samples from deep structural levels, sillimanite and metamorphic potassium feldspar coexist in rocks that are nearly devoid of muscovite, suggesting that peak metamorphism may have reached the second sillimanite isograd. As noted above, much of the sillimanite shows textural relationships that are pre- or early synkinematic relative to emplacement of the Winchell Lake fold-nappe, and therefore pre-kinematic with respect to the later extensional shearing. For example, mats of sillimanite are folded in the hinge zone of the Winchell Lake fold-nappe, and in the mylonitic zone bundles of sillimanite are commonly boudinaged, deflected by extensional crenulation cleavage, or cut by microfractures oriented perpendicular to Tertiary stretching lineation. Below we argue that this initial phase of sillimanite growth occurred synchronously with fold-nappe emplacement (M_n) and was Late Cretaceous. Nevertheless, textural relationships commonly record more than one phase of sillimanite growth, and the final phase of sillimanite growth (M_{n+1}) probably occurred during Oligocene extensional deformation. For example, fine-grained intergrowths of dynamically recrystallized quartz, fibrolite, and biotite occur along some extensional shear bands.

Many shear band fabrics and extensional microfractures also contain relatively late-stage minerals (M_{n+2}) such as chlorite and muscovite, demonstrating that mylonitic deformation continued through a range of progressively lower grade conditions during extensional exhumation. Although muscovite occurs at all structural levels, overprinting of earlier fabrics and assemblages by coarse, patchy muscovite becomes increasingly conspicuous at higher levels in the mylonitic shear zone.

The assemblages described above are amenable to quantitative thermobarometry based on electron microprobe analysis using the Thermocalc computer program of Powell and Holland (1988) and the internally consistent thermodynamic data set of Holland and Powell (1990). P-T estimates obtained by this method define a linear trend from approximately 8.7 kb, 790°C to 2 kb, 540°C (Fig. 20) (Hurlow et al., 1991; Hodges et al., 1992; McGrew and Peters, unpublished data). We believe that this steeply inclined P-T trend records decompressional metamorphism that accompanied exhumation of the East Humboldt Range from the Late Cretaceous to late Oligocene (see below). The samples yielding the lowest P-T estimates (2–4.2 kb, 540°C–650°C) include minerals such as muscovite that grew synkinematically with extensional shear-

ing as part of the equilibrium assemblage (Hurlow et al., 1991; Hodges et al., 1992; McGrew and Peters, unpublished data). Accordingly, these results represent the best estimate for P-T conditions accompanying mylonitic deformation. In addition, because the closure temperature range for $^{40}\text{Ar}/^{39}\text{Ar}$ dating of hornblende (480°C–580°C) overlaps these P-T estimates, cooling ages of 26–32 Ma in the northern Ruby Mountains (Dallmeyer et al., 1986) and 29–36 Ma at deep structural levels in the East Humboldt Range (McGrew and Snee, 1994) probably record the approximate timing of this final stage of metamorphic equilibration (see below).

Metacarbonate and metabasite mineral parageneses are largely compatible with the results from pelitic schists reported above. For a discussion of calc-silicate phase equilibria see the section on metamorphic fluids below. Metabasite mineral assemblages most commonly occur in small amphibolite bodies in the Paleoproterozoic and Archean gneiss sequences of Angel Lake near the northern end of the range. Characteristic assemblages commonly include amphibole + plagioclase ± biotite ± garnet ± quartz ± clinopyroxene ± ilmenite ± sphene ± magnetite ± rutile ± apatite ± chlorite. Many amphibolites contain moderately to severely resorbed garnet porphyroblasts surrounded by a symplectite of plagioclase ± hornblende ± biotite. This classic decompression texture lends additional support to the decompressional PTt-path outlined above. Depending on fluid activities, P-T results for the above assemblage range from 6.1 kb, 470°C for $a_{\text{H}_2\text{O}} = 0.1$ to 8.4 kb, 600°C for $a_{\text{H}_2\text{O}} = 1.0$ (Fig. 20) (McGrew and Peters, unpublished data). The temperature range for this sample corresponds quite closely with the closure temperature range for $^{40}\text{Ar}/^{39}\text{Ar}$ dating of hornblende, so an $^{40}\text{Ar}/^{39}\text{Ar}$ hornblende cooling age of 51.0 ± 2 Ma on a nearby amphibolite provides a plausible estimate for the timing of equilibration. The lower temperature of this P-T estimate as compared with pelitic assemblages raises the possibility that the amphibolite sample records a cooling event at this time that is not seen in the results from the metapelites.

Radiometric age constraints and an integrated PTt-path

A variety of radiometric age data including U-Pb, $^{40}\text{Ar}/^{39}\text{Ar}$, and fission-track data provide critical constraints on the timing of metamorphism in the East Humboldt Range. The key date constraining the timing of peak metamorphism (M_n) comes from a preliminary U-Pb, zircon age of 70–90 Ma (J. E. Wright, personal comm., 1992) on a small body of pegmatitic leucogranite collected in the hinge zone of the Winchell Lake fold-nappe. The leucogranite in question is clearly folded around the nose of the Winchell Lake fold-nappe, but larger-scale field relationships strongly suggest that it was emplaced synkinemati-

cally with the fold-nappe. It belongs to a suite of leucogranitic bodies that are strongly associated with a rusty-weathering, graphite-rich pelitic schist and paragneiss unit that forms a continuous, distinctive layer within the inferred Paleozoic miogeoclinal sequence on the upper limb of the Winchell Lake fold-nappe (McGrew, 1992). As this unit is traced into the hinge zone of the Winchell Lake fold-nappe, the volume percent of leucogranite increases gradationally but dramatically, from <25% to >65% over a distance of ~2 km. In addition, relict kyanite on the upper limb of the Winchell Lake fold-nappe occurs most commonly in this same unit, but it is completely replaced by sillimanite over this same interval. The volume percent of leucogranite in the weakly migmatitic marbles that surround these rocks show no systematic variations over this same interval. On the lower limb of the fold-nappe this same unit never exceeds 5 m in thickness, and in many localities it is completely absent or exists only as isolated rafts of graphitic, biotite-rich melanosome suspended in small bodies of leucogranite. Commonly, the leucogranite can be traced into the country rock where it forms small pods and seams intricately interdigitated with selvages of melanosome enriched in biotite, iron oxide, and graphite, suggesting an origin by localized partial melting. In any case, the observation that migmatitic layering clearly wraps around the fold hinge in combination with the fact that leucogranite isopleths cut the Winchell Lake fold-nappe, implies that leucogranite generation and emplacement was synkinematic to fold-nappe emplacement. Therefore, the Late Cretaceous U-Pb zircon age of 70–90 Ma referred to above probably dates both fold-nappe emplacement and a major syntectonic magmatic-metamorphic event (M_n). We suggest that the highest P-T results shown on Figure 20 (approximately 8.7 kb, 790°C) probably date from this time.

The thermal history of the East Humboldt Range following peak metamorphism in the Late Cretaceous depends mostly on $^{40}\text{Ar}/^{39}\text{Ar}$ and fission-track cooling age constraints summarized in Figure 21. Temperature estimates for pelitic assemblages in the northern half of the East Humboldt Range are all well above the nominal closure temperature range for $^{40}\text{Ar}/^{39}\text{Ar}$ dating of hornblende (480°C–580°C), and thus $^{40}\text{Ar}/^{39}\text{Ar}$ hornblende cooling ages bracket the age of metamorphism. For samples collected above 9600 ft (2930 m) this age limit is defined by hornblende cooling ages between 50 and 63 Ma (McGrew and Snee, 1994). However, at lower elevations final cooling through $^{40}\text{Ar}/^{39}\text{Ar}$ hornblende closure temperatures did not occur until the early Oligocene (30–36 Ma), resulting in a much broader age bracket. Samples from higher structural levels yield P-T estimates in the range 6.4 to 8.7 kb, 635°C to 800°C (for $a_{\text{H}_2\text{O}} = 1.0$), whereas those from deeper structural levels range from 4.5 to 9.1 kb and

PT Results, East Humboldt Range

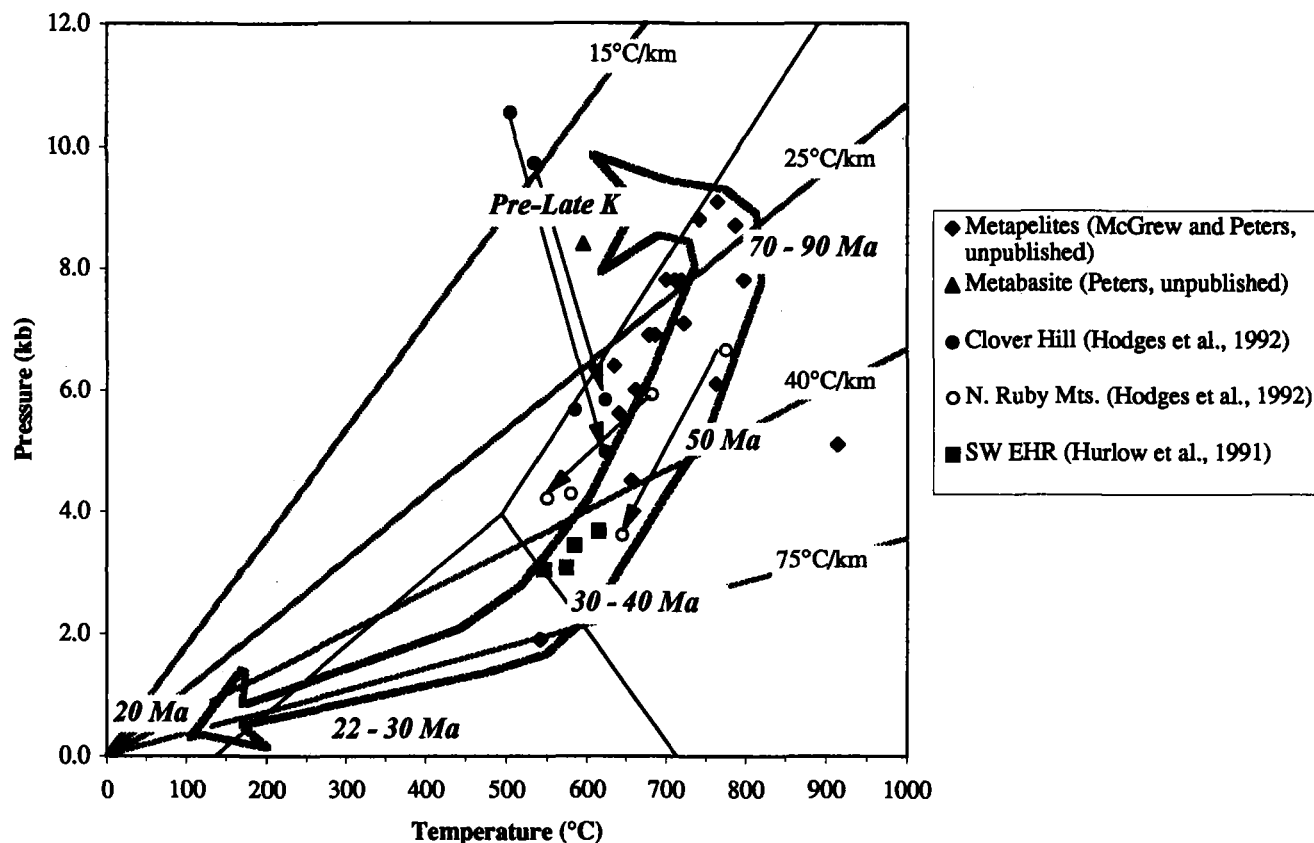


Figure 20. Synoptic diagram of P - T estimates from the central and northern East Humboldt Range determined by the authors using the updated, internally consistent thermodynamic data set of Holland and Powell (1990) and the Thermocalc computer program of Powell and Holland (1988) combined with previously published P - T results from elsewhere in the Ruby-East Humboldt metamorphic complex (Hurlow et al., 1991; Hodges et al., 1992). The large shaded arrow represents the general PTt -path inferred for the East Humboldt Range for late Mesozoic time to ~ 20 Ma. The light arrows represent P - T -paths based on Gibbs Method modeling of garnet zoning profiles reported in Hodges et al. (1992). Shaded lines provide reference geotherms of $15^\circ\text{C}/\text{km}$, $25^\circ\text{C}/\text{km}$, $40^\circ\text{C}/\text{km}$, and $75^\circ\text{C}/\text{km}$. The modern day geothermal gradient in the Basin and Range province is approximately $25^\circ\text{C}/\text{km}$, whereas the Battle Mountain heat flow high is characterized by geothermal gradients on the order of 40 – $75^\circ\text{C}/\text{km}$ (Lachenbruch and Sass, 1978). Stability fields for the Al_2SiO_5 polymorphs are also provided for reference (also calculated using the data of Holland and Powell [1990] and Powell and Holland [1988]).

640°C to 765°C (McGrew and Peters, unpublished data). The broader range in pressures recorded at deep levels suggests that the lower pressure samples were probably reset during reheating accompanying Oligocene extensional unroofing. In addition, one sample from the central part of the range yields a much lower pressure estimate of 2 kb, 540°C , and exhibits textural relationships that strongly imply that it reequilibrated during extensional shearing. This sample was collected at approximately the level of the transition between the younger and older hornblende cooling ages, so an Oligocene age for final equilibration is plausible (Hurlow et al., 1991; McGrew and Peters, unpublished data). Important implications of

this history are that the northern East Humboldt Range must have experienced ≥ 20 km of unroofing before it experienced dramatic cooling, and that over 7 km (> 2 kb) of this unroofing may have occurred before middle Eocene time. This lends credence to previously published suggestions that extensional unroofing in northeastern Nevada began as early as Eocene or even Late Cretaceous time (Hodges et al., 1992; McGrew and Snee, 1994; Camilleri and Chamberlain, 1997).

Following cooling through $^{40}\text{Ar}/^{39}\text{Ar}$ hornblende closure temperatures (480°C – 580°C), the cooling history of the northern East Humboldt Range is constrained mostly by $^{40}\text{Ar}/^{39}\text{Ar}$ mica and fission-track apatite cooling ages

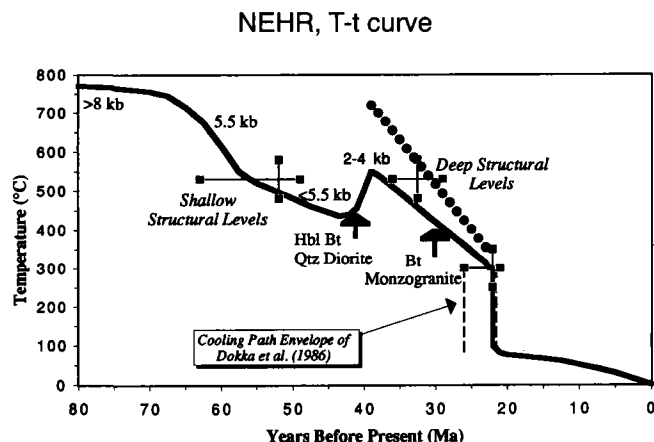


Figure 21. A proposed time-temperature history for the northern East Humboldt Range from the Late Cretaceous to Present, integrating the $^{40}\text{Ar}/^{39}\text{Ar}$ results of McGrew and Snee (1994) with older thermochronometric results (Dallmeyer et al., 1986; Dokka et al., 1986). Pressure estimates are also included, based on integration of P-T results reported by McGrew (1992), Peters (1992), and Hurlow et al. (1991) (see also Fig. 20). The solid curve represents relatively shallow structural levels (and thus also a lower temperature bound for relatively deep structural levels), whereas the dotted curve represents an upper temperature bound for relatively deep structural levels. Heavy arrows denote important igneous events: (a) intrusion of the hornblende-biotite quartz dioritic orthogneiss sheet at 40 ± 3 Ma and eruption of andesitic to rhyolitic tuffs; and (b) intrusion of biotite monzogranitic dikes and sheets at 29 ± 0.5 Ma (Wright and Snoke, 1993). We favor a distinct thermal pulse at the time of quartz dioritic intrusion and widespread ignimbrite eruption (~ 40 Ma), but we cannot rule out the alternative interpretation of gradual slow cooling from ~ 50 Ma to ~ 30 Ma.

(Dallmeyer et al., 1986; Dokka et al., 1986; McGrew and Snee, 1994). In any given area $^{40}\text{Ar}/^{39}\text{Ar}$ muscovite and biotite cooling ages are identical to each other and to fission-track apatite cooling ages within analytical uncertainties, thus implying cooling rates on the order of $100^\circ\text{C}/\text{m.y.}$ in the northern part of the range during the late Oligocene and early Miocene (Fig. 21) (Dokka et al., 1986; McGrew and Snee, 1994). In addition, $^{40}\text{Ar}/^{39}\text{Ar}$ mica cooling ages document diachronous cooling of the East Humboldt Range through $^{40}\text{Ar}/^{39}\text{Ar}$ biotite closure temperatures (250°C – 300°C), from ~ 32 Ma in the south to ~ 21 Ma in the north (Dallmeyer et al., 1986; McGrew and Snee, 1994). Moreover, geographic comparison of fission-track and mica cooling ages indicates that the southeastern part of the range had cooled through fission-track apatite closure temperatures ($\sim 110^\circ\text{C}$) while areas as little as 7 km to the west had not yet cooled through $^{40}\text{Ar}/^{39}\text{Ar}$ muscovite closure temperatures (300°C – 350°C). McGrew and Snee (1994)

show how these cooling age relationships could be explained by progressive rolling-hinge style unroofing of the footwall of a west-northwest-directed normal fault system.

METAMORPHIC FLUIDS: GEOCHEMISTRY, EVOLUTION, AND RELATIONSHIP TO LEUCOGRANITE PETROGENESIS

In this section we outline the relationship between fluid geochemistry and the metamorphic and magmatic evolution of the East Humboldt Range, with particular attention to the origin and significance of the abundant leucogranitic bodies that occur throughout the range. At relatively high structural levels throughout the northern half of the range, variations in leucogranite percentage are primarily controlled by the host lithology. Marbles and pure quartzites commonly contain $<10\%$ leucogranite, whereas pelitic or semi-pelitic units, impure metapsammitic rocks, and quartzo-feldspathic gneiss contain variable amounts of leucogranite, ranging from $<15\%$ to $>75\%$ by volume (McGrew, 1992).

At deeper structural levels, beneath the hornblende-biotite quartz diorite sill, leucogranite proportions in the paragneiss sequence of Lizzies Basin increase systematically and dramatically, from values generally $<50\%$ above 9400 ft (2865 m) to values $>65\%$ (locally $>90\%$) at elevations below 9000 ft. (2745 m) (see Fig. 7B in Camilleri et al., this volume) (McGrew, 1992; Peters and Wickham, 1995). Textural relationships, such as fine-scale interdigitations of leucosome and melanosome, suggest that some rocks represent in situ partial melts. However, the sheer volume of leucogranite suggests that a sizable fraction must have been externally-derived (Peters and Wickham, 1995). We refer to this sequence of extremely migmatitic rocks informally as the migmatite complex of Lizzies Basin, and we take the 65% leucogranite isopleth as its upper boundary, although it should be remembered that this boundary is actually gradational across a narrow interval. In addition, large, finger-like bodies of leucogranite originating from the Lizzies Basin migmatite complex locally penetrate upward into the overlying rocks. No age dates currently exist for the Lizzies Basin leucogranite suite, but we note that some of the leucogranitic bodies cut the 40-Ma quartz dioritic sill and 29-Ma monzogranitic sheets.

The roof of the migmatite complex of Lizzies Basin also coincides with an important oxygen isotope discontinuity (the contact between the lower zone and the upper zone in Figure 9) and with the nearly complete replacement of marble by calc-silicate rock below (Wickham and Peters, 1990; McGrew, 1992; Peters and Wickham, 1995). The metasedimentary rocks of the lower zone (i.e., the migmatite complex) exhibit uniformly low $\delta^{18}\text{O}$ values implying equilibration with a large, isotopically light fluid reser-

voir (see also Wickham and Peters, 1992; Wickham et al., 1993; Bickle et al., 1995). By contrast, the rocks of the upper zone show higher and generally more variable $\delta^{18}\text{O}$ values (Wickham and Peters, 1990; Peters and Wickham, 1995). Furthermore, all calc-silicate samples in the Lizzies Basin migmatite complex show extensive late-stage overgrowths of amphibole \pm epidote \pm garnet, suggesting a late-stage, high-temperature, H_2O -rich fluid infiltration event (Peters and Wickham, 1994). In addition, where this late-stage assemblage is well-developed at shallower structural levels it is generally associated with nearby leucogranites, further documenting the relationship between metasomatism and magmatism (Peters and Wickham, 1994; 1995). Finally, this late-stage assemblage occurs locally in extensional shear bands, pull-apart zones, or veins orthogonal to the extensional stretching lineation, suggesting a synextensional origin for both the migmatite complex of Lizzies Basin and the final episode of high-grade metamorphism.

SUMMARY AND CONCLUSIONS

The northern East Humboldt Range preserves a complex, evolving record of deep-crustal metamorphism, fluid infiltration, and anatexis during large-scale contractional and extensional tectonism from the late Mesozoic to early Miocene. Relict kyanite + staurolite assemblages record tectonic deep burial of the northern East Humboldt Range during the earliest stages of this history before the Late Cretaceous. Peak metamorphism occurred in the Late Cretaceous synkinematically with emplacement of a large, southward-closing recumbent fold-nappe, the Winchell Lake nappe. Peak metamorphism attained P–T conditions as high as 8.7 kb, 790°C, approaching or exceeding the second sillimanite isograd, and resulting in the generation and emplacement of abundant leucogranitic bodies. Primary assemblages in calc-silicate rocks may date from this time and indicate equilibration with an internally buffered([?]), CO_2 -rich pore fluid.

Following the Late Cretaceous the rocks experienced decompressional metamorphism through much of the Tertiary, with decompression of at least 2 kb (>7 km of unroofing) before approximately 50 Ma. Rocks at high

structural levels cooled through the closure temperature range for $^{40}\text{Ar}/^{39}\text{Ar}$ dating of hornblende (480°C–580°C) by ~50 Ma, but rocks at deeper structural levels did not finally close to argon diffusion in hornblende until early Oligocene time (30–36 Ma). During this time period, metamorphism at conditions of at least 2.0–4.2 kb, 540°C–650°C developed synkinematically with the early stages of west-northwest-directed extensional mylonitic deformation. However, fault rocks in the northern East Humboldt Range show a continuous ductile through brittle deformational evolution. In addition, $^{40}\text{Ar}/^{39}\text{Ar}$ mica and fission-track cooling age constraints indicate that the East Humboldt Range was ultimately exhumed by diachronous unroofing in the footwall of an evolving, west-rooted normal fault system from the late early Oligocene to early Miocene (Mueller and Snoke 1993a).

Secondary subassemblages of amphibole + epidote + garnet in calc-silicate rocks probably also grew during synextensional Oligocene metamorphism, recording intensive metasomatism by water-rich brines that probably came from crystallization of abundant leucogranitic bodies at deep structural levels. During this late stage, H_2O -rich fluid infiltration event metamorphic conditions probably evolved from early high temperature (600°C–750°C) to later, lower temperature conditions (<525°C). Pervasive fluid infiltration at deep structural levels produced wholesale reequilibration and homogenization of the oxygen isotope systematics to uniformly low values of $\delta^{18}\text{O}$. We suggest that the leucogranitic melts acted as a proxy, or vector of transport for fluids that ultimately derived from injection of mantle-derived basaltic magma at lower crustal levels. In contrast, rocks at higher structural levels show higher and more variable values of $\delta^{18}\text{O}$ that reflect the original sedimentary isotope systematics. If these conclusions are true, then much of the deep crust of northeastern Nevada may have been buffered at melting conditions during the primary phases of extensional tectonism and metamorphic core complex development. Consequently, we envision a deep-crustal environment that was rheologically weak and subject to asthenosphere-like flow on geologically reasonable time-scales.

Grand Tour—Part 3: Geology and petrology of Cretaceous and Tertiary granitic rocks, Lamoille Canyon, Ruby Mountains, Nevada

SANG-YUN LEE
CALVIN G. BARNES

Department of Geosciences, Texas Tech University, Lubbock, Texas 79409-1053

INTRODUCTION

Deep structural levels of the Ruby Mountains core complex are exposed in the Lamoille Canyon area (Figs. 1 and 16). Howard (1980) showed that the proportion of granitic rocks increases structurally downward, and cross-sections by MacCready et al. (in press) show that several granitic units in the Ruby Mountains were deformed during development of the core complex. Therefore, Lamoille Canyon is an excellent locality to study the structural and petrogenetic relationships between core complex formation and granitic magmatism.

Here, we report the results of field studies and preliminary laboratory analysis of granitic rocks collected predominantly from upper Lamoille Canyon. The field data show that consistent cross-cutting relationships are present, which permits identification of distinct, mappable granitic rock units. The geochemical data indicate that many of these units are compositionally distinct and that more than a single petrogenetic mechanism is necessary to explain their origins.

IGNEOUS ROCKS OF THE LAMOILLE CANYON AREA

The intrusive sequence was determined on the basis of cross-cutting relationships, an example of which is shown in Figure 22. From oldest to youngest, the sequence is equigranular muscovite-biotite granitic gneiss (Kgn), sillimanite-bearing pegmatitic two-mica granitic gneiss (Kt), a suite of biotite monzogranites (Tbm), fine-grained biotite tonalite dikes (Tdd), and undeformed biotite-muscovite granitic pegmatite (Tp).

Equigranular muscovite-biotite granitic gneiss (Cretaceous or Jurassic)

This unit consists of medium- to coarse-grained, equigranular muscovite-biotite monzogranitic and leucogranitic gneiss. Foliation is typically well developed and gneissic

banding is common. This rock unit is composed of medium- to coarse-grained anhedral quartz, alkali feldspar, and plagioclase. Biotite and muscovite occur as subhedral grains in a groundmass of alkali feldspar, quartz, and plagioclase. Anhedral garnet is locally present, as are rare sillimanite grains. The gneissic texture that is apparent in the field is less clear in most thin sections.

Sillimanite-bearing two-mica granitic gneiss (Cretaceous)

This unit, qualitatively the most abundant in the area, is coarse- to very coarse-grained (commonly pegmatitic) sillimanite-bearing two-mica granitic gneiss. It grades into muscovite-bearing pegmatitic granitic gneiss which locally has the appearance of leucosomes in host two-mica pegmatitic gneiss. On outcrop scales, the unit forms networks of sills and dikes, or irregular bodies. Metasedimentary enclaves are common.

Biotite is more abundant than muscovite, except in the pegmatitic rocks. Accessory garnet is sparse. Where present, sillimanite most commonly occurs as needles and fibrolitic mats in biotite. Perthitic alkali feldspar crystals form large anhedral plates. Plagioclase is commonly sericitized and myrmekite is also common.

Age of the gneissic units

Monazite from a sillimanite-bearing, pegmatitic muscovite leucogranite collected near the Terraces day-use area in upper Lamoille Canyon (STOP 3-3) yielded a Late Cretaceous age (data cited in Wright and Snoke, 1993). We view this rock as correlative with the sillimanite-bearing two-mica granitic gneiss. At all locations where cross-cutting relations were observed, this unit cuts the equigranular muscovite-biotite granitic gneiss (e.g., Fig. 19C). Therefore, the latter unit is Late Cretaceous or older in age. The close association of these two units in the field, and locally indistinct contacts, suggest that the two share

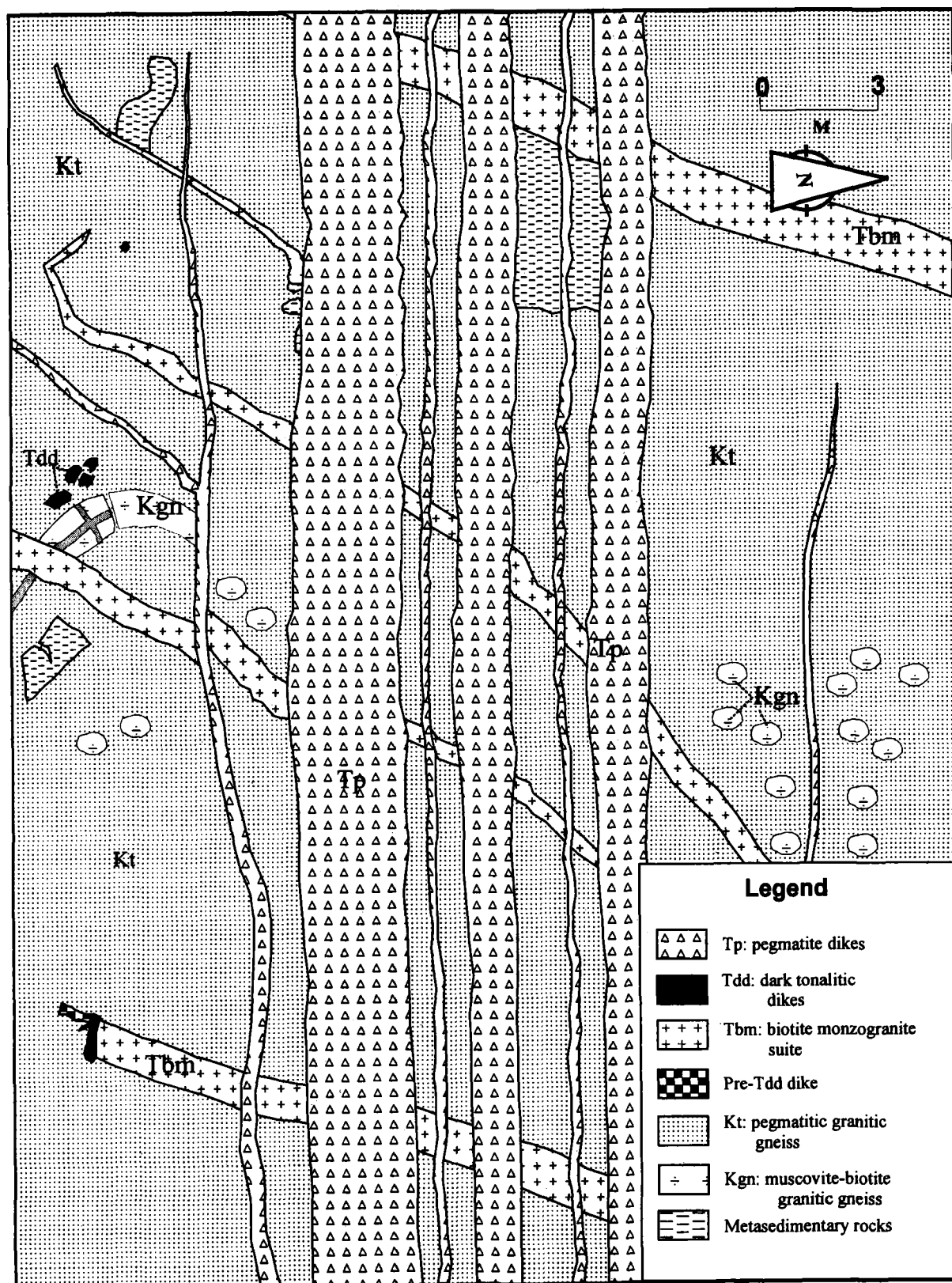


Figure 22. Simplified outcrop sketch map of cross-cutting relationships in upper Lamoille Canyon.

similar ages. As shown below, they also share similar geochemical features, so both are thought to be Late Cretaceous in age.

Biotite monzogranite suite (Oligocene)

This unit consists of massive to foliated, medium-grained, equigranular biotite monzogranitic dikes and sheets, some of which form interconnected networks. These intrusions cut earlier granitic gneisses as well as foliation, folds, and lithologic layering in the host rocks (Howard, 1980; Wright and Snoke, 1993). Biotite-rich schlieren were observed locally, particularly near the base of a shallowly-dipping sheet in upper Lamoille Canyon.

In thin section, quartz, alkali feldspar, and plagioclase are subhedral to anhedral. Poikilitic alkali feldspar crystals enclose sericitized plagioclase and irregularly-shaped, fine-grained quartz. Biotite is the predominant varietal mineral, but blue-green hornblende is sparsely present. Accessory minerals are apatite, allanite, zircon, and opaque oxides. Muscovite locally replaces plagioclase and sericite is common, as is myrmekite. The biotite monzogranite intrusions are cut by leucocratic muscovite-biotite monzogranitic dikes. Many of these dikes are composite, with rims of pegmatite and cores of medium-grained leucocratic monzogranite. The leucocratic dikes are petrographically similar to the biotite monzogranite, but magmatic muscovite and sparse garnet are present. A complete compositional gradation exists between the biotite monzogranite and leucocratic monzogranite (see below); therefore, we treat them as the "biotite monzogranite suite."

Zircon fractions from biotite monzogranite suite dikes yielded discordant U-Pb ages with lower intercepts of ~29 Ma (Wright and Snoke, 1993; MacCready et al., in press). These ages are similar to ages of biotite monzogranitic dikes elsewhere in the Ruby Mountains and East Humboldt Range and were interpreted to be crystallization ages (Wright and Snoke, 1993).

Tonalitic dikes (Oligocene?)

Fine-grained biotite tonalitic to quartz dioritic dikes intrude both of the gneissic units. These dark-colored dikes also locally intrude rocks of the Oligocene biotite monzogranite suite. However, leucogranitic two-mica monzogranites of this suite cut the tonalitic dikes. Nevertheless, the intrusive relationships of this unit are commonly unclear because it crops out as irregular, discontinuous dikes (Fig. 19A). Most samples are fine- to medium-grained, weakly foliated, assemblages of anhedral to subhedral plagioclase, quartz, and biotite. Blue-green hornblende is present in some of the most mafic samples, and muscovite,

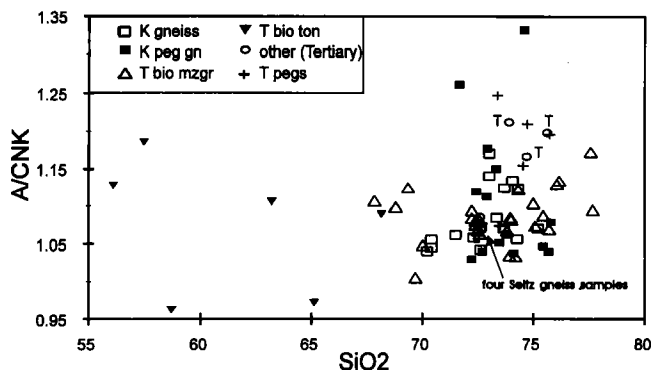


Figure 23. A/CNK (molar Al_2O_3 divided by the sum of CaO , Na_2O , and K_2O) plotted against SiO_2 for Cretaceous and Tertiary granitic rocks from the Lamoille Canyon area.

alkali feldspar, zircon, and minute prismatic apatite are accessory minerals.

Pegmatitic dikes (Oligocene?)

The youngest granitic intrusions in Lamoille Canyon are undeformed muscovite- and biotite-muscovite pegmatitic granite. They form parallel-walled dikes that range up to at least 5 m wide and are locally associated with aplitic garnet-bearing muscovite leucogranite. Alkali feldspar crystals range in diameter to at least 30 cm and graphic texture is common. These Tertiary pegmatitic dikes are distinct from the Cretaceous ones in their lack of deformation, predominance of muscovite over biotite, lack of sillimanite, and more common occurrence of garnet. Where these pegmatites cut calc-silicate wall rocks, garnet-idocrase-diopside skarns are common.

Other analyzed granitic rocks: gneiss of Seitz Canyon (Tertiary, Cretaceous, or Jurassic?) and gneiss of Thorpe Creek (Eocene)

The gneiss of Seitz Canyon crops out in the core of the Lamoille Canyon fold-nappe (Howard, 1980; see also mileage point 62.85 on DAY THREE). It is a medium- to coarse-grained biotite granodioritic orthogneiss with traces of garnet and muscovite. A cross-cutting medium-grained biotite monzogranitic gneiss is tentatively considered to be part of the Seitz gneiss. Muscovite and euhedral garnet are varietal minerals; accessory minerals are apatite and zircon. Myrmekitic intergrowths occur next to large poikilitic alkali feldspar.

The orthogneiss of Thorpe Creek is a medium-grained, garnet-biotite-muscovite leucogranitic gneiss that is locally sillimanite-bearing (see mileage point 59.9 on DAY THREE). Wright and Snoke (1993) reported a U-Pb (mona-

GEOCHEMICAL DATA

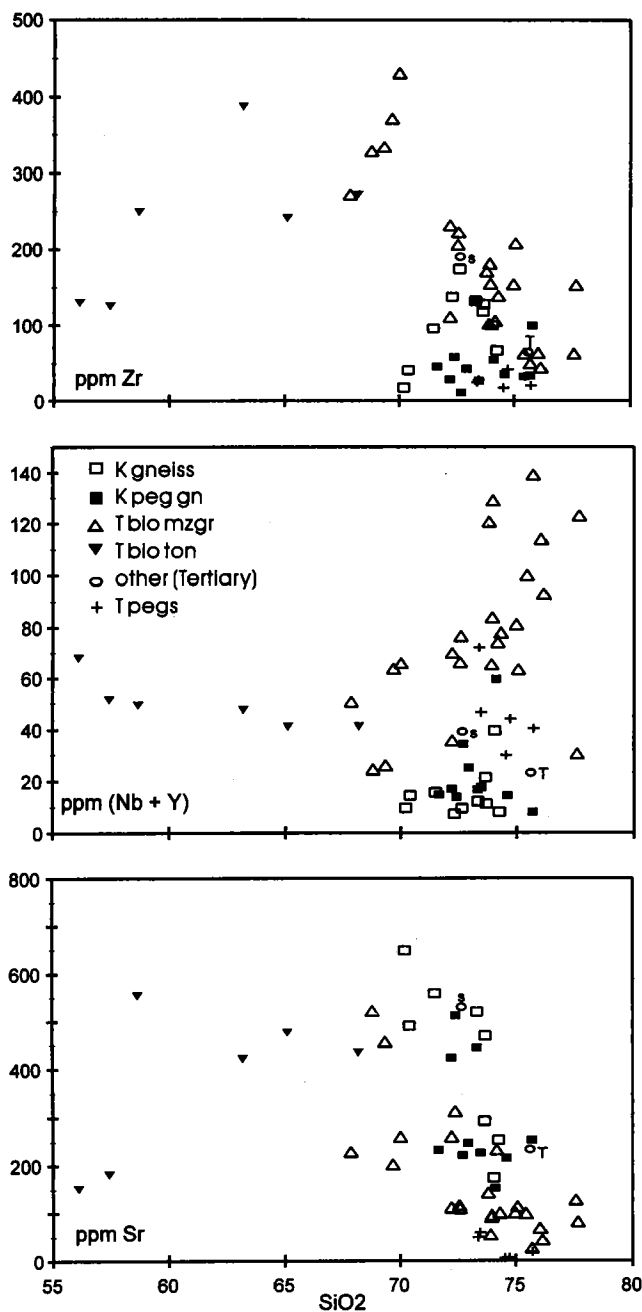


Figure 24. Zr, (Nb+Y), and Sr abundances plotted against SiO_2 for Cretaceous and Tertiary granitic rocks in the Lamoille Canyon area. Data points for Thorpe Creek and Seitz Creek gneisses labelled with "T" and "S," respectively.

zite) age of ~ 39 Ma. MacCready et al. (in press) have analyzed additional monazite samples of the orthogneiss of Thorpe Creek that yield dates that range from 36.1 to 37.9 Ma. Both Wright and Snoke (1993) and MacCready et al. (in press) conclude that these dates indicate an Eocene crystallization age.

Most of the data used in this report were obtained by ICP-AES analysis for major and trace elements at Texas Tech University. Rb was determined by flame emission and the rare-earth elements (REE), Th, U, Ta, and Hf by INAA at Oregon State University as part of the DOE Reactor Sharing Program. Additional data are from the U.S. Geological Survey (K. A. Howard, written comm., 1996).

Granitic rocks from the Lamoille Canyon area are predominantly peraluminous. That is, A/CNK , molar $\text{Al}_2\text{O}_3/(\text{CaO} + \text{Na}_2\text{O} + \text{K}_2\text{O}) > 1$ (Fig. 23). Most samples are silica rich, in accord with their granitic nature, but it is noteworthy that less evolved compositions are present, particularly among the biotite monzogranite suite.

Cretaceous(?) granitic and pegmatitic gneisses

These gneisses occupy a rather narrow range of major element contents. Although their compositions tend to overlap, the muscovite-biotite granitic gneiss has higher contents of total iron (Fe_2O_3^*) and MgO, and $\text{Na}_2\text{O}/\text{K}_2\text{O}$ ratios > 1 , compared to the pegmatitic gneiss. The latter unit is also characterized by higher Al_2O_3 , K_2O , and $A/\text{CNK} > 1.12$, and by its low $\text{Na}_2\text{O}/\text{K}_2\text{O}$ ratios (< 1). The gneissic units display large variations of Rb, Sr, and Ba, and are Sr-rich compared with Oligocene biotite monzogranites with similar SiO_2 contents. In contrast, abundances of Zr, and especially Nb, and Y are relatively low when compared to younger granites (Fig. 24). Rare-earth element contents (Fig. 25) are highly fractionated ($\text{La}_N/\text{Lu}_N = 49\text{--}165$) and the heavy REE are strongly depleted, which results in steep negative slopes. Most REE patterns for these samples lack Eu anomalies.

Tertiary(?) tonalitic, granitic, and pegmatitic rocks

The tonalitic samples contain relatively low silica abundances (< 68 wt% SiO_2 ; Fig. 23) and are characterized by relatively high Al_2O_3 (most > 17 wt.%), Fe_2O_3 (> 5.2 wt.%), MgO (> 1.1 wt.%) and CaO (> 2.7 wt.%) contents. In spite of their relatively mafic nature, their A/CNK values are larger than 1.1. These values reflect the high proportions of biotite in the tonalitic rocks. The biotite monzogranite suite displays the widest range of elemental contents (Fig. 26). Most elemental abundances decrease with increasing SiO_2 , but K_2O , Na_2O , and Rb are exceptions. The lowest silica samples (< 70 wt.% SiO_2) are broadly similar in elemental contents to the most siliceous tonalites. Leucocratic members of this suite are all high silica (> 74 wt.% SiO_2).

In comparison with the Cretaceous(?) gneisses, the tonalites and biotite monzogranite suite are characterized

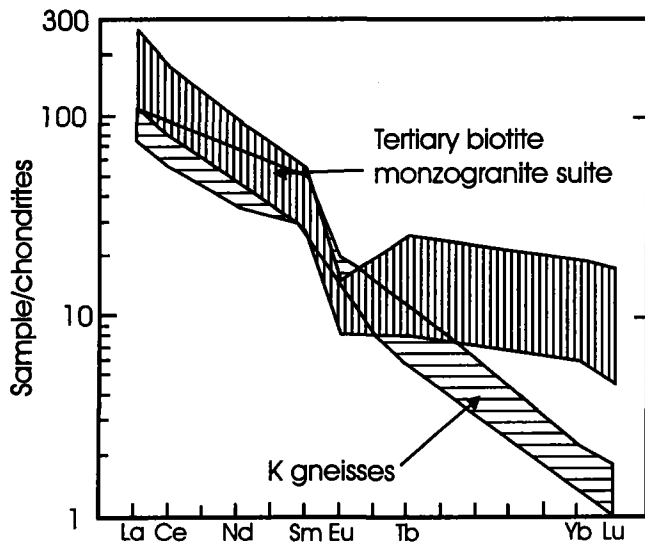


Figure 25. Plots of rare earth element abundances. The field with horizontal ruling is for Cretaceous(?) monzogranitic and pegmatitic gneisses. The field with vertical ruling is for the biotite monzogranite suite.

by higher, and relatively variable, contents of Zr, and especially Y and Nb (Fig. 24). Zr abundances tend to decrease with increasing SiO_2 , but Y and Nb behave incompatibly. This relationship is best seen when Rb is used as a differentiation index (Fig. 27) because SiO_2 values vary only slightly among the leucocratic granites.

REE patterns for samples of the biotite monzogranite suite (Fig. 25) are characterized by a "dog-leg," with nearly flat HREE patterns and HREE abundances $\sim 7\text{--}15\times$ chondrites. All of these samples have negative Eu anomalies. Resultant La_N/Lu_N ratios are in the range of 6 to 36. In general, light REE abundances decrease with differentiation, whereas heavy REE abundances increase. This type of variation suggests that REE abundances are controlled by light REE-rich, accessory phases such as allanite and/or monazite.

The late pegmatitic dikes exhibit the lowest Fe_2O_3^* , MgO, CaO, TiO_2 contents. The $\text{Na}_2\text{O}/\text{K}_2\text{O}$ ratios are variable for this rock unit. All are alumina oversaturated; four of the five analyzed samples have $\text{A}/\text{CNK} > 1.15$. Abundances of Sr and Ba are quite low (< 59 ppm and < 52 ppm, respectively), as are Zr contents (< 50 ppm).

Samples of the gneiss of Thorpe Creek are strongly peraluminous (Fig. 23) and the single sample analyzed for trace elements is broadly similar to the Cretaceous gneisses in terms of Sr and Nb + Y contents (Fig. 24). Except for high Sr contents, the few analyses of the gneiss of Seitz Creek are similar to the biotite monzogranites.

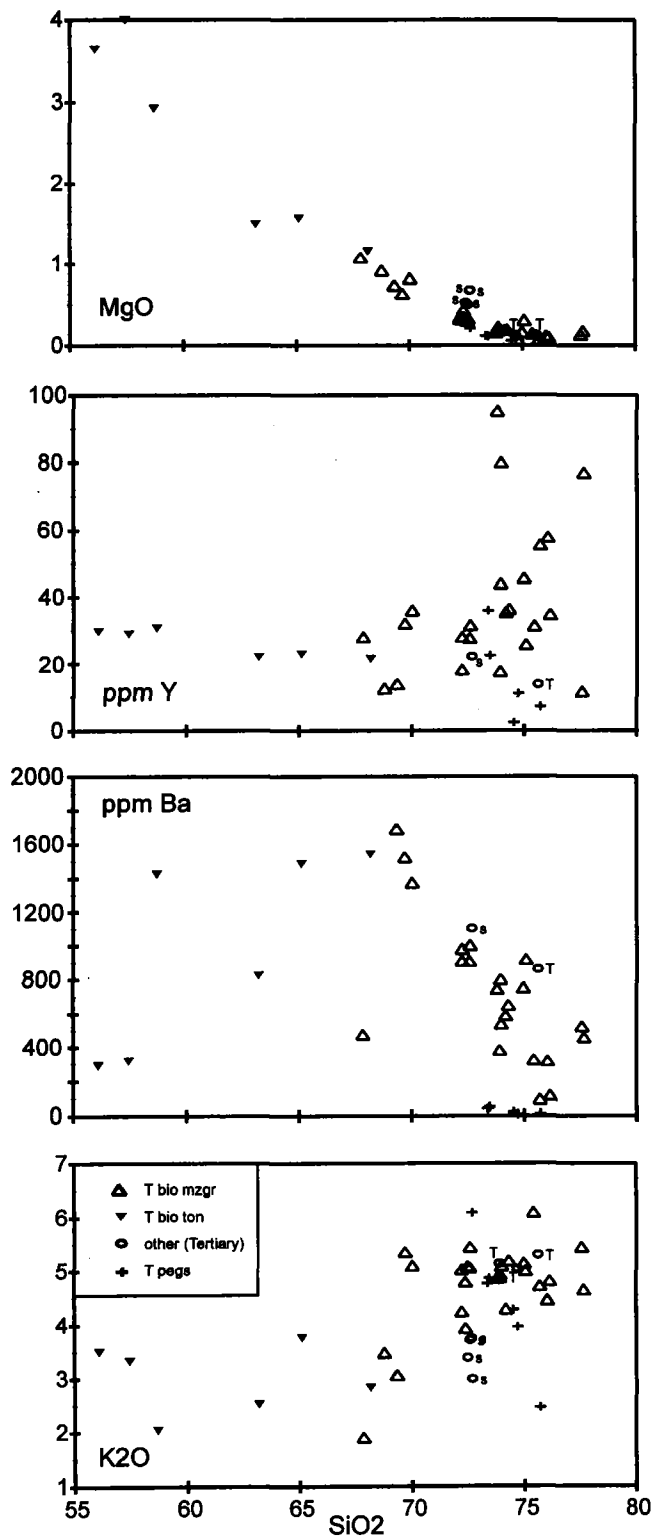


Figure 26. Major oxides and trace element concentrations plotted against SiO_2 for the Tertiary tonalitic dikes and granitic rocks from Lamoille Canyon. "S" and "T" label Seitz Creek and Thorpe Creek gneisses, respectively.

PETROGENETIC CONSIDERATIONS

Cretaceous(?) granitic and pegmatitic gneisses

Limited isotopic data for the Cretaceous pegmatitic gneisses ($^{87}\text{Sr}/^{86}\text{Sr} = 0.72609$, $\epsilon\text{Nd} = -15.1$, Wright and Snoke, 1993; $\delta^{18}\text{O}(\text{qtz}) = +13.0$, H. Karlsson, unpublished data) combined with their high $\text{K}_2\text{O}/\text{Na}_2\text{O}$, and strongly peraluminous nature suggests crustal anatexis of metasedimentary rocks as a likely origin. The markedly depleted heavy REE patterns and low Y contents of these samples indicate that garnet was residual in the source region. Furthermore, Eu anomalies are small or absent among these samples, and Sr contents are relatively high. These features suggest that feldspars were not important residual minerals during the melting event. If one assumes a metasedimentary source, as indicated by the isotopic data, such features are consistent with one of two conditions in the source region: partial melting under H_2O -saturated conditions with feldspars melting nearly entirely in early (low-T) melt fractions, or partial melting of an eclogitic assemblage in which feldspars were entirely absent (e.g., Martin, 1987). In either case, garnet was residual, which is indicative of relatively high-pressure anatexis.

Zircon saturation temperatures for these rocks are low (639°C to 749°C), which is also consistent with relatively high H_2O contents. Inasmuch as these temperatures represent near-solidus conditions, comparison with experimental melting studies of haplogranite is appropriate (Ebadi and Johannes, 1991) and suggests H_2O activity between 0.5 and 1.0.

Finally, Late Cretaceous (~ 83 – 75 Ma) magmatism is broadly associated with crustal thickening during the Sevier orogeny (e.g., Wright and Wooden, 1991; Camilleri and Chamberlain, 1997). The relatively high pressures implied by residual garnet in the source region is consistent with an origin of the Cretaceous(?) granitic gneisses by anatexis of deep-seated crustal rocks during the peak of Sevier-age metamorphism.

Tertiary tonalitic and monzogranitic rocks

Initial $^{87}\text{Sr}/^{86}\text{Sr}$ and ϵNd values for the biotite monzogranite suite belong to an array of isotopic data that Wright and Snoke (1993) and Wright and Wooden (1991) interpreted as a mixing line between mantle-derived magmas and partial melts of Proterozoic basement rocks. Similar explanations were proposed for Tertiary volcanic rocks in the Snake and Egan ranges to the south (Gans et al., 1989; Feeley and Grunder, 1991; Grunder, 1992). If the tonalitic rocks are assumed to be associated with the biotite monzogranite suite, the geochemical data are consistent with a mixed source. In such a case, the tonalitic rocks would represent magmas with higher proportions of mantle component, whereas the leucogranitic members of

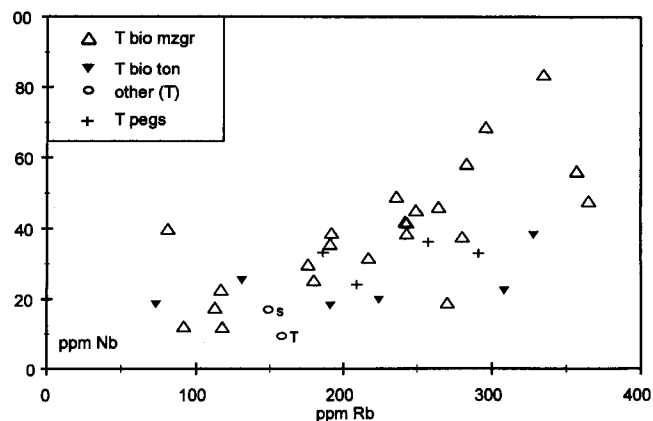


Figure 27. Nb content plotted against Rb for tonalitic dikes and biotite monzogranitic suite. Note the positive correlation between the two elements which is an indication that both elements are incompatible in the biotite monzogranite suite.

the biotite monzogranite suite would represent crustal melts. However, our preliminary work suggests that the trend from tonalitic to biotite monzogranitic rocks could be a fractional crystallization trend. Furthermore, trace element compositions suggest that two distinct compositional populations might exist among the monzogranite suite. Thus, a thorough understanding of the origin of the Tertiary granitic and tonalitic rocks will require more detailed geochemical and isotopic data and modeling.

At the present time, we can say that the rock compositions do not plot near minimum-melt compositions for water-saturated granites in the normative Ab-Or-Qz system, but instead cluster near an anhydrous 4 kb, 1000°C minimum determined by Steiner et al. (1975). Higher magmatic temperatures are consistent with zircon saturation temperatures, which range from 807°C to 867°C . By comparison to experimentally determined solidus conditions, zircon saturation temperatures indicate activities of H_2O less than 0.35 (Ebadi and Johannes, 1991), consistent with the low H_2O contents implied by normative compositions.

No matter what the origin of the Tertiary granites, their prominent Eu anomalies and compatible behavior of Sr and Ba (but not Rb) indicate that residual plagioclase and alkali feldspar played a significant role in differentiation. The lack of heavy REE depletion shows that garnet did not. In addition, whether the granites formed by fractional crystallization, partial melting, or mixing, the anticorrelation of light and heavy REE contents indicates that one or more accessory minerals controlled REE concentrations.

Tectonic discrimination diagrams

For those who appreciate discrimination diagrams for granitic rocks, we provide the following. Diagrams that

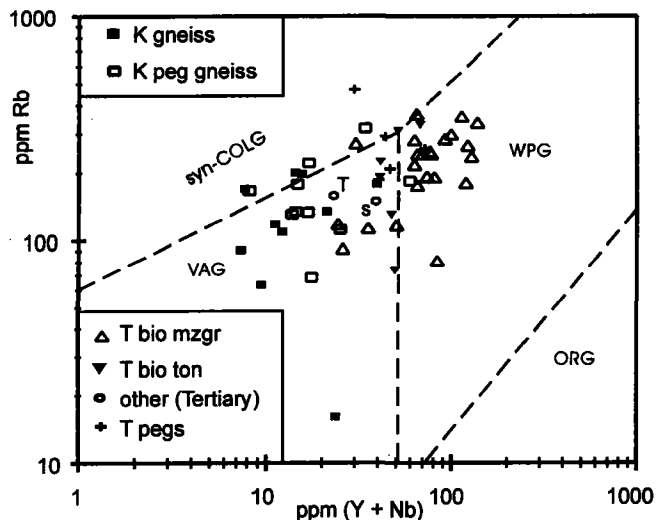


Figure 28. Discrimination diagram (Pearce et al., 1984). Note the clear distinction between "K" (Cretaceous[?]) granitic gneisses and the "T" (Tertiary) biotite monzogranite suite on the basis of Y+Nb contents. VAG = volcanic-arc granites, ORG = ocean-ridge granites, WPG = within-plate granites, syn-COLG = syn-collisional granites.

utilize Rb, Y, and Nb contents (Fig. 28; Pearce et al., 1984) imply a volcanic arc setting for the Cretaceous(?) muscovite-biotite granitic gneiss. However, compositions of the Cretaceous pegmatitic gneiss, which show a geochemical relationship to the older gneissic unit, plot in a scattered zone among the syn-collisional and volcanic arc fields.

The Oligocene biotite monzogranite suite plots in the within-plate granitic field. Its geochemical characteristics, high concentrations of high field strength elements (Zr,

Nb, Y, etc.), combined with high $\text{Fe}_2\text{O}_3^*/\text{MgO}$ and low transition metal concentrations, are consistent with a classification as A-type granite (Loiselle and Wones, 1979). However, although A-type granites are commonly thought to be fluorine-rich (e.g., Eby, 1990), normative Ab-Or-Qz compositions of the biotite monzogranite suite lack evidence of fluorine control of melt compositions.

Conclusions

Granitic rocks in the Lamoille Canyon area can be broadly divided into at least two groups: Cretaceous(?) granitic and pegmatitic gneisses and Tertiary granitic gneisses and monzogranites, tonalites, and related rocks. The youngest granitic magmatism in the area is represented by undeformed pegmatitic dikes. The older gneissic rocks are distinct in their higher concentrations of Sr, their lower concentrations of Nb, Y, and Zr, their steep REE patterns with strongly depleted heavy REE, and their lack of appreciable Eu anomalies. These features suggest an origin by crustal melting at conditions where garnet was a residual mineral but feldspars were not. Such an origin is consistent with deep-seated melting of crust thickened during the Sevier orogeny. Tertiary tonalitic dikes and the biotite monzogranite suite may represent a compositionally extended suite of related magmas. Their rather complex trace and major element behaviors can presently be explained in several ways, including anatexis of widely variable Proterozoic crust, source mixing among crustal and mantle reservoirs, and mixing of mantle- and crustally-derived magmas. In all cases, fractional crystallization is likely to have played a role as well. Therefore, a thorough understanding of these granites requires further detailed analytical work and modeling.

Grand Tour—Part 4: Geology and geochemistry of the Harrison Pass pluton, central Ruby Mountains, Nevada

BRADFORD R. BURTON

Department of Geology and Geophysics, University of Wyoming, Laramie, Wyoming 82071-3006

CALVIN G. BARNES

TRINA BURLING

Department of Geosciences, Texas Tech University, Lubbock, Texas 79409-1053

JAMES E. WRIGHT

Department of Geology and Geophysics, Rice University, Houston, Texas 77005

ABSTRACT

Harrison Pass pluton is a late Eocene, composite granitoid body with related mafic and hypabyssal rocks. The pluton was emplaced at upper-crustal levels probably during the initiation of a phase of large-magnitude crustal extension that resulted in the eventual exhumation of the Ruby Mountains core complex. Post-emplacement tilting facilitated the exposure of a partial cross section of the pluton from a roof zone exposed on the east side of the range to granitic rocks on the west side of the range that were originally about 5 km deeper than the roof zone.

The pluton is composed of two distinct suites of granitic rocks. The oldest suite consists of granodiorite and minor, related rock types that occupy the structurally higher eastern half of the pluton. Compositional variation within the weakly peraluminous to metaluminous granodioritic suite can be explained by crystal fractionation and magma-mixing processes. This plutonic suite was the magmatic source of hypabyssal dikes and sills that cut country rocks in the roof zone. Emplacement of the granodioritic suite was accommodated by stoping, wall-rock shortening, and uplift.

Slightly younger granitic rocks comprise the monzogranitic suite which underlies much of the western half of the pluton. Three distinct rock types are recognized: two-mica monzogranite which forms a body informally called the “granite of Green Mountain Creek,” other two-mica monzogranitic rocks, and biotite monzogranite. These granitoids are peraluminous and chemically, but not isotopically, similar to Jurassic monzogranite exposed in the central Ruby Mountains. Except for the granite of Green Mountain Creek, much of the monzogranitic suite consists of layered, tabular units that were emplaced as composite sheets intruded into rocks of the granodioritic suite.

INTRODUCTION

The central Ruby Mountains are a zone of transition between the metamorphic and igneous infrastructure of the Ruby Mountains core complex to the north, and low-grade to non-metamorphosed rocks to the south (Fig. 1) (Hudec, 1990, 1992; Snoke et al., 1990b). During the late Eocene, this transition zone was intruded by the composite Harrison Pass pluton (Fig. 1), which underlies an area of subdued topography on either side of Harrison Pass. U-Pb

zircon geochronology indicates that the two major intrusive units of the pluton were emplaced ~36 Ma (Wright and Snoke, 1993). The Harrison Pass pluton and its wall rocks were then cut by a large-magnitude, normal-sense, plastic-to-brittle fault zone called the Ruby Mountains shear zone. Discontinuities in mid- to lower-crustal density and seismic velocity indicate that the Harrison Pass pluton also lies above a major, northward-dipping crustal structure (Stoerzel, 1996). Eastward tilting of the footwall of

the Ruby Mountains shear zone has exposed a partial cross-section through the Harrison Pass pluton (Kistler et al., 1981).

Harrison Pass pluton is particularly interesting in regard to core complex development, because magmatism occurred just prior to, or perhaps concurrent with, large-magnitude crustal extension and exhumation of the Ruby Mountains core complex. Cooling of the pluton through the closure temperature for ^{40}Ar in biotite occurred by 35 Ma in parts of the eastern roof zone, and by 25 Ma in the western part of the pluton (Kistler et al., 1981). Thus, the pluton represents a short-duration, high-intensity thermal-magmatic episode in the development of a core complex during which at least four distinct granitoid magmas were generated and emplaced.

GEOLOGY OF THE HARRISON PASS PLUTON

Harrison Pass pluton is exposed over an area of more than 110 km² (43 sq mi) in the central Ruby Mountains (Figs. 1 and 29). A thickness of more than 1,200 m (4,000 ft) of plutonic rocks is exposed, but the true overall thickness of the pluton is unknown. Wide-angle seismic reflection studies conducted along Ruby Valley road, east of the pluton, and a short seismic line recorded between Ruby Valley and Harrison Pass do not image the base of the intrusion (Stoerzel, 1996), nor do gravity and aeromagnetic data from the area define this subsurface boundary. Field relations indicate that most of the monzogranite intrusive units are tabular in shape and dip gently to moderately eastward, whereas the granodiorite unit, and the "granite of Green Mountain Creek" (petrographic description provided later in this article) are internally massive to foliated. Fabric elements are roughly parallel to adjacent wall-rock contacts.

The exposed part of the Harrison Pass pluton is interpreted to represent an upper-crustal cross section from deeper structural levels in the west, to shallower levels in the east (Fig. 30). This interpretation is supported by the observation that the Paleozoic sedimentary rocks of the southern Ruby Mountains, which are intruded by the Harrison Pass pluton, comprise a monotonous eastward-dipping homocline (Sharp, 1942; Willden et al., 1967; Willden and Kistler, 1967, 1969, 1979). In the pluton, hypabyssal dikes, stopped blocks, and porphyries are more common along the eastern margin of the pluton, suggesting that this area was structurally higher than the western part of the body. Perhaps the most convincing evidence of variation in structural level across the exposed part of the Harrison Pass pluton is the biotite K-Ar age contours delineated by Kistler et al. (1981, their figure 1). These data indicate a biotite K-Ar age progression from <25 Ma on the west side of the pluton to ≥ 35 Ma on the east side of the pluton.

This systematic progression in biotite K-Ar cooling ages thus suggests eastward tilting of the range subsequent to the emplacement of the ~ 36 -Ma pluton. Fission-track data on apatite and zircon as summarized in Blackwell et al. (1984, 1985) and Reese (1986) also support eastward tilting of the range, although additional thermochronologic studies are in progress to further explore the post-emplacement kinematic history.

PLUTONIC UNITS

Harrison Pass pluton is a composite granitic body consisting of two major intrusive suites: the granodioritic and monzogranitic suites, each characterized by a variety of rock types (Snoke and Lush, 1984; Wright and Snoke, 1993). The suites differ in relative age, mechanisms of emplacement, geochemistry, and petrogenesis.

Granodioritic suite

Granodioritic rocks comprise the bulk of the oldest intrusive suite (Fig. 29). These rocks are present at all levels of the pluton and are the principal rock type in the structurally highest part of the pluton which includes part of the original roof zone. Small bodies of granodiorite also occur within wall rocks along the western extent of the southern margin of the pluton; it is apparent that granodioritic magma occupied deeper structural levels of the pluton. This intrusive suite consists mainly of granodiorite, but includes related tonalite, quartz monzonite, and biotite monzogranite (Fig. 31). Several mela- and leucocratic varieties are also present. Contacts between these small-volume units are only locally observed, and the granodiorite suite is mapped as a single unit (Fig. 29). Within the granodiorite unit is a distinctive biotite monzogranite, here informally called the "granite of Corral Creek" for outcrops near the head of Corral Creek; the unit is also exposed along Harrison Pass Creek (Fig. 29). External contacts of the granite of Corral Creek cut a fabric in the granodiorite defined by aligned feldspar megacrysts. This relationship suggests that the granite of Corral Creek is younger than the granodiorite; however, it is geochemically gradational with the granodiorite. Conversely, the granite of Corral Creek is geochemically distinct from rocks of the monzogranitic suite.

Rocks of the granodioritic suite are coarse- to very coarse-grained, and contain megacrysts of alkali feldspar. Biotite is the principal mafic mineral; hornblende is most common as a constituent mineral in the northeastern exposures of the unit. Sphene is a prominent accessory mineral and is visible in hand sample as isolated crystals that may reach 12 mm long. Allanite, apatite, opaque minerals, and zircon are microscopic accessory minerals. Mafic enclaves are ubiquitous but are generally sparse, except in several

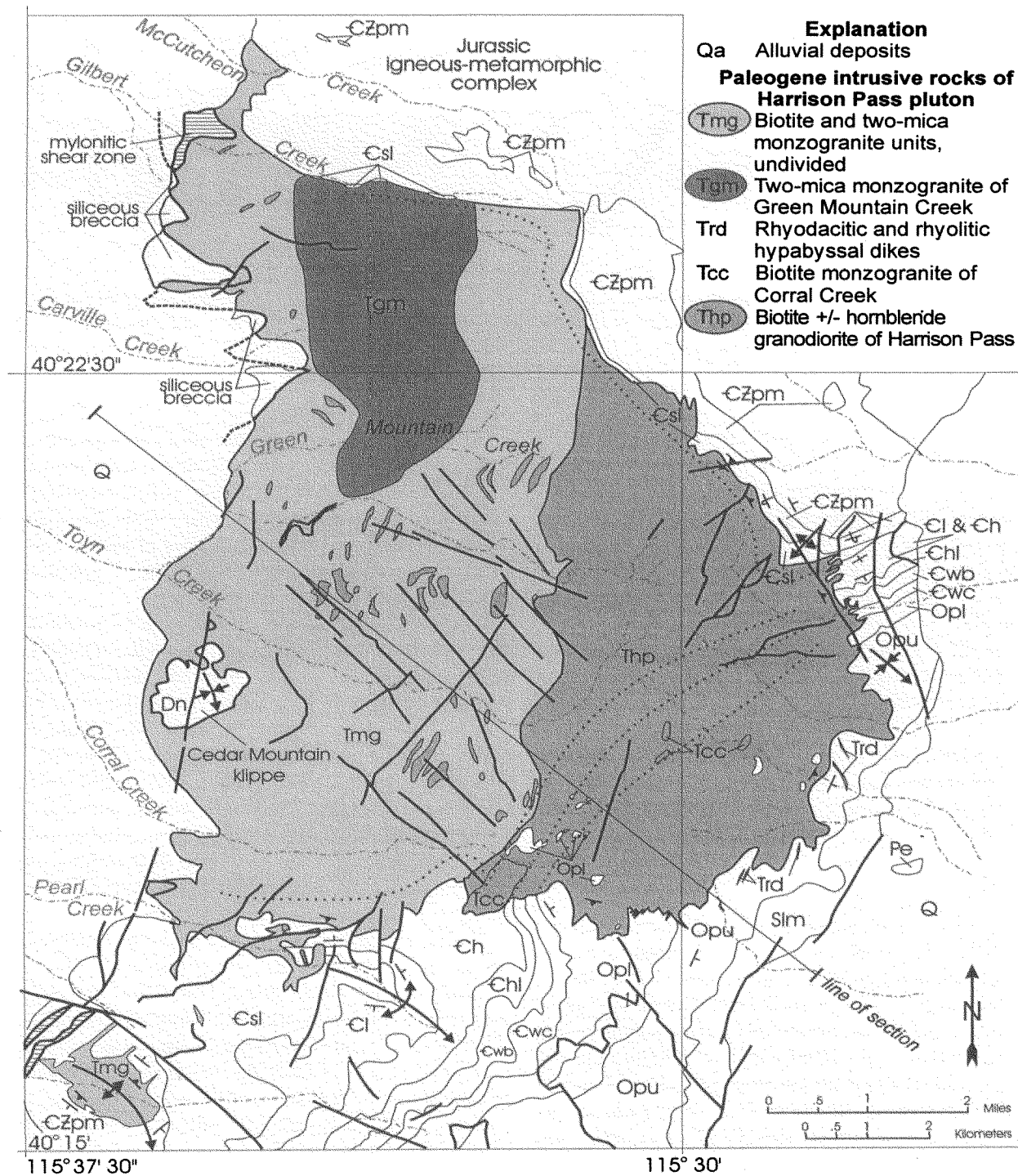


Figure 29. Simplified geologic map of the Harrison Pass pluton and environs. Wavy lines indicate mylonitic rocks. Geology by B. R. Burton.

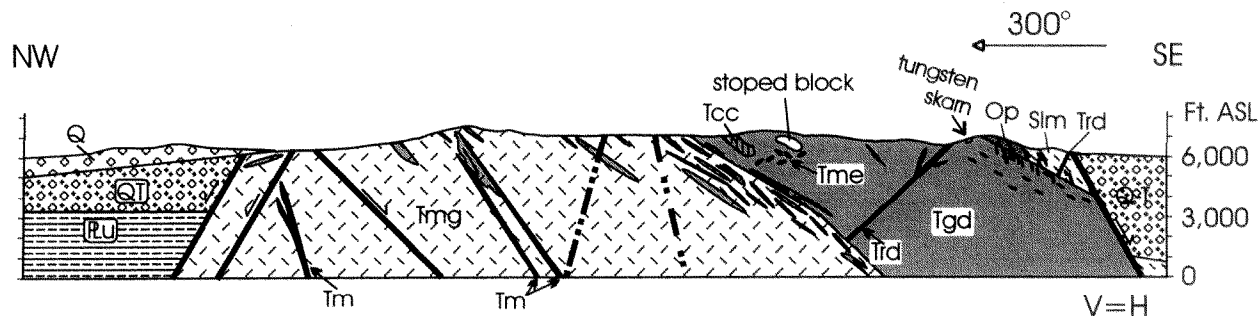


Figure 30. Simplified cross-section across the Harrison Pass pluton drawn parallel to the direction of displacement of the hanging wall of the Ruby Mountains shear zone and perpendicular to the inferred axis of rotation of the footwall. Tm = mafic sheets, Tme = mafic enclaves, other symbols same as Fig. 29. Geology by B. R. Burton.

localities in the northeastern part of the pluton where they occur in dense swarms. The enclaves vary in composition from microdiorite to quartz monzodiorite. Scarce epidote-bearing hornblende-biotite tonalitic synplutonic dikes are also present.

The granodioritic suite was cut by biotite-bearing aplitic and alaskitic dikes, and a small number of microgranular dacitic dikes prior to emplacement of the monzogranitic suite. In the border facies, where granodioritic rocks are in contact with carbonate wall and roof rocks, these intrusive rocks are medium- to coarse-grained and lack megacrysts. Along the eastern contact of the pluton, in the roof zone, porphyritic dikes of granodioritic composition intrude the carbonate wall rocks. These dikes are characterized by phenocrysts of plagioclase, quartz, and relict mafic minerals in a fine-grained groundmass.

Monzogranitic suite

The monzogranitic suite (Fig. 29) includes numerous distinct intrusive units. These are predominantly biotite monzogranite and two-mica monzogranite, but include a small volume of leucocratic rocks such as two-mica aplite, alaskite, and pegmatite. Scarce dikes of syenogranite and mafic rocks also occur. Tabular bodies of biotite monzogranite intrude the granodioritic unit producing abundant screens of granodiorite within monzogranitic rocks. These relationships clearly indicate that the monzogranitic suite is younger than the granodiorite suite. Petrographic and geochemical data show that the monzogranite unit can be divided into at least three subunits: two-mica monzogranite of Green Mountain Creek, other two-mica monzogranites, and biotite monzogranite.

In an area north of Green Mountain Creek (i.e., in the northern part of the pluton), a distinctive intrusive body here informally named the "granite of Green Mountain Creek" crops out (Fig. 29). This unit is a relatively homo-

geneous, massive body of two-mica monzogranite that lacks internal layering, distinguishing it from most other monzogranite bodies in the pluton. It is characterized by moderately uniform, medium- to coarse grain size, a distinct orange weathering, and the presence of sparse, but distinctive coarse-grained, mica-rich enclaves and cm-scale clots of massive quartz.

Two-mica granites are abundant in the west-central part of the pluton, but also intrude the granodioritic unit in the eastern part of the pluton. They are distinct from the granite of Green Mountain Creek in texture and homogeneity. They range from medium- to coarse-grained and commonly show compositional and textural layering. This "line-rock" texture is characterized by segregation of alkali feldspar and plagioclase. Pegmatitic segregation is also common, and generally increases in grain size and abundance from west to east in the central part of the pluton. Mafic enclaves have been found within these rocks, but they are scarce.

Biotite monzogranite dikes crop out as small masses, predominantly in the south-central part of the pluton and as small, isolated, oblate-shaped bodies in wall rocks adjacent to the southwest margin of the pluton. Microgranular dikes of dacitic and monzonitic composition are uncommon components of both the granodiorite and monzogranite suites of the pluton. In several exposures, these rocks dip moderately east, concordant with associated tabular units of monzogranite. At some localities, monzogranitic rocks cut mafic rocks.

GEOCHEMICAL DATA

More than 60 samples from the Harrison Pass pluton were analyzed by ICPS and INAA for major- and trace-element abundances. Although relatively few analyses are available from rocks of older or equivalent age in the region, the data are compared to available compositional data for

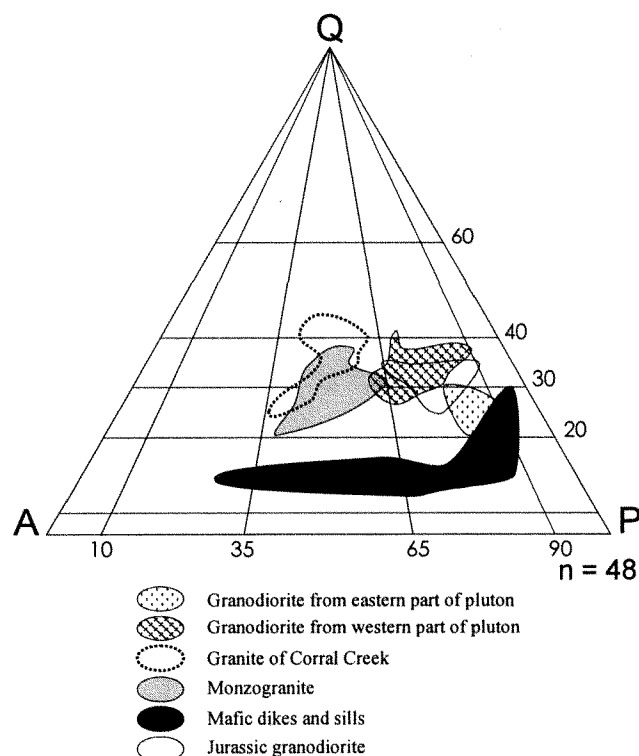


Figure 31. Summary of modal data from granitic rocks of the Harrison Pass pluton.

the granite of Dawley Canyon, a Late Jurassic intrusive unit (Hudec, 1990; Hudec and Wright, 1990) that crops out just north of the Harrison Pass pluton (Figs. 32–37).

Major element data show that the bulk of the rocks of the Harrison Pass pluton are mildly peraluminous (alumina saturation index [ASI = molar $\text{Al}_2\text{O}_3/(\text{CaO} + \text{Na}_2\text{O} + \text{K}_2\text{O})$] less than 1.1 but greater than 1.0) (Fig. 32). The granodioritic unit, roof dikes, and a synplutonic tonalitic dike show distinct $\text{Mg}/(\text{Mg} + \text{Fe})$ values (Fig. 33), which, with two exceptions, range from 0.33 to 0.39. The $\text{Mg}/(\text{Mg} + \text{Fe})$ values of enclaves are similar to those of the host granodiorite, but $\text{Mg}/(\text{Mg} + \text{Fe})$ values of mafic (monzonitic) dikes are significantly higher (0.46 to 0.59). In addition to their $\text{Mg}/(\text{Mg} + \text{Fe})$ values, the roof dikes from the eastern side of the pluton are compositionally quite similar to what could be considered an “average” value for the granodioritic unit.

The granite of Green Mountain Creek, most other two-mica granites, and the Jurassic granite of Dawley Canyon are strongly peraluminous ($\text{ASI} > 1.1$). The two-mica granites of Green Mountain Creek and biotite monzogranite dikes have $\text{Mg}/(\text{Mg} + \text{Fe})$ values less than 0.28. Two samples of two-mica granitic dikes display low $\text{Mg}/(\text{Mg} + \text{Fe})$ values, whereas three samples have values between 0.40 and 0.52, the highest observed among felsic rocks in the area.

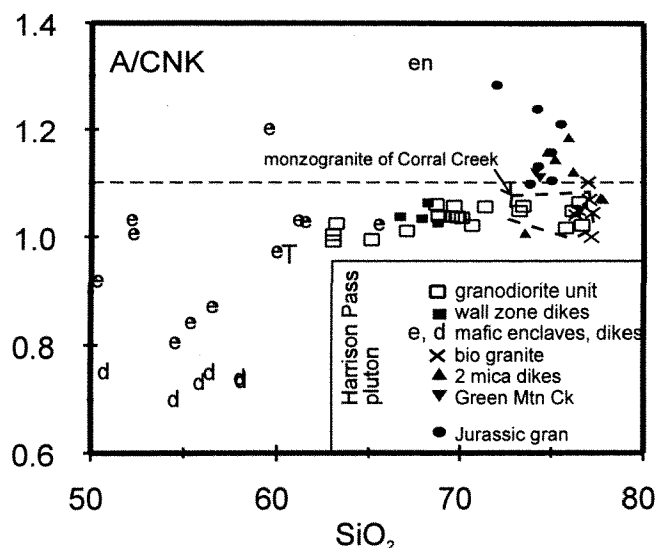


Figure 32. A/CNK (molar Al_2O_3 divided by CaO , Na_2O , and K_2O) plotted against SiO_2 for granitic rocks of the Harrison Pass pluton. Monzogranitic rocks of the granodiorite unit (monzogranite of Corral Creek) enclosed by a dashed line, “en” represents enclaves in the two-mica granite of Green Mountain Creek. “T” represents synplutonic tonalitic dike in the granodiorite unit.

Mafic dikes and mafic enclaves from the granodioritic unit are typically metaluminous. Micaceous enclaves from the two-mica granite of Green Mountain Creek are strongly peraluminous and have low $\text{Mg}/(\text{Mg} + \text{Fe})$ values nearly identical to that of their host rocks.

Two geochemical groups can be distinguished on the basis of Y abundances (Fig. 34). Samples of the granodioritic suite, its enclaves, and mafic dikes, are typically low in Y (most < 40 ppm) over a large range of SiO_2 values; Y and SiO_2 display a weak negative correlation. Samples of the monzogranitic suite show a range of Y contents from 10 to > 90 ppm. Members of this group include both groups of two-mica granite, biotite monzogranite dikes, and Jurassic two-mica granite of Dawley Canyon. At these high SiO_2 values, no correlation between Y and SiO_2 is present.

Most samples from the granodioritic unit of the Harrison Pass pluton display subparallel rare earth element (REE) patterns characterized by negative slope, a slight negative Eu anomaly, and a weak dog-leg with a lower slope among the heavy REE (Fig. 35). The patterns of two roof dike samples are identical to those of the granodioritic unit, and two quartz monzonite dikes are also similar but have slightly higher REE abundance. Biotite monzogranites from the granite of Corral Creek (part of the granodioritic suite) show distinct REE patterns in that they contain lower total REE concentrations and lack Eu anomalies. Mafic enclaves in the granodioritic unit range widely in REE abundance

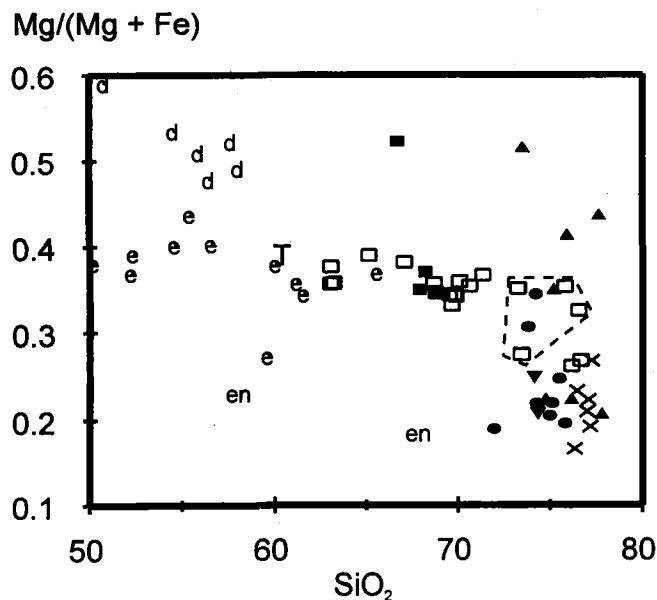


Figure 33. Plot of $Mg/(Mg+Fe)$ against SiO_2 for the granitic rocks of the Harrison Pass pluton. Symbols as in Fig. 32.

but generally display patterns similar to those of their host rocks, but with more pronounced negative Eu anomalies.

Biotite monzogranites of the younger intrusive suite have relatively low REE abundances, the most prominent negative Eu anomalies, and flat to slightly positive slopes. The REE pattern of the granite of Green Mountain Creek is similar to rocks of the granodioritic suite except for its large Eu anomaly. The REE pattern of a micaceous enclave from the granite of Green Mountain Creek is similar to that of its host, but the enclave contains higher REE contents, with La at 1000X chondrites, consistent with an origin by accumulation of accessory minerals. Other two-mica granites of the pluton (sheets and dikes) are characterized by variable, shallow negative slopes, negative Eu anomalies, and variable REE abundances.

Most of the isotopic data for the Harrison Pass pluton cluster in a narrow range of initial $^{87}Sr/^{86}Sr$ from 0.7097 to 0.7116 and ϵNd from -10.2 to -15.9 (Fig. 36). These data are distinct from those for two samples from the two-mica granite of Green Mountain Creek (monzogranite and a granitic enclave) which have initial $^{87}Sr/^{86}Sr$ about 0.725 and ϵNd of -21.3.

Quartz from rocks of the granodioritic unit has $\delta^{18}O$ (SMOW) values of about +10‰ (H. Karlsson, unpublished data). In contrast, the two-mica granite of Green Mountain Creek has $\delta^{18}O$ of about +8.5‰. The fact that the two-mica granites have lower $\delta^{18}O$ values is of note, because in many granitic systems, initial $^{87}Sr/^{86}Sr$ and $\delta^{18}O$ are positively correlated.

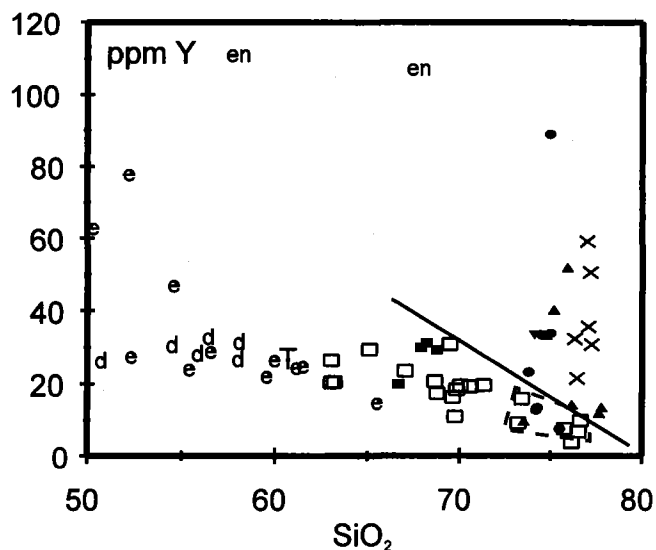


Figure 34. Plot of Y against SiO_2 for the granitic rocks of the Harrison Pass pluton. Symbols as in Fig. 32. Line separates high-Y, high- SiO_2 samples from other samples of the pluton.

DISCUSSION OF GEOCHEMICAL DATA

Granodioritic suite

For the granodiorite unit and roof dikes, when SiO_2 , $Mg/(Mg+Fe)$, and CaO/Al_2O_3 are used as differentiation indices, other elemental concentrations and ratios tend to plot in linear arrays with variable scatter (Fig. 37). In virtually all plots, the mafic end of these arrays is a hornblende-biotite tonalite dike (sample BB-70-94), which is a large mafic enclave that is part of an aligned, disarticulated mafic dike ~5 m thick. The dike cuts porphyritic granodiorite but is also cut by the host granodiorite and by leucogranitic pegmatite. Petrographically similar hornblende-bearing rocks of the granodioritic unit are slightly more evolved than this sample. In binary elemental plots, biotite monzogranites from the granodioritic unit plot at the felsic end of the data array.

This linear relationship can result from magma mixing or from fractional crystallization. Fractional crystallization models (Burling, 1996) show that major- and trace-element concentrations can be explained by removal of plagioclase from a hornblende-bearing granodioritic parent. However, textural evidence indicates that the granodioritic magma was saturated with plagioclase, quartz, biotite, sphene, and allanite \pm hornblende \pm alkali-feldspar \pm zircon \pm opaque minerals. Thus, models in which plagioclase is the only fractionated phase are unlikely.

Major element data are also consistent with a simple mixing model between tonalitic and monzogranitic end members. A mixing model would also explain linear varia-

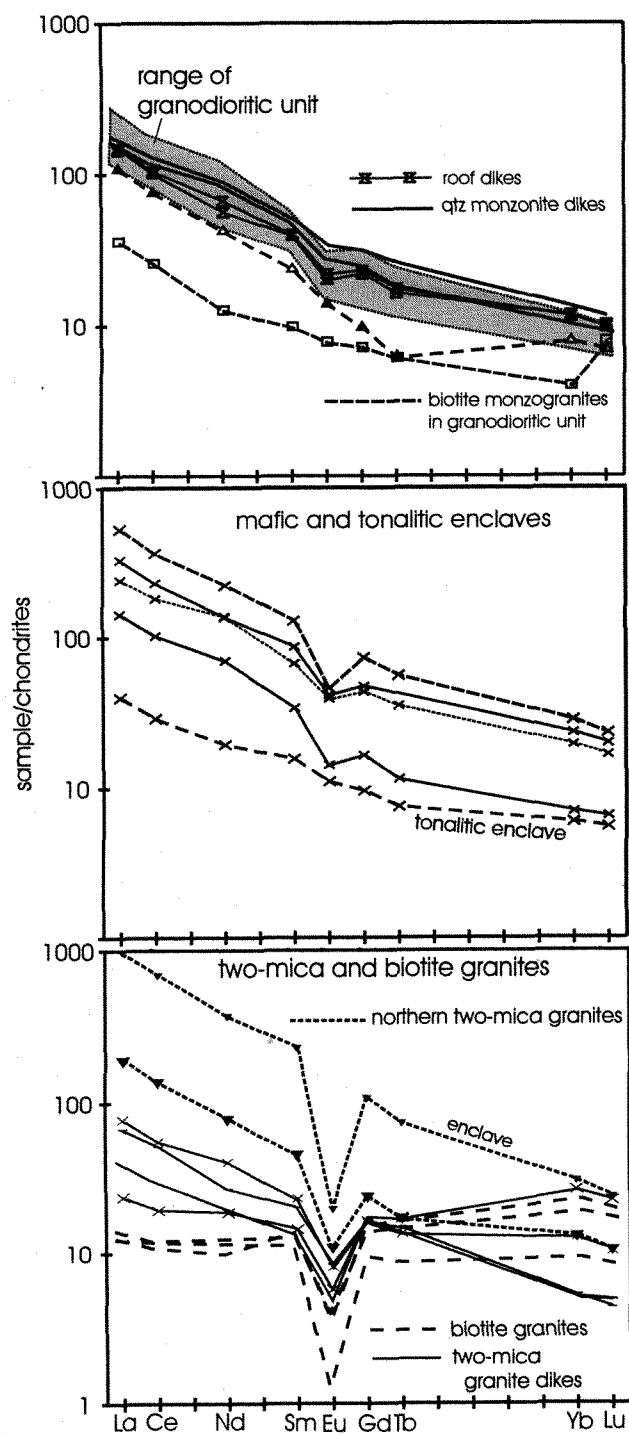


Figure 35. Plots of rare earth elements abundances.

tion among the trace elements. Scatter among Ba concentrations is probably due to local flow sorting of alkali-feldspar, whereas local enrichments in Rb and K_2O suggest late-stage, fluid-enhanced enrichment of these elements.

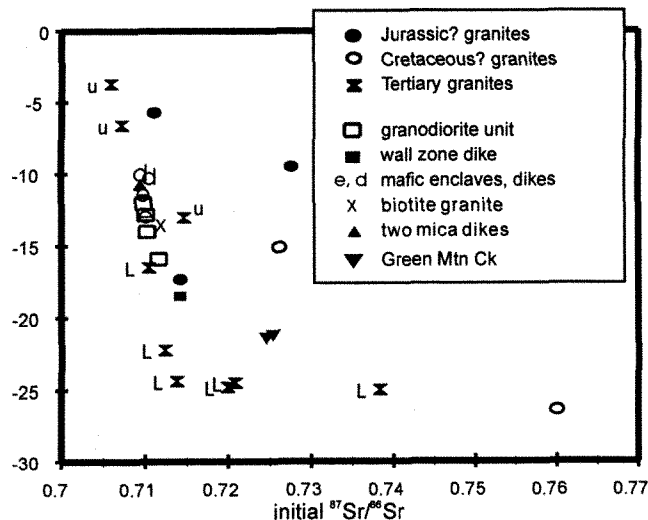


Figure 36. Plot of ϵNd against initial $^{87}Sr/^{86}Sr$ for selected granitic rocks of the Ruby Mountains including samples from the Harrison Pass pluton. Tertiary granitic rocks labelled with an "L" or "U," which denote possible Archean or Proterozoic source (or contaminant) regions, respectively (Wright and Snoke, 1993).

Chemical similarities among the granodioritic unit and roof dikes suggest that the roof dikes represent "leaks" from the granodiorite magma chamber. This is supported by the observation that most roof dike compositions lie on a major and trace element mixing line defined by the granodioritic rocks (Fig. 37).

Monzogranitic suite

Late stage biotite monzogranitic rocks are distinct from the biotite monzogranites of the granodioritic group (e.g., granite of Corral Creek) in a number of ways. The younger rocks have lower $Mg/(Mg+Fe)$, Al_2O_3 , Ba, Sr, Zr, Hf, and Th contents and generally higher concentrations of Nb, Ta, and U. In addition, they display positive REE slopes and large negative Eu anomalies. This combination of elemental data indicate that this unit is unrelated to the granodioritic unit. Mass balance calculations show that it is also an unsuitable felsic end member in the granodiorite mixing models.

The granite of Green Mountain Creek contains higher contents of Rb, Nb, Zr, and Zn than other monzogranites in the pluton, and higher Y contents than any sample from the granodioritic unit. Its REE patterns are distinct from those of the granodioritic unit because of their pronounced negative Eu anomaly.

Other two-mica granites are distinct from the granodioritic unit in their strongly peraluminous nature, their wide variation in $Mg/(Mg+Fe)$, their range of REE patterns

CaO

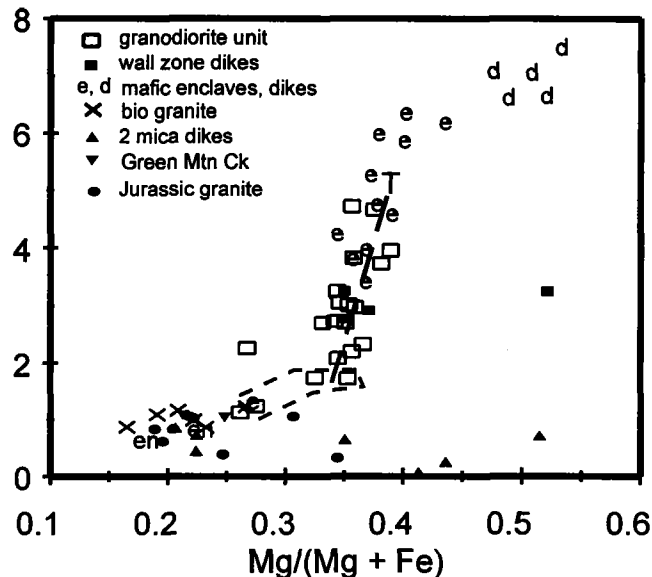


Figure 37. Plot of CaO against Mg/Mg+Fe for granitic rocks of the Harrison Pass pluton. Symbols as in Fig. 32. Long-dashed line indicates possible mixing line between mafic tonalitic and monzogranitic end members.

and La/Lu values, and their pronounced negative Eu anomalies. In addition, when total Fe contents as Fe_2O_3 are used as a differentiation index, most samples of this group do not plot on an extension of the granodioritic trend. These features are not readily explained by fractional crystallization from an granodioritic composition; therefore, the late two-mica monzogranites are thought to represent distinct batches of magma unrelated to earlier phases of the pluton.

In summary, geochemical data indicate the following: (1) the granodiorite unit is compositionally distinct from all younger intrusive units in the pluton; (2) compositional variation within the granodioritic suite is predominantly the result of magma mixing between tonalitic and monzogranitic end members, with lesser crystal-liquid fractionation processes; (3) the low ϵNd , high $^{87}\text{Sr}/^{86}\text{Sr}$, and relatively low $\delta^{18}\text{O}$ of the two-mica granite of Green Mountain suggest source rocks that are quite different from those of other monzogranites in the pluton; (4) dikes and sills of biotite monzogranite and two-mica granite cannot be readily related to either the granodioritic unit or the granite of Green Mountain Creek. Therefore, the Harrison Pass pluton consists of at least one intermediate magma composition (tonalitic end member of the granodiorite unit) plus at least four distinct monzogranitic magmas: felsic end member of the granodioritic unit, granite of Green Mountain Creek, late biotite monzogranite, and late two-mica monzogranite.

EMPLACEMENT HISTORY

Emplacement of the granodioritic and monzogranitic suites was accommodated by distinctly different mechanisms which may have been controlled by the temperature and viscosity of the different magmas, the difference in depth of emplacement between the two intrusive suites, and the rheology of the rocks into which they were emplaced. Emplacement of the granodioritic suite was accommodated by a combination of "passive" and "forceful" intrusive mechanisms as reflected by structural studies of the contact metamorphic aureole and pluton. These mechanisms are summarized in Figure 38. The monzogranitic suite was subsequently emplaced into a thermally and structurally prepared zone which was occupied by rocks of the earlier granodioritic suite.

Granodioritic suite

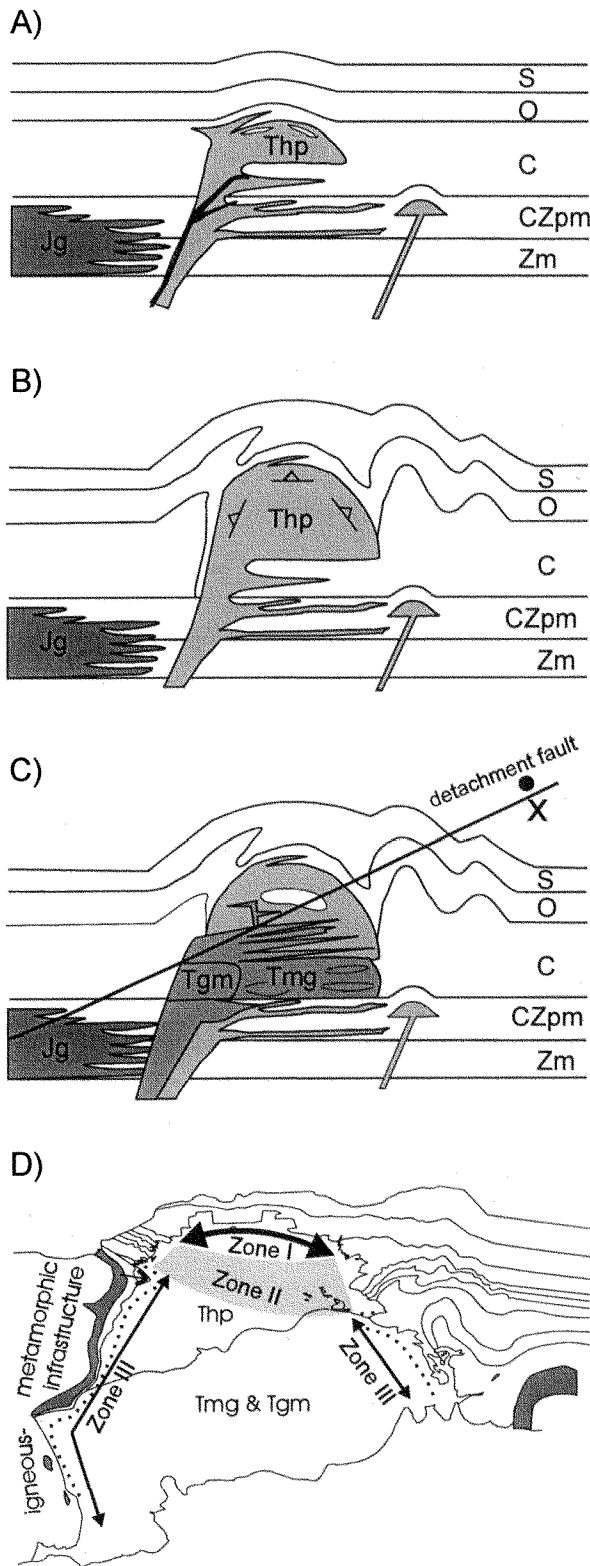
Stoping

Emplacement of the granodiorite suite was accommodated in part by stoping of existing wall and roof rocks. Numerous large pendants are present within the granodioritic unit, especially adjacent to the southern margin of the pluton and eastern roof zone where the pluton-wall rock contacts are discordant (zone 1 on Fig. 38). These blocks consist of impure calcite marble and calc-silicate rocks that have irregular, angular contacts with the surrounding host granodiorite. Leucocratic granitoid dikes form a marginal facies to most of these blocks and also occur within the stoped blocks. Tungsten skarn mineralization is present along many of these granodiorite-calc-silicate rock contacts (Tingley, 1992).

Excellent exposures in the Road Canyon area (STOP 4-2) illustrate a mechanism by which stoping occurred. Here, stoped blocks (1–10 m thick) are separated from the adjacent wall rocks by a network of dikes and sills. The stoped blocks have been translated westward and rotated clockwise about a steeply plunging pole of rotation. The magnitude of rotation and translation is roughly equivalent to the thickness of the overlying network of dikes and sills. Intrusive units generally follow the compositional layering in the greenschist-facies wall rocks, but step upward to higher stratigraphic levels via thin dikes. Thus, an overall "stair step" geometry characterizes much of the granodiorite-wall rock contact along the eastern margin of the pluton.

Wall-rock strain

Penetrative deformation of wall rocks has occurred adjacent to the Harrison Pass pluton and has accommodated emplacement space. Small amplitude folds (5–20 cm) are present in a contact-metamorphic aureole, about 500 to 800 m thick, adjacent to the granodiorite suite. An axial



planar fabric of contact-metamorphic calc-silicate minerals suggests that the folds formed during pluton emplacement. Hinge lines of the folds trend approximately parallel to the pluton-wall rock contact and plunge eastward. The folds are commonly overturned, and some are recumbent and isoclinal. Measurements of these folds suggest that about 50% shortening of the wall rocks occurred throughout much of this aureole, which accounts for a two-dimensional shortening of $\sim 20 \text{ km}^2$.

Large-amplitude folds (0.3–1 km) also are present in wall rocks adjacent to the southern margin of the pluton (Fig. 29). These folds have accommodated 30% shortening over an area of $\sim 40 \text{ km}^2$. Wall-rock stratigraphic units are attenuated in the limbs of the folds, and the hinge zones are thickened.

Uplift

South of the Harrison Pass pluton, the southern Ruby Mountains are a simple homocline of eastward tilted Paleozoic rocks which strike $\sim \text{N}10\text{E}$. Adjacent to the southern margin of the Harrison Pass pluton, the strike is deflected sharply eastward and dips increase to $\sim 60^\circ$. The deformed beds describe a southeast-plunging synform. Adjacent to the northeastern margin of the pluton, a tight synform exists in which the limbs are highly attenuated. These synforms are separated by a broad, open antiform which forms the roof zone of the pluton, and which is structurally displaced

Figure 38. Model of the emplacement for the Harrison Pass pluton. **A**, Early emplacement of granodioritic suite was accommodated by brittle emplacement of dikes and sheets that produced stoping of the wall rocks and minor uplift. **B**, Emplacement of the remainder of the granodioritic suite produced substantial strain in thermally and mechanically weakened wall rocks, uplift of the roof zone, minor stoping in the roof and pluton margins, and internal strain. **C**, Subsequent emplacement of the monzogranitic suite (Tmg) as layered tabular units that pervasively intruded the granodioritic suite and wall rocks, and the emplacement of the granite of Green Mountain Creek (Tgm) as a homogeneous mass which shortened and attenuated Jurassic igneous and metamorphic rocks (Jg) (i.e., wall rocks to the north). Oblique line shows the future position of the Ruby Mountains shear zone. **D**, Oblique-angle cross section through the Harrison Pass pluton from transposed and rotated map view showing final state of emplacement-related strain and stoping. Zone I is the concordant roof zone of the pluton that shows evidence of stoping and uplift. Zone II is the discordant wall zone where stoping and wall-rock strain were important emplacement mechanisms. Structurally deeper Zone III is characterized by transposed and highly strained, concordant wall-rock contacts.

from the projected trajectory of strata south of the pluton. Uplift of these rocks during emplacement of the Harrison Pass pluton is considered to be an important mechanism of emplacement. The structural thickness of the pluton is ~5 km, and it was emplaced into a wall-rock succession ~2.7 km thick.

Internal Strain

Mafic enclaves within the granodiorite suite are ellipsoids of oblate spheroidal shape. Measurement of a-c axes of these bodies and quantitative strain analysis using the Rf- ϕ method (Ramsey and Huber, 1983) show that the enclaves were subject to 30% flattening. Shortening is oriented perpendicular to the pluton wall-rock contact. Foliation in the granodiorite also describes a great circle with β point to the southeast, consistent with a southeastern orientation of the direction of maximum shortening. The direction of maximum elongation described by the 2-dimensional strain ellipses of the mafic enclaves defines a gently east-dipping great circle which is coincident with the shortening direction reflected by wall-rock folds.

Monzogranitic suite

The monzogranitic suite of the pluton was emplaced into a complex zone that was previously occupied by granodiorite. In the central part of the pluton, emplacement of tabular intrusions of monzogranite into a granodioritic host was accommodated by stoping. Here, the monzogranitic rocks are layered line rock. Dilation by the monzogranitic sheets produced translation of the granodiorite. Brittle propagation of the monzogranitic sheets is indicated by truncation of alkali feldspar megacrysts and mafic enclaves in the host granodiorite. The sheets strike northeastward and dip moderately eastward, consistent with the tilt of the mountain range, suggesting that the sheets were initially subhorizontal.

The granite of Green Mountain Creek lacks the internal segregation and layering of the monzogranites described above and was apparently emplaced as a homogeneous mass. Crystal-plastic strain produced a foliation in these rocks which is parallel to the orientation of the Ruby Mountains shear zone, so that any magmatic foliation that may have been present is no longer identifiable. Along its northern margin, the granite of Green Mountain Creek is

in contact with Jurassic monzogranite. A thin screen of hornfels along this zone marks the contact between the two rock types. This screen represents a highly attenuated portion of the Paleozoic wall rocks that are found south and northeast of the pluton.

Other bodies of monzogranite are dikes and sills that are emplaced into older plutonic rocks or into the adjacent wall rocks. The southern margin of the pluton is pervasively intruded by small monzogranite dikes, sills, and lensoidal intrusive bodies. Emplacement of these units is thought to have been accommodated by brittle dike and sill propagation and localized wall-rock shortening.

CONCLUDING REMARKS

The Harrison Pass pluton was emplaced in the footwall of a major core complex during an early stage of regional crustal extension. This tectonic event was accommodated by mid-crustal flow which has been recognized in the northern Ruby Mountains (MacCready et al., in press). Crustal extension in the Ruby Mountains and East Humboldt Range may have initiated in the Eocene along a west-rooted, plastic-to-brittle shear zone-detachment fault system (Mueller and Snoke, 1993a). Cooling data suggest that a significant component of tectonic denudation occurred within one million years of the emplacement of the Harrison Pass pluton. However, a direct relationship between tectonism and magmatism is not reflected in the mechanisms of emplacement of the pluton. Instead, Harrison Pass pluton was emplaced by the combination of mechanisms including: stoping, wall-rock strain, and localized uplift.

The presence of intermediate magma compositions (mafic tonalite as an end member of the granodioritic unit and monzodioritic dikes among the late-stage intrusions) suggests the likelihood of a mantle-derived component in the pluton. Similar conclusions were reached for coeval, extension-related volcanic rocks in the Snake and Egan ranges (e.g., Gans et al., 1989; Grunder, 1992). A direct relationship between granitoid plutonism and crustal extension is thus reflected in the presence of these intermediate magmas in that advected heat from parental mafic magmas is probably necessary to explain the abundance of crustally-derived monzogranitic magmas. In addition, the compositional variety of the monzogranitic rocks suggests that crustal source region(s) were of diverse rock type.

REFERENCES CITED

(for all 4 parts)

- Allmendinger, R.W., and Jordan, T.E., 1984, Mesozoic structure of the Newfoundland Mountains, Utah: Horizontal shortening and subsequent extension in the hinterland of the Sevier belt: *Geological Society of America Bulletin*, v. 95, p. 1280–1292.
- Anderson, R.E., Zoback, M.L., and Thompson, G.A., 1983, Implications of selected subsurface data on the structural form and evolution of some basins in the northern Basin and Range province, Nevada and Utah: *Geological Society of America Bulletin*, v. 94, p. 1055–1072.
- Armstrong, R.L., 1968, Sevier orogenic belt in Nevada and Utah: *Geological Society of America Bulletin*, v. 79, p. 429–458.
- Armstrong, R.L., and Hansen, E., 1966, Cordilleran infrastructure in the eastern Great Basin: *American Journal of Science*, v. 264, p. 112–127.
- Babcock, R.C., Jr., Ballantyne, C.H., and Phillips, C.H., 1995, Summary of the geology of the Bingham district, Utah, in Pierce, F.W., and Bolm, J.G., eds., *Porphyry copper deposits of the America Cordillera*: Tucson, Arizona Geological Society Digest 20, p. 316–335.
- Bickle, M.J., Chapman, H.J., Wickham, S.M., and Peters, M.T., 1995, Strontium and oxygen isotope profiles across marble-silicate contacts, Lizzies Basin, East Humboldt Range, Nevada: constraints on metamorphic permeability contrasts and fluid flow: *Contributions to Mineralogy and Petrology*, v. 121, p. 400–413.
- Blackwell, D.D., Kelley, S.A., and Reese, M., 1984, Fission track evidence on the Late Cenozoic deformation of the Ruby Mountains, Nevada: *Geological Society of America Abstracts with Programs*, v. 16, p. 446.
- Blackwell, D.D., Reese, N.M., and Kelley, S.A., 1985, Evolution of Basin and Range structure in the Ruby Mountains and vicinity, Nevada, in Lucchitta, I., Morgan, P., and Soderblom, L.A., eds., *Proceedings volume for the conference on heat and detachment in crustal extension on continents and planets*: Houston, Texas, Lunar and Planetary Institute Contribution 575, p. 12–14.
- Brooks, W.E., Thorman, C.H., Snee, L.W., 1995, The $^{40}\text{Ar}/^{39}\text{Ar}$ ages and tectonic setting of the middle Eocene northeast Nevada volcanic field: *Journal of Geophysical Research*, v. 100, p. 10,403–10,416.
- Burling, T.C., 1996, Magmatism associated with extension, Harrison Pass pluton, Ruby Mountains, Nevada [M.S. thesis]: Lubbock, Texas, Texas Tech University, 136 p.
- Burton, B.R., in preparation, Structural geology and emplacement history of the Harrison Pass pluton, central Ruby Mountains, Elko County, Nevada [Ph.D. dissertation]: Laramie, University of Wyoming.
- Camilleri, P.A., 1994, Mesozoic and Cenozoic tectonic and metamorphic evolution of the Wood Hills and Pequop Mountains, Elko County, Nevada [Ph.D. dissertation]: Laramie, University of Wyoming, 196 p.
- Camilleri, P.A., and Chamberlain, K.R., 1997, Mesozoic tectonics and metamorphism in the Pequop Mountains and Wood Hills region, northeast Nevada: implications for the architecture and evolution of the Sevier orogen: *Geological Society of America Bulletin*, v. 109, p. 74–94.
- Cashman, P.H., 1992, Structural geology of the northeastern Stansbury Mountains, in Wilson, J.R., ed., *Field guide to geologic excursions in Utah and adjacent areas of Nevada, Idaho, and Wyoming*: Utah Geological Survey Miscellaneous Publication 92-3, p. 171–178.
- Crittenden, M.D., Jr., Coney, P.J., and Davis, G.H., eds., 1980, *Cordilleran metamorphic core complexes*: Boulder, Colorado, Geological Society of America Memoir 153, 490 p.
- Dallmeyer, R.D., Snoke, A.W., and McKee, E.H., 1986, The Mesozoic-Cenozoic tectonothermal evolution of the Ruby Mountains–East Humboldt Range, Nevada: A Cordilleran metamorphic core complex. *Tectonics*, v. 5, p. 931–954.
- Dickinson, W.R., 1991, Tectonic setting of faulted Tertiary strata associated with the Catalina core complex in southern Arizona: Boulder, Colorado, Geological Society of America Special Paper 264, 106 p.
- Doelling, H., 1989, Antelope Island State Park, the history, the geology, and wise planning for future development: Survey Notes, Utah Geological & Mineral Survey, v. 23, no. 1, p.2–14.
- Doelling, H.H., Willis, G.C., Jensen, M.E., Hecker, S., Case, W.F., and Hand, J.S., 1990, Geologic map of Antelope Island, Davis County, Utah: Utah Geological and Mineral Survey Map 127, scale 1:24,000, accompanying booklet 27 p.
- Dokka, R.K., Mahaffie, M.J., and Snoke, A.W., 1986, Thermochronologic evidence of major tectonic denudation associated with detachment faulting, northern Ruby Mountains–East Humboldt Range, Nevada: *Tectonics*, v. 5, p. 995–1006.
- Ehadi, A., and Johannes, W., 1991, Beginning of melting and composition of first melts in the system $\text{Qz-Ab-Or-H}_2\text{O-CO}_2$: Contributions to Mineralogy and Petrology, v. 106, p. 286–295.
- Eby, G.N., 1990, The A-type granitoids: A review of their occurrence and chemical characteristics and speculations on their petrogenesis: *Lithos*, v. 26, p. 115–134.
- Effimoff, I., and Pinezich, A.R., 1981, Tertiary structural development of selected valleys based on seismic data: Basin and Range province, northeastern Nevada. Royal Society of London, *Philosophical Transactions, Series A*, v. 300, p. 435–442.
- Feeley, T.C., and Grunder, A.L., 1991, Mantle contribution to the evolution of middle Tertiary silicic magmatism during early stages of extension: the Egan Range volcanic complex, east-central Nevada: Contributions to Mineralogy and Petrology, v. 106, p. 154–169.
- Fricke, H.C., Wickham, S.M., and O'Neil, J.R., 1992, Oxygen and hydrogen isotope evidence for meteoritic water infiltration during mylonitization and uplift in the Ruby Mountains–East Humboldt Range core complex, Nevada: Contributions to Mineralogy and Petrology, v. 111, p. 203–221.
- Gans, P.B., Mahood, G.A., and Schermer, E., 1989, Synextensional magmatism in the Basin and Range province: A case study from the eastern Great Basin: Boulder, Colorado, Geological Society of America Special Paper 233, 53 p.
- Gilbert, G.K., 1890, Lake Bonneville: U.S. Geological Survey Monograph 1, 438 p.
- Glick, L.L., 1987, Structural geology of the northern Toano Range, Elko County, Nevada [M.S. thesis]. San Jose, California, San Jose State University, 141 p.
- Good, S.C., Nester, P.L., and Snoke, A.W., 1995, Lacustrine molluscs from the lower Humboldt formation, northeastern Nevada, and possible late Eocene to Oligocene age: *Geological Society of America Abstracts with Programs*, v. 27, no. 1, p. 49.
- Grunder, A.L., 1992, Two-stage contamination during crustal assimilation: isotopic evidence from volcanic rocks in eastern Nevada: Contributions to Mineralogy and Petrology, v. 112, p. 219–229.
- Grunder, A.L., 1995, Material and thermal roles of basalt in crustal magmatism: case study from eastern Nevada: *Geology*, v. 23, p. 952–956.
- Hacker, B.R., Yin, A., Christie, J.M., and Snoke, A.W., 1990, Differential stress, strain rate, and temperature of mylonitization in the Ruby Mountains, Nevada: implications for the rate and duration of uplift: *Journal of Geophysical Research*, v. 95, p. 8569–8580.
- Hodges, K.V., Snoke, A.W., and Hurlow, H.A., 1992, Thermal evolution of a portion of the Sevier hinterland: the northern Ruby Mountains–East Humboldt Range and Wood Hills, northeastern Nevada: *Tectonics*, v. 11, p. 154–164.
- Holland, T.J.B., and Powell, R., 1990, An enlarged and updated internally consistent thermodynamic dataset with uncertainties and correlations: the system $\text{K}_2\text{O-Na}_2\text{O-CaO-MgO-MnO-FeO-Fe}_2\text{O}_3\text{-Al}_2\text{O}_3\text{-TiO}_2\text{-SiO}_2\text{-C-H}_2\text{-O}_2$: *Journal of Metamorphic Geology*, v. 8, p. 89–124.

- Hope, R.A., 1972, Geologic map of the Spruce Mountain quadrangle, Elko County, Nevada: U.S. Geological Survey Quadrangle Map GQ-942, 3 p., scale 1:62,500
- Howard, K.A., 1966, Structure of the metamorphic rocks of the northern Ruby Mountains, Nevada [Ph.D. dissertation]: New Haven, Yale University, 170 p.
- Howard, K.A., 1968, Flow direction in triclinic folded rocks: *American Journal of Science*, v. 266, p. 758–765.
- Howard, K.A., 1971, Paleozoic metasediments in the northern Ruby Mountains, Nevada. *Geological Society of America Bulletin*, v. 82, p. 259–264.
- Howard, K.A., 1980, Metamorphic infrastructure in the northern Ruby Mountains, Nevada, in Crittenden, M.D., Jr., Coney, P.J., and Davis, G.H., eds., *Cordilleran metamorphic core complexes*. Boulder, Colorado, Geological Society of America Memoir 153, p. 335–347.
- Howard, K.A., 1987, Lamoille Canyon nappe in the Ruby Mountains metamorphic core complex, Nevada, in Hill, M.L., ed., *Geological Society of America Centennial Field Guide—Cordilleran Section*. Boulder, Colorado, Geological Society of America, p. 95–100.
- Hudec, M.R., 1990, The structural and thermal evolution of the central Ruby Mountains, Elko County, Nevada [Ph.D. dissertation]: Laramie, University of Wyoming, 272 p.
- Hudec, M.R., 1992, Mesozoic structural and metamorphic history of the central Ruby Mountains metamorphic complex, Nevada. *Geological Society of America Bulletin*, v. 104, p. 1086–1100.
- Hudec, M.R., and Wright, J.E., 1990, Mesozoic history of the central part of the Ruby Mountains-East Humboldt Range metamorphic core complex, Nevada. *Geological Society of America Abstracts with Programs*, v. 22, no. 3, p. 30.
- Hurlow, H.A., Snoke, A.W., and Hodges, K.V., 1991, Temperature and pressure of mylonitization in a Tertiary extensional shear zone, Ruby Mountains-East Humboldt Range, Nevada. *tectonic implications*. *Geology*, v. 19, p. 82–86.
- Jaeger, K.B., 1987, Structural geology and stratigraphy of the Elko Hills, Elko County, Nevada [M.S. thesis]: Laramie, University of Wyoming, 70 p.
- Ketner, K.B., 1990, Geologic map of the Elko Hills, Elko County, Nevada: U.S. Geological Survey Miscellaneous Investigations Series Map I-2082, scale 1:24,000.
- Ketner, K.B., and Ross, R.J., Jr., 1990, Geologic map of the northern Adobe Range, Elko County, Nevada. U.S. Geological Survey Miscellaneous Investigations Series Map I-2081, scale 1:24,000.
- Ketner, K.B., and Smith, J.F., Jr., 1974, Folds and overthrusts of Late Jurassic or Early Cretaceous age in northern Nevada. *Journal of Research U.S. Geological Survey*, v. 2, p. 417–419.
- King, C., 1878, *Systematic Geology—geological exploration of the Fortieth Parallel*, v. 1. Washington, D.C., U.S. Government Printing Office, 803 p.
- Kistler, R.W., Ghent, E.D., and O'Neil, J.R., 1981, Petrogenesis of garnet two-mica granites in the Ruby Mountains, Nevada. *Journal of Geophysical Research*, v. 86, p. 10,591–10,606.
- Lachenbruch, A.H., and Sass, J.H., 1978, Models of an extending lithosphere and heat flow in the Basin and Range province, in Smith, R.B., and Eaton, G.P., eds., *Cenozoic tectonics and regional geophysics of the western Cordillera*. Denver, Colorado, Geological Society of America Memoir 152, p. 209–250.
- Lanier, G., John, E.C., Swensen, A.J., Reid, J., Bard, C.E., Caddey, S.W., and Wilson, J.C., 1978, General geology of the Bingham mine, Bingham Canyon, Utah. *Economic Geology*, v. 73, p. 1228–1241.
- Lapointe, D.D., Tingley, J.V., and Jones, R.R., 1991, Mineral resources of Elko County, Nevada. Reno, Nevada Bureau of Mines and Geology Bulletin 106, 236 p.
- Lipten, E.J.H., 1984, The geology of Clover Hill and classification of the Wells tungsten prospect, Elko County, Nevada [M.S. thesis]. West Lafayette, Indiana, Purdue University, 239 p.
- Lister, G.S., and Snoke, A.W., 1984, S-C mylonites. *Journal of Structural Geology*, v. 6, p. 617–638.
- Loiselle, M.C., and Wones, D.R., 1979, Characteristics and origin of anorogenic granites. *Geological Society of America Abstracts with Programs*, v. 11, no. 7, p. 468.
- Lush, A.P., McGrew, A.J., Snoke, A.W., and Wright, J.E., 1988, Allochthonous Archean basement in the northern East Humboldt Range, Nevada. *Geology*, v. 16, p. 349–353.
- MacCready, T., Snoke, A.W., and Wright, J.E., 1993, Evidence for nearly orthogonal Oligocene crustal flow beneath the coeval mylonitic shear zone of the Ruby Mountains core complex, Nevada. *Geological Society of America Abstracts with Programs (Combined Cordilleran–Rocky Mountain Sectional Meeting)*, v. 25, no. 5, p. 112.
- MacCready, T., Snoke, A.W., Wright, J.E., and Howard, K.A., in press, Mid-crustal flow during Tertiary extension in the Ruby Mountains core complex, Nevada. *Geological Society of America Bulletin*.
- Martin, H., 1987, Petrogenesis of Archean trondhjemites, tonalites, and granodiorites from eastern Finland. major and trace element geochemistry. *Journal of Petrology*, v. 28, p. 921–953.
- McGrew, A.J., 1992, Tectonic evolution of the northern East Humboldt Range, Elko County, Nevada [Ph.D. dissertation]. Laramie, University of Wyoming, 191 p.
- McGrew, A.J., and Snee, L.W., 1994, $^{40}\text{Ar}/^{39}\text{Ar}$ thermochronometric constraints on the tectonothermal evolution of the northern East Humboldt Range metamorphic core complex, Nevada. *Tectonophysics*, v. 238, p. 425–450.
- Miller, D.M., and Allmendinger, R.W., 1991, Jurassic normal and strike-slip faults at Crater Island, northwestern Utah. *Geological Society of America Bulletin*, v. 103, p. 1239–1251.
- Miller, D.M., and Camilleri, P.A., 1992, Day 2. Road log from the Pilot Range to Wells, Nevada, in Wilson, J.E., ed., *Field guide to geologic excursions in Utah and adjacent areas of Nevada, Idaho, and Wyoming*: Utah Geological Survey Miscellaneous Publication 92-3, p. 40–46.
- Miller, D.M., and Hoisch, T.D., 1992, Mesozoic structure, metamorphism, and magmatism in the Pilot and Toano Ranges, in Wilson, J.E., ed., *Field guide to geologic excursions in Utah and adjacent areas of Nevada, Idaho, and Wyoming*. Utah Geological Survey Miscellaneous Publication 92-3, p. 77–92.
- Miller, D.M., and Lush, A.P., 1981, Preliminary geologic map of the Pilot Peak quadrangle and adjacent quadrangles, Elko County, Nevada, and Box Elder County, Utah. U.S. Geological Survey Open-File Report 81-658, 21 p., 2 sheets, scale 1:24,000.
- Miller, D.M., Hillhouse, W.C., Zartman, R.E., and Lanphere, M.A., 1987, Geochronology of intrusive and metamorphic rocks in the Pilot Range, Utah and Nevada, and comparison with regional patterns. *Geological Society of America Bulletin*, v. 99, p. 886–879.
- Misch, P., and Hazzard, J.C., 1962, Stratigraphy and metamorphism of late Precambrian rocks in central northeastern Nevada and adjacent Utah. *American Association of Petroleum Geologists Bulletin*, v. 46, p. 289–343.
- Moore, W.J., 1973, A summary of radiometric ages of igneous rocks in the Oquirrh Mountains, north-central Utah. *Economic Geology*, v. 68, p. 97–101.
- Moore, W.J., and McKee, E.H., 1983, Phanerozoic magmatism and mineralization in the Tooele $1^\circ \times 2^\circ$ quadrangle, Utah, in Miller, D.M., Todd, V.R., and Howard, K.A., eds., *Tectonic and stratigraphic studies in the eastern Great Basin*. Boulder, Colorado, Geological Society of America Memoir 157, p. 183–190.

- Mueller, K.J., and Snoke, A.W., 1993a, Progressive overprinting of normal fault systems and their role in Tertiary exhumation of the East Humboldt-Wood Hills metamorphic complex, northeast Nevada: *Tectonics*, v. 12, p. 361–371.
- Mueller, K.J., and Snoke, A.W., 1993b, Cenozoic basin development and normal fault systems associated with the exhumation of metamorphic complexes in northeast Nevada, in Lahren, M.M., Trexler, J.H., Jr., and Spinosa, C., editors, *Crustal evolution of the Great Basin and Sierra Nevada: Cordilleran/Rocky Mountain Section*, Geological Society of America Guidebook, Department of Geological Sciences, University of Nevada, Reno, p. 1–34.
- Noble, L.F., 1941, Structural features of the Virgin Spring area, Death Valley, California. *Geological Society of America Bulletin*, v. 52, p. 941–1000.
- Palmer, A.R., 1983, Decade of North American Geology 1983 geologic time scale: *Geology*, v. 11, p. 503–504.
- Palmer, H.C., MacDonald, W.D., and Hayatsu, A., 1991, Magnetic, structural and geochronologic evidence bearing on volcanic sources and Oligocene deformation of ash flow tuffs, northeast Nevada. *Journal of Geophysical Research*, v. 96, p. 2185–2202.
- Patterson, E.B., 1977, What's in a name? A history of Elko County place names: Elko, Nevada, *Northeastern Nevada Historical Society Quarterly*, Spring and Summer 1977, p. 3–47.
- Pearce, J.A., Harris, N.B.W., and Tindle, A.G., 1984, Trace element discrimination diagrams for the tectonic interpretation of granitic rocks: *Journal of Petrology*, v. 25, p. 956–983.
- Peters, M.T., 1992, A petrologic and stable isotope study of the role of fluids in high-grade metamorphism: the East Humboldt Range, Nevada, USA [Ph.D. dissertation]: Chicago, Illinois, The University of Chicago, 279 p.
- Peters, M.T., and Wickham, S.M., 1994, Petrology of upper amphibolite facies marbles from the East Humboldt Range, Nevada, USA; evidence for high-temperature, retrograde, hydrous volatile fluxes at mid-crustal levels: *Journal of Petrology*, v. 35, p. 205–238.
- Peters, M.T., and Wickham, S.M., 1995, On the causes of ^{18}O -depletion and $^{18}\text{O}/^{16}\text{O}$ homogenization during regional metamorphism; the East Humboldt Range core complex, Nevada: *Contributions to Mineralogy and Petrology*, v. 119, p. 68–82.
- Peters, M.T., Wickham, S.M., and Miller, D.M., 1992, High $\delta^{13}\text{C}$ Late Proterozoic carbonates of the North American Cordillera: *Geological Society of America Abstracts with Programs*, v. 24, no. 7, p. A114.
- Powell, R., and Holland, T.J.B., 1988, An internally consistent dataset with uncertainties and correlations: 3. Applications to geobarometry, worked examples and a computer program: *Journal of Metamorphic Geology*, v. 6, p. 173–204.
- Ramsey, J.G., and Huber, M.I., 1983, *The techniques of modern structural geology*, volume 1: Strain analysis: New York, Academic Press, 307 p.
- Reese, N.M., 1986, Cenozoic tectonic history of the Ruby Mountains and adjacent areas, northeastern Nevada: constraints from radiometric dating and seismic reflection profiles [M.S. thesis]: Dallas, Texas, Southern Methodist University, 88 p.
- Rigby, J.K., 1958, Geology of the Stansbury Mountains, eastern Tooele County, Utah: *Utah Geological Society Guidebook to the geology of Utah*, no. 13, p. 1–134.
- Schaeffer, F.E., editor, 1960, *Geology of the Silver Island Mountains, Box Elder and Tooele counties, Utah and Elko County, Nevada*: Utah Geological Society Guidebook to the geology of Utah, no. 15, 185 p.
- Schalla, R.A., 1992, Results of exploratory drilling in Hungington Valley near Jiggs, Elko County, Nevada, in Trexler, J.H., Jr., and others, eds., *Structural geology and petroleum potential of southwest Elko County, Nevada*: Reno, Nevada, 1992 Fieldtrip Guidebook, Nevada Petroleum Society, Inc., p. 71–85.
- Sharp, R.P., 1938, Pleistocene glaciation in the Ruby-East Humboldt Range, northeastern Nevada: *Journal of Geomorphology*, v. 1, no. 4, p. 296–323.
- Sharp, R.P., 1939a, The Miocene Humboldt Formation in northeastern Nevada: *Journal of Geology*, v. 47, p. 133–160.
- Sharp, R.P., 1939b, Basin-Range structure of the Ruby-East Humboldt Range, northeastern Nevada: *Geological Society of America Bulletin*, v. 50, p. 881–920.
- Sharp, R.P., 1940, Geomorphology of the Ruby-East Humboldt Range, Nevada: *Geological Society of America Bulletin*, v. 51, p. 337–372.
- Sharp, R.P., 1942, Stratigraphy and structure of the southern Ruby Mountains, Nevada: *Geological Society of America Bulletin*, v. 53, p. 647–690.
- Smith, J.F., Jr., and Howard, K.A., 1977, Geologic map of the Lee 15-minute quadrangle, Elko County, Nevada: U.S. Geological Survey Geologic Quadrangle Map GQ-1393, scale 1:62,500.
- Smith, J.F., Jr., and Ketner, K.B., 1976, Stratigraphy of post-Paleozoic rocks and summary of resources in the Carlin-Pinon Range area, Nevada with a section on Aeromagnetic Survey by D.R. Mabey. U.S. Geological Survey Professional Paper 867-B, 48 p.
- Smith, J.F., Jr., and Ketner, K.B., 1978, Geologic map of the Carlin-Pinon Range area, Elko and Eureka counties, Nevada. U.S. Geological Survey Miscellaneous Investigations Series Map I-1028, scale 1:62,500.
- Snelson, S., 1957, The geology of the northern Ruby Mountains and the East Humboldt Range, Elko County, Nevada [Ph.D. dissertation]: Seattle, University of Washington, 214 p.
- Snoke, A.W., 1975, A structural and geochronological puzzle: Secret Creek gorge area, northern Ruby Mountains, Nevada. *Geological Society of America Abstracts with Programs*, v. 7, no. 7, p. 1278–1279.
- Snoke, A.W., 1980, Transition from infrastructure to suprastructure in the northern Ruby Mountains, Nevada, in Crittenden, M.D., Jr., Coney, P.J., and Davis, G.H., eds., *Cordilleran metamorphic core complexes*: Boulder, Colorado, Geological Society of America Memoir 153, p. 287–333.
- Snoke, A.W., 1992, Clover Hill, Nevada: Structural link between the Wood Hills and East Humboldt Range, in Wilson, J.R., ed., *Field guide to geologic excursions in Utah and adjacent areas of Nevada, Idaho, and Wyoming*: Utah Geological Survey Miscellaneous Publication 92-3, p. 107–122.
- Snoke, A.W., 1994, Oblique views of the crust in the Ruby Mountains-East Humboldt Range, northeastern Nevada: implications for superposed Mesozoic and Cenozoic metamorphism. *Geological Society of America Abstracts with Programs*, v. 26, no. 2, p. 94.
- Snoke, A.W., and Howard, K.A., 1984, Geology of the Ruby Mountains-East Humboldt Range, Nevada: A Cordilleran metamorphic core complex (includes road log), in Lintz, J., Jr., editor, *Western Geological Excursions*, v. 4: Reno, Nevada, Department of Geological Sciences of the Mackay School of Mines, p. 260–303.
- Snoke, A.W., and Lush, A.P., 1984, Polyphase Mesozoic-Cenozoic deformational history of the northern Ruby Mountains-East Humboldt Range, in Lintz, J., ed., *Western Geological Excursions*, v. 4: Reno, Nevada, Department of Geological Sciences of the Mackay School of Mines, p. 232–260.
- Snoke, A.W., McKee, E.H., and Stern, T.W., 1979, Plutonic, metamorphic, and structural chronology in the northern Ruby Mountains, Nevada: A preliminary report: *Geological Society of America Abstracts with Programs*, v. 11, p. 520–521.
- Snoke, A.W., Durgin, S.L., and Lush, A.P., 1982, Structural variations in the northern Ruby Mountains-East Humboldt Range, Nevada. *Geological Society of America Abstracts with Programs* 1982, v. 14, no. 4, p. 235.
- Snoke, A.W., Hudec, M.R., Hurlow, H.A., and McGrew, A.J., 1990a, The anatomy of a Tertiary extensional shear zone, Ruby Mountains-East

- Humboldt Range, Nevada. Geological Society of America Abstracts with Programs, v. 22, no. 3, p. 66.
- Snoke, A.W., McGrew, A.J., Valasek, P.A., and Smithson, S.B., 1990b, A crustal cross-section for a terrain of superimposed shortening and extension: Ruby Mountains-East Humboldt Range metamorphic core complex, Nevada, in Salisbury, M.H., and Fountain, D.M., eds., Exposed cross-sections of the continental crust, NATO Advanced Studies Institute. Dordrecht, The Netherlands, Kluwer Academic Publishers, p. 103-135.
- Snoke, A.W., Wright, J.E., Hudec, M.R., and McGrew, A.J., 1992, Mesozoic magmatic-metamorphic-deformational history of the Ruby Mountains-East Humboldt Range, Nevada: Geological Society of America Abstracts with Programs, v. 24, no. 6, p. 63.
- Solomon, B.J., McKee, E.H., and Anderson, D.W., 1979, Stratigraphy and depositional environments of Paleogene rocks near Elko, Nevada, in Armentrout, J.M., Cole, M.R., and TerBest, H., Jr., eds., Cenozoic paleogeography of the western United States, Pacific Coast Paleogeography Symposium 3: Los Angeles, California, The Pacific Section, Society of Economic Paleontologists and Mineralogists, p. 75-88.
- Solomon, B.J., and Moore, S.W., 1982, Geologic map and oil shale deposits of the Elko East quadrangle, Elko County, Nevada: U.S. Geological Survey Map MF-1421, scale 1:24,000.
- Steiner, J.C., Jahns, R.H., and Luth, W.C., 1975, Crystallization of alkali feldspar and quartz in the haplogranite system $\text{NaAlSi}_3\text{O}_8$ - KAlSi_3O_8 - SiO_2 - H_2O at 4 kb: Geological Society of America Bulletin, v. 86, p. 83-98.
- Stoerzel, A., 1996, Implications on the nature of extended crust from multi-component seismic studies of the Ruby Mountains metamorphic core complex, northeastern Nevada [Ph.D. dissertation]: Laramie, University of Wyoming, 281 p.
- Strecker, U., Smithson, S.B., and Steidtmann, J.R., 1996, Cenozoic basin extension beneath Goshute Valley, Nevada, in Beratan, K.K., ed., Reconstructing the history of Basin and Range extension using sedimentology and stratigraphy: Boulder, Colorado, Geological Society of America Special Paper 303, p. 15-26.
- Swisher, C.C., III, and Prothero, D.R., 1990, Single-crystal $^{40}\text{Ar}/^{39}\text{Ar}$ dating of the Eocene-Oligocene transition in North America: Science, v. 249, p. 760-762.
- Taylor, G.K., 1984, Stratigraphy, metamorphism, and structure of the southeastern East Humboldt Range, Elko County, Nevada [M.S. thesis]: Columbia, University of South Carolina, 148 p.
- Thorman, C.H., 1962, Structure and stratigraphy of the Wood Hills and a portion of the northern Pequop Mountains, Elko County, Nevada [Ph.D. dissertation]: Seattle, University of Washington, 218 p.
- Thorman, C.H., 1970, Metamorphosed and nonmetamorphosed Paleozoic rocks in the Wood Hills and Pequop Mountains, northeast Nevada. Geological Society of America Bulletin, v. 81, p. 2417-2448.
- Thorman, C.H., Ketner, K.B., Snoke, A.W., Brooks, W.E., and Mueller, K.J., 1991, Evidence for the involvement of the Roberts Mountains allochthon in Mesozoic tectonics and its effect on mineral deposits and petroleum accumulation models in northeast Nevada, in Buffa, R.H., and Coyner, A.R., eds., Geology and ore deposits of the Great Basin, Field Trip Guidebook Compendium, volume 2: Reno, Nevada, Geological Society of Nevada, p. 869-905.
- Tingley, J.V., 1992, Mining districts of Nevada. Reno, Nevada Bureau of Mines and Geology Report 47, 80 p.
- Tooker, E.W., 1983, Variations in structural style and correlation of thrust plates in the Sevier foreland thrust belt, Great Salt Lake area, Utah, in Miller, D.M., Todd, V.R., and Howard, K.A., eds., Tectonic and stratigraphic studies in the eastern Great Basin. Boulder, Colorado, Geological Society of America Memoir 157, p. 61-73.
- Tooker, E.W., and Roberts, R.J., 1970, Upper Paleozoic rocks in the Oquirrh Mountains and Bingham Mining District, Utah: U.S. Geological Survey Professional Paper 629-A, 76 p.
- Tooker, E.W., and Roberts, R.J., 1971, Structures related to thrust faults in the Stansbury Mountains, Utah: U.S. Geological Survey Professional Paper 750-B, B1-B12.
- Warnaars, F.W., Smith, W.H., Bray, R.E., Lanier, G., and Shafiqullah, M., 1978, Geochronology of igneous intrusions and porphyry copper mineralization at Bingham, Utah. Economic Geology, v. 73, p. 1242-1249.
- Wernicke, B., and Burchfiel, B.C., 1982, Modes of extensional tectonics. Journal of Structural Geology, v. 4, p. 105-115.
- Wickham, S.M., and Peters, M.T., 1990, An oxygen isotope discontinuity in high-grade rocks of the East Humboldt Range, Nevada. Nature, v. 345, p. 150-153.
- Wickham, S.M., and Peters, M.T., 1992, Oxygen and carbon isotope profiles in metasediments from Lizzies Basin, East Humboldt Range, Nevada: constraints on mid-crustal metamorphic and magmatic volatile fluxes: Contributions to Mineralogy and Petrology, v. 112, p. 46-65.
- Wickham, S.M., and Peters, M.T., 1993, High $\delta^{13}\text{C}$ Neoproterozoic carbonate rocks in western North America. Geology, v. 21, p. 165-168.
- Wickham, S.M., Taylor, H.P., Jr., Snoke, A.W., and O'Neil, J.R., 1991, An oxygen and hydrogen isotope study of high-grade metamorphism and anatexis in the Ruby Mountains-East Humboldt Range core complex, Nevada, in Taylor, H.P., Jr., O'Neil, J.R., and Kaplan, I.R., eds., Stable isotope geochemistry. A tribute to Samuel Epstein. The Geochemical Society, Special Publication No. 3, p. 373-390.
- Willden, R., and Kistler, R.W., 1967, Ordovician tectonism in the Ruby Mountains, Elko County, Nevada. U.S. Geological Survey Professional Paper 575-D, p. D64-D75.
- Willden, R., and Kistler, R.W., 1969, Geologic map of the Jiggs quadrangle, Elko County, Nevada. U.S. Geological Survey Map GQ-859, scale 1:62,500.
- Willden, R., and Kistler, R.W., 1979, Precambrian and Paleozoic stratigraphy in central Ruby Mountains, Elko County, Nevada, in Newman, G.W., and Goode, H.D., eds., Basin and Range symposium and Great Basin field conference: Denver, Colorado, Rocky Mountain Association of Geologists, p. 221-243.
- Willden, R., Thomas, H.H., and Stern, T.W., 1967, Oligocene or younger thrust faulting in the Ruby Mountains, northeastern Nevada. Geological Society of America Bulletin, v. 78, p. 1345-1358.
- Wright, J.E., and Snoke, A.W., 1986, Mid-Tertiary mylonitization in the Ruby Mountain-East Humboldt metamorphic core complex, Nevada. Geological Society of America Programs with Abstracts, v. 18, no. 6, p. 795.
- Wright, J.E., and Snoke, A.W., 1993, Tertiary magmatism and mylonitization in the Ruby-East Humboldt metamorphic core complex, northeastern Nevada. U-Pb geochronology and Sr, Nd, and Pb isotope geochemistry: Geological Society of America Bulletin, v. 105, p. 935-952.
- Wright, J.E., and Wooden, J.L., 1991, New Sr, Nd, and Pb isotopic data from plutons in the northern Great Basin. Implications for crustal structure and granite petrogenesis in the hinterland of the Sevier thrust belt. Geology, v. 19, p. 457-460.
- Young, J.C., 1955, Geology of the southern Lakeside Mountains, Utah. Utah Geological and Mineralogical Survey Bulletin 56, 110 p.